Regulation of natural killer cell cytotoxic pathways during serial killing activity

Dissertation

submitted to the

Faculty of Chemistry and Biological Chemistry

at the Technische Universität Dortmund

for the degree of

Doctor of Natural Sciences

Thesis by Isabel Prager

(born in Gelsenkirchen)

Referees Prof. Dr. Carsten Watzl

Prof. Dr. Jan Hengstler

Meinen Eltern

Table of contents

Acknowledgments

First of all, I would like to thank Prof. Dr. Carsten Watzl. Thank you for all your research advise and for all your support, guidance, valuable comments, suggestions that benefited me much in the completion and success of this study.

Furthermore, I highly appreciate that Prof. Dr. Jan Hengstler for his considerate acceptance of acting as second examiner.

I also thank all past and present members of the Watzl lab.

Moritz Anft	Linda Drenkelforth	Jens Niemann
Lea Boller	Nicole Dychus	Martin Obholzer
Vivian Bönnemann	Anke Flegel	Mina Sandusky
Peter Bröde	Leonie Fleige	Elena Schwendich
Nora Bruning	Markus Gilles	Doris Teutsch
Silvia Capellino	Alisa Kahler	Doris Urlaub
Maren Claus	Julia Luo	Karolin Wieber
Jürgen Damaschke	Sarah Metzler	Sabine Wingert

Thank you not only for the good working atmosphere and everything you have been teaching me, but also for the huge support and inspiring discussion, which benefited me even more for the success of my final thesis.

A special thanks goes to Björn Önfelt and Hanna van Ooijen for their collaboration in the experiments and constitutive sugesstions.

Thank you to all collaboration partners Dr. Wenjie Bi, Prof. Dr. Lothar Jänsch and Dr. Jana Götz, Prof. Dr. Adelheid Cerwenka to getting me the opportunity to think out of the box.

Moreover, I would like to thank my family. Thank you mom and dad, for your love and unconditional support. You are the best parents, I could ever wish for. Last but not least, a special thanks to Niklas Uhlenbrock, who always supported me and gave me a lot of courage and strength. I´m look forward to spending the rest of my life with you.

Abstract

Natural Killer (NK) cells act as the front line of the body´s defense in the immune system and they are key players in efficiently recognizing and eliminating virus-infected and tumor cells. Individual NK cells can eliminate multiple target cells in a sequential manner during a process named serial killing. There are two major pathways NK cells use to induce apoptosis in their target cells: By releasing the content of cytotoxic granules containing the serine protease granzyme B (GrzB) and the pore-forming protein perforin or by the engagement of death receptors, which initiates caspase cascades via Caspase-8 (Casp8). The contribution of both cell death processes to NK cell cytotoxicity and serial killing remains poorly understood. Therefore, investigating the interplay between these pathways in more detail is important for a better understanding of NK cell cytotoxicity. To visualize the GrzB and death receptor-mediated target cell death in a time-dependent manner, we used fluorescent localization reporters that enabled us to simultaneously measure the activities of GrzB and of Casp8 in target cells upon contact with NK cells by life cell imaging.

In this study we observed that NK cells kill their initial targets via the fast GrzB-induced pathway and switch to a slow death receptor-mediated killing for the final target. During the target cell contact NK cells lost GrzB and perforin, whereas the expression of CD95L, a main death cell ligand, was increased on the NK cell surface. The reduction of the lytic granules can be efficiently restored by the stimulation with different cytokines such as IL-15, IL-2 or IL-21. Perforin deficient NK cells or ILC3 cells were unable to perform GrzB-mediated killing and no serial killing could be mediated without this pathway. In contrast, the absence of death receptor CD95 on the target cell and/or the absence of death receptor ligands on the NK cell had no direct influence on the GrzB-mediated serial killing. This demonstrates that the use of GrzB vs. death receptor-mediated target cell killing is differentially regulated during the serial killing activity of NK cells. Taken together, we observed a rapid target cell death which was induced by GrzB and originated from early established NK : target contacts. In contrast, cell death mediated by Casp-8 was a result of later target cell engagements and took much longer from NK : target cell contact to target cell death.

Zusammenfassung

Natürliche Killerzellen (NK) fungieren als Frontlinie der körpereignen Verteidigung und spielen eine Schlüsselrolle bei der effektiven Immunantwort gegen virusinfizierte Zellen und Tumorzellen, da sie in der Lage sind, transformierte und infizierte Zellen zu erkennen und abzutöten. Einzelne NK-Zellen können mehrere Zellen nacheinander töten, wobei dieser Prozess serielle Tötung genannt wird. Es gibt zwei Wege, über die NK-Zellen Apoptose in ihren Zielzellen induzieren. Zum einen besitzen NK Zellen zytotoxische Granula, welche die Serinprotease Granzym B (GrzB) und das porenbildende Protein Perforin enthalten. Zum anderen können NK Zellen durch Bindung an Todesrezeptoren Apoptose induzieren, was über eine Initiierung einer Caspase Kaskade via Caspase-8 (Casp8) erfolgt. Es konnte jedoch bislang nicht gezeigt werden, welche Mechanismen zur seriellen Abtötung der NK-Zellen genutzt werden. Um ein besseres Verständnis der Zytotoxizität von NK-Zellen zu erlangen, ist es wichtig, das Zusammenspiel dieser Wege genauer zu untersuchen. Aus diesem Grund wurden in dieser Arbeit Fluoreszenzlokalisationsreporter verwendet, mit denen simultan und unabhängig die Aktivitäten von GrzB und Casp8 in Zielzellen bei Kontakt mit NK-Zellen gemessen werden konnten.

In der Anfangsphase der Kokultur mit HeLa Zellen wird der Zelltod nahezu ausschließlich über den schnellen GrzB-vermittelten Todesweg induziert. Erst bei späteren Kontakten mit Tumorzellen wechselten die NK Zellen zu der langsameren Todesrezeptor-vermittelten Tötung. Während des Zielzellenkontakts reduziert sich bei den degranulierenden NK-Zellen GrzB und Perforin, wohingegen die Expression von CD95L auf der NK-Zelloberfläche zunimmt. Die Reduktion der lytischen Granula kann durch die Stimulation mit IL-2, IL-15 oder IL-21 effizient wiederhergestellt werden. Perforin-defiziente NK-Zellen oder ILC3-Zellen konnten keine GrzB-vermittelte Tötung induzieren und waren nicht in der Lage serielle Tötungen mehrerer Zielzellen durch den Todesrezeptorweg zu vermitteln. Zusätzlich konnte gezeigt werden, dass das Fehlen von Todesrezeptoren und/oder das Fehlen von Todesrezeptorliganden keinen direkten Einfluss auf die GrzB-vermittelte serielle Tötung hat. Zusammenfassend konnte gezeigt werden, dass die NK Zellen zunächst schnell über den GrzB-vermittelten Todesweg Apoptose induzierten, der von früh etablierten NK : Zielkontakten herrührte. Im Gegensatz dazu war der durch Casp8 vermittelte Zelltod ein Ergebnis späterer Zielzellkontakte und dauerte von NK-Zielzellkontakt bis zum Zielzelltod deutlich länger.

1 Introduction

1.1 Natural killer cells

Since the discovery of natural killer (NK) cells in humans and mice in 1975, NK cells were described as “naturally” cytotoxic, which enable them to kill certain tumorous cells without prior activation (Kiessling et al., 1975). NK cells represent one of three subpopulations of peripheral blood lymphocytes (PBL) beside the T and B cells. In the peripheral blood, NK cells can be divided into two subtypes based on their relative expression of the surface markers CD16 and CD56. Accordingly, NK cells can be mainly grouped in $CD56^{bright}$ $CD16^{-}$ or $CD56^{dim}$ $CD16^{+}$, with the $CD56^{dim}$ $CD16^{+}$ population being dominant (90 %) in healthy individuals (Poli et al., 2009). In addition, these two populations are also functionally different: $CD56^{dim}$ $CD16^{+}$ NK cells are more cytotoxic than the $CD56^{bright}$, but $CD56^{bright}$ are more responsive to stimulation by inflammatory cytokines than $CD56^{dim}$ NK cells (Nagler et al., 1989). Moreover, several experimental findings indicated that $CD56^{bright}$ NK cells are the precursors of the more mature $CD56^{dim}$ NK cells (Poli et al., 2009). As a part of the innate immune system, NK cells contribute to first line of defense against a variety of virally infected or transformed / malignant cells. NK cells derive from precursors (multipotent $CD34^{+}$ haematopoietic cells) in the bone marrow and can be found as mature NK cells in the bloodstream and in some lymphatic or non-lymphatic tissues such as the liver, kidney, tonsil, lungs and uterus during pregnancy (Carrega and Ferlazzo, 2012). NK cells are potent producers of pro-inflammatory cytokines and display immunomodulatory functions. The most prominent cytokines produced by NK cells are tumor necrosis factor alpha (TNF) and interferon gamma, (IFN-γ), which play an important role during the early and late phases of immune responses (Murphy et al., 2001). In particular, IFN-γ enhances on the one hand the innate immune response and on the other hand helps to shape the adaptive immune response (Robb and Hill, 2012). This demonstrates that NK cells act as a connection between the innate and the adaptive immune system. Apart from the immune regulatory function, NK cells play an important role removing infected and transformed cells via cell-mediated cytotoxicity. The induction of the cytotoxic function is regulated by a balance of inhibitory and activating germ line encoded receptors. Activating receptors mostly recognize stress-induced ligands on malignantly transformed or virally infected cells. The Natural Cytotoxicity Receptors (NCRs) NKp30, NKp44 and NKp46, the C-type lection receptor NKG2D, DNAM-1, SLAM family receptors such as 2B4 and activating Killer Ig-like receptors (KIRs) are the main activating receptors inducing cytotoxicity (Farag et al., 2002). This activation enables the NK cells to detect and eliminate potentially dangerous cells. Inhibitory receptors primarily

bind to major histocompatibility complex class I (MHC-I) and thereby differentiate between self versus non-self (Elliott and Yokoyama, 2011). Inhibitory receptors include inhibitory KIRs and C-type lectin like receptors such as NKG2A (Joyce and Sun, 2011). NK cells express a wide variety of inhibitory receptors, but there are clonally expressed on individual NK cells. Early studies reported that all mature human NK cell clones from two individuals expressed at least one inhibitory receptor for self-MHC I (Valiante et al., 1997). However, recent studies have detected that there are also NK cells known that lack any inhibitory receptors that recognized a self MHC-I, resulting in a hyporesponsiveness, a mechanism for self-tolerance (Diefenbach and Raulet, 2001). This indicates that only the engagement of inhibitory receptors with self MHC-I molecules provides all of the signals during NK cell development that would lead to fully functional competent NK cells. The acquisition of functional competence in NK-cell is called education. So far, several mechanisms were postulated to explain the induction of proper self-tolerance in NK cells. The “disarming model” implies that during continuous stimulation via activating receptors NK cells are “disarmed” (hyporesponsive) when they lack the inhibitory signals to balance the continuous activating stimulation (He and Tian, 2017). In contrast, the “arming model” suggests that NK cells become fully functional through signals from at least one inhibitory receptor that recognize self-MHC I (Shifrin et al., 2014). These educated NK cells were also described to have increased dense-core secretory granules and therefore better NK cell effector functions (Goodridge et al., 2019).

The MHC-I receptors are important for education but also take a main part in NK cell activation. Diseased and stressed cells down-regulate or lose their MHC-I receptors on their surface (missing-self), leading to induction of apoptosis by the NK cell (Khanna, 1998). The integration of multiple signals delivered by activating and inhibitory receptors determines if the NK cell becomes effectively activated or not (Kumar, 2018). The NK cell cytotoxicity can be triggered by two distinct ways. The initial mechanism to induce cytotoxicity is based on granule exocytosis (degranulation) upon formation of an immunological synapse (Orange, 2008). NK cells possess preformed granules that contain amongst others granzymes such as granzyme B (GrzB) and perforin. Upon activation, NK cells rapidly release the cytotoxic granule contents and induce apoptosis via the granzyme-mediated pathway (Talanian et al., 1997). The second pathway to induce apoptosis is the death receptor-mediated pathway. The two main death receptor ligands to induce apoptosis are CD95L (FasL) and TNF-related apoptosis-inducing ligand (TRAIL) (Kumar et al., 2005). Binding of TRAIL and CD95L to its receptors, TRAILR1/ TRAILR2 or CD95, results in receptor oligomerization on the cell membrane, which leads

by the activation of caspases to death receptor-mediated apoptosis (Guicciardi and Gores, 2009).

NK cells belong to the larger group of innate lymphoid cells (ILCs), which originate from the common lymphoid progenitor (CLP), like T- and B-cells. ILCs were discovered in the late nineties as lymphoid tissue inducer cells (LTi), and since the last 2000s they are grouped in three different subpopulations ILC1s, ILC2s and ILC3s (include LTi cells) (Spits et al., 2013). ILCs are defined as cell linage marker negative (Lin^-), but do express CD25 (IL-2 receptor-α) and CD127 (IL-7 receptor-α). ILCs are present in intestinal, pulmonary and oropharyngeal mucosal tissue and less well represented in circulating blood. ILC1 rely on the transcriptional factor T-bet to generate IFN-γ when stimulated by IL-12, IL15 and IL-18 (Bernink et al., 2015, Spits et al., 2016). ILC2 are ROR-α and GATA3-dependent and produce IL-5 and IL-13 upon the stimulation by IL-25 and thymic stromal lymphopoietin (TSLP) (Brestoff et al., 2015). ILC3 produce IL-17A, IL-22 and granulocyte macrophage-colony stimulating factor (GM-CSF) upon stimulation by IL-1beta and/or IL-23 and rely on the transcription factor ROR-γ-t and aryl hydrocarbon receptor (AHR) (Atreya et al., 2019). Furthermore, ILC3 can be divided according to the expression of NKp44 and $NKp44^+$ ILC3 produce IL-22, whereas $NKp44^-$ ILC3 secret IL-17A. These three subpopulations of ILCs have different roles. ILC3s provide protection against extracellular microbial pathogen (Guo et al., 2015), ILC2s respond to parasitic worms (Herbert et al., 2019), but they are also implicated in obesity, dietary stress and allergic disease (Everaere et al., 2018), ILC1 defend against to intracellular parasites and bacteria (Dunay and Diefenbach, 2018).

1.2 Trafficking and storage of GrzB and perforin in lytic granules

One mechanism of NK cells to induce target cell death is mediated by releasing cytotoxic molecules like perforin and granzymes. These proteins are stored in secretory lysosomes, which are also known as cytotoxic granules (Bossi and Griffiths, 2005). Secretory lysosomes are dual-function organelles combining the degradative function of conventional lysosomes with the capacity to fuse with the plasma membrane (regulated exocytosis) (Burkhardt et al., 1990, Topham and Hewitt, 2009). Granzymes were discovered in the late 1980s and early 1990s (Masson and Tschopp, 1987) and belong to the serine protease family. There are five known human granzymes (A, B, H, K and M). Granzyme B (GrzB) as well as perforin represent main components of the granules of NK cells and cytotoxic T cells (CTLs) (Voskoboinik et al., 2015).

The best-characterized granzymes are Granzyme A (GrzA) and GrzB, while the other granzymes are much less described (Masson and Tschopp, 1987). GrzB was initially named “cytotoxic T lymphocyte-associated serine esterase 1” or granzyme 2. It has a wide range of substrate specificities and cleaves after aspartate in the P1 position, which GrzB shares with different caspases (Thornberry et al., 1997). Therefore, it can process numerous caspases *in vitro* including Casp3, -6, -7, -8 and -10 (Darmon et al., 1995, Chinnaiyan et al., 1996, Duan et al., 1996). It was shown that GrzB can cleave Casp3 and Casp7 resulting in a cascade of caspases, which induces caspase-dependent cell death (Yang et al., 1998). GrzB can also induce cell death independently of caspases by cleaving the BH3-only proapoptotic Bcl-2 family member, Bid, which finally results in apoptosis (Pinkoski et al., 2001). This efficient cleavage of Bid can only be observed for human GrzB but not in mice (Casciola-Rosen et al., 2007).

The biosynthesis of GrzB and perforin is a highly ordered and tightly regulated process. GrzB is expressed as a pre-pro-protein (inactive zymogen) with a N-terminal signal sequence (pre) and a N-terminal inhibitory dipeptide (pro) (**Fig. 1**). The signal peptide directs it to the endoplasmic reticulum (ER) (Jenne and Tschopp, 1988). At the ER, the protein is synthesized and the signal peptide is cleaved off, which results in an inactive proenzyme. This proenzyme is transported to the *cis* compartment of the Golgi apparatus. Within the Golgi, it is modified with a mannose-6-phosphate (M6P) tag by the *N*-acetlyglucosamine-1-phospodieser α-*N*-acetyl-glucosamiadase on its carbohydrate chains, targeting the proenzyme from the Golgi to secretory lysosomes via the M6P-receptor (cytotoxic granules) (Griffiths and Isaaz, 1993). Human GrzB has two potential sites for the addition of asparagine (N)-linked carbohydrates. In the granules the environment is acidic (pH 5.5) (Einstein and Gabel, 1991) and when GrzB enters the granules this may result in a removal of the M6P tag. However, this aspect remains a matter of debate since different studies suggested that GrzB may be able to retain its M6P moiety. Within or en route to the granules the pro-peptide of GrzB is cleaved by the cysteine protease cathepsin C (dipeptidly peptidase I) (Smyth et al., 1995). However, genetically deficient cathepsin C mice or humans, showed only a partially reduced GrzB activity, which lead to the suggestion that there are alternative ways to activate GrzB. As an alternative, some studies reported that cathepsin H is an additional convertase to activate GrzB. However, in mice lacking both cathepsins (C and H), the activity of GrzB was still not completely reduced (D'Angelo et al., 2010). The removal of the dipeptide transforms GrzB into its active form, resulting in storage of active GrzB in the granules. Some studies revealed that GrzB is released in both active and inactive forms, which lead to the suggestion that there is an extracellular GrzB activator (Prakash et al., 2009). Inside

the granules, GrzB is inhibited by binding the acidic sulphate preoteoglycan serglycin and by the acidic pH. Serglycin is also responsible for the electron dense core of granules. An alternative pathway to the secretory pathway for GrzB is the constitutive nongranule biosynthesis pathway, which seems to play a role in the NK cell lines YTS, CTL and NK92 cells but not in IL-2 human activated NK cells (Prakash et al., 2009).

Perforin is a key shaped molecule comprised of 3 domains: a C-terminal membrane and Ca^{2+}/lipid binding C2 domain, a central epidermal growth factor (EGF) domain and the N-terminal membrane attack complex perforin like (MACPF)-dependent cytolysin pore-forming domain (Praper et al., 2010, Voskoboinik et al., 2005). The pore formation of perforin is highly dependent on pH and Ca^{2+} concentration (minimum of 0.2 mM required for pore formation). Under acidic conditions of less than a pH of 6 perforin remains inactive (Young et al., 1987). However, how perforin is trafficking to and stored within the granules is not fully understood. Two hypotheses are currently proposed to explain the processing and trafficking of perforin from the ER to the granules. Noteworthy, the environment in the ER is pH neutral and the concentration of Ca^{2+} is above 0.2 mM, which provides perfect conditions to form pores for perforin. One hypothesis is that perforin is synthesized as an inactive precursor. This precursor consists of an inhibitory C-terminal dodecapeptide to block Ca^{2+} access to the C2 domain. Nevertheless, this is contradicted by the fact that perforin with an intact C-terminus possessed the same activity and stability as perforin that lacks the C-terminus (Brennan et al., 2011). The X-ray structure of perforin also indicates that the C-terminus is located far from the Ca^{2+} -binding region of the C2 domain (> 60 Å), indicating that the hypothesis may not be correct (Law et al., 2010). The second hypothesis is that perforin is N-glycosylated at residue Asn549 close to the C-terminus, which blockes oligomerization of perforin monomers during the biosynthesis of perforin (House et al., 2017). Additionally, a rapid export of perforin from the ER to the Ca^{2+}-poor Golgi apparatus is also promoted by the N-linked glycosylation, which minimizes the concentration of active perforin in the ER (Brennan et al., 2018). In line with this observation, mutation or deletion of the last 12 amino acids causes retention of Perforin in the ER (Law et al., 2010). Perforin contains the binding amino acid sequence KVFF (residues 439-442), which supports calreticulin binding. Calreticulin forms complexes with perforin to limit perforin from pore-forming (Fraser et al., 2000). Also the protein lysosomal-associated membrane protein 1 (LAMP1, CD107a) seems to play a critical role in routing perforin to the lytic granules (Krzewski et al., 2013). Inside the granules, perforin can be cleaved via cathepsin-L or other proteases to generate a fully functional perforin (Konjar et al., 2010).

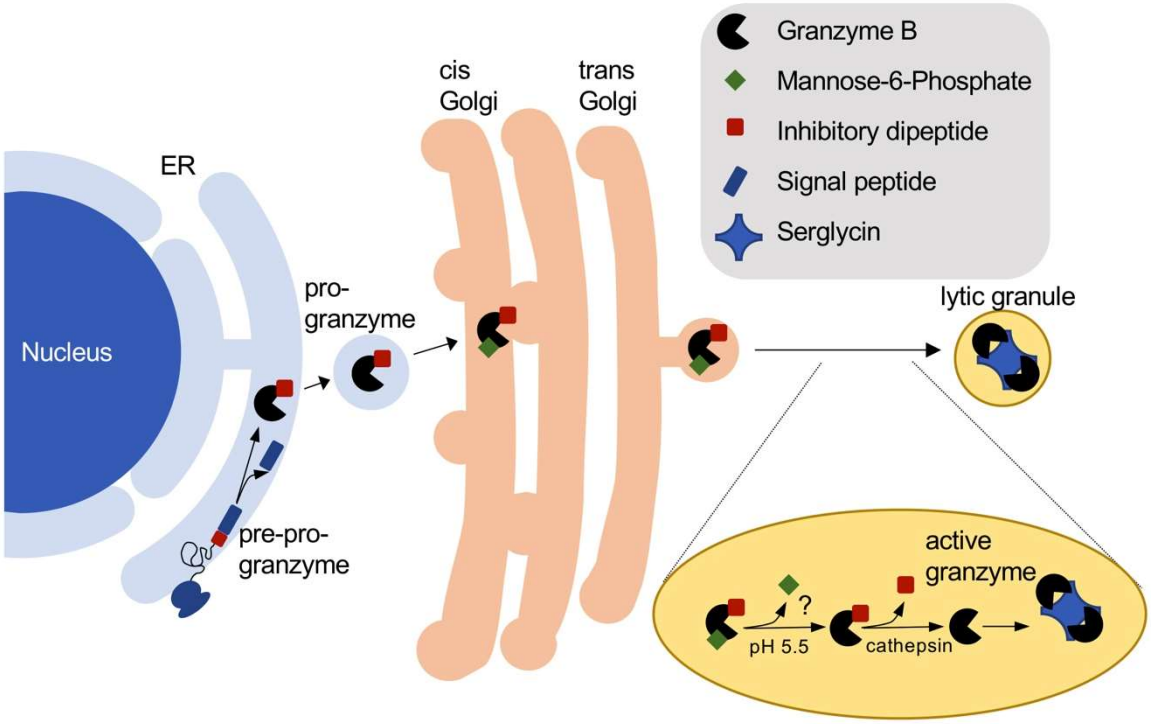

Figure 1: Trafficking of granzymes. Most of the events described in this figure stem from studies investigating GrzB. Grzs are synthesized into the ER as a pre-pro-Grz, the signal peptide is cleaved off (pre-protein), which results in inactive pro-protein. The proenzyme is modified with a M6P, providing the necessary signal for sorting into lytic granules in the cis-Golgi. M6P may be removed due to the acidic environment and cathepsin C or cathepsin H cleave the inhibitory dipeptide in the granules. Active granzymes are stored in complex with serglycin.

1.3 Degranulation and entry of GrzB and perforin

The induction of apoptosis is initiated by integrin-mediated NK cell adhesion to the target cell and the formation of the immunologic synapse. The formation of a functional immunologic synapse proceeds in three different stages: the initiation stage, the effector stage and the termination stage (Orange, 2008). For the initiation step to form a lytic synapse close cell-cell contact, intracellular signaling and initial adhesion of the NK cell to its target cell are needed, which leads to NK-cell activation. Subsequently, a firm adhesion between NK and target cell is established, which is mainly mediated by higher affinity interactions of integrins and their ligands. Two examples for well described intregrins expressed on NK cells include macrophage receptor 1 (MAC1;CD11b-CD18) and lymphocyte function-associated antigen 1 (LFA1;CD11a-CD18) (Orange et al., 2003). Beside these integrins, adapter proteins such as Adhesion and Degranulation-promoting Adapter Protein ADAP (also known as Fyn-binding protein (Fyb) or SLAP-130) are essential for the firm adhesion process. ADAP is expressed in cells of the hematopoietic

system such as NK cells, T cells, platelets and myeloid cells (Rajasekaran et al., 2013). While the impact of ADAP on the activation and effector function of T cells has been well described, several recent studies showed conflicting data about the function of ADAP in NK cells. Some studies showed that ADAP has no impact on the development or the cytotoxic function of NK cells (Fostel et al., 2006), whereas another study claimed the opposite, that ADAP has a strong influence on the NK cell function (May et al., 2013). Especially BÖNING et. al showed in an *in vivo Lm (Listeria monocytogenes)* infected mouse model that ADAP KO NK cells have reduced cytotoxic activity and an altered integrin expression (Boning et al., 2019).

Once the NK cell becomes fully activated to kill the target cell, the intracellular network of actin microfilaments is reorganized (effector stage). The lytic granules efficiently engage and move along the microtubules to the microtubule organizing center (MTOC) (Mace et al., 2014). The movement of the lytic granules along the microtubules is driven by the motor protein dynein, which polarize them towards the synapse together with the MTOC. At the synapse, the lytic granules undergo docking and fusion with the plasma membrane. With the help of small GTPases of the Rab family, MUNC proteins and the formation of a SNARE complex, this step results in the release of the granules in the synaptic cleft (Mace et al., 2014). During the fusion with the plasma membrane, CD107a appears on the cell surface and can be used as a marker for the degranulation process (Krzewski et al., 2013). Once secreted into the synaptic cleft, the neutral pH environment of the extracellular space and the presence of Ca^{2+} enables perforin to bind to the target cell membrane and to form pores in the membrane (**Fig. 2A**). These pores consist of 20 to 22 perforin monomers, contributing two β-hairpains to a membrane-spanning β-barrel (Rosado et al., 2008). In addition, the calcium-dependent C2 domain at the C terminus of perforin has a relatively low affinity (minimum of 200-250 µM) for Ca^{2+} in contrast to homologous C2 domains that function inside the cell (Voskoboinik et al., 2005). As described for membranes of cancerous or virus-infected cells the size of these oligomeric pores have a 10-20 nm inner diameter (Leung et al., 2017). These pores are structural equivalents to a transmembrane channel, which could merge into larger pores by recruiting additional perforin monomers (Leung et al., 2017). Considering these aspects, the entry of Grz directly through perforin pores seems to be possible, as the Stokes radius of GrzB is 2.5 nm (Kurschus et al., 2008). This hypothesis is underlined by results of recent studies (Lopez et al., 2013b, Lopez et al., 2013a). An alternative pathway, how GrzB could enter the target cell is the endocytotic mechanism. Thereby, the cellular uptake of GrzB is driven by binding of GrzB to the cation-independent mannose-6-phosphate receptor or by the membrane repair process, which is induced by perforin-

mediated plasma membrane disruption and Ca^{2+} influx (Keefe et al., 2005). Stored in so-called gigantosomes, GrzB could then be released into the target cell by means of perforin. During this endocytosis, perforin form pores into the endosomal membranes, which are large enough to transport granzymes efficiently (Thiery et al., 2011). Nevertheless, as the delivery process of Grz through the perforin pores just takes 80 s, these findings suggest that the direct delivery of Grz seems to be the dominant pathway (Lopez et al., 2013b). However, while direct delivery of Grz through perforin pores provides a convenient platform for Grz to enter the target cell, the endocytotic delivery of Grz cannot be excluded. Therefore, it is likely that these two processes are operating in parallel, where the endocytotic pathway works as a potential backup mechanism to ensure efficient delivery of lethal Grz to kill the target cells. After the lytic-granule contents have been secreted, the termination stage is reached (Orange, 2008). During this final step, downregulation of the accumulated activating receptors can be observed (Anft et al., 2020). This leads to the detachment of the NK cells from the target cells, which restore their ability to kill another target cell.

1.4 Death receptor signaling

In addition to the exocytosis of lytic granules, NK cells can also kill target cells by death-receptor-mediated killing (**Fig 2B**). Mainly two different receptor/ligand complexes exist that mediate apoptosis upon activation: CD95L binding to CD95 (APO-1/Fas) receptor and TRAIL mediating their effects via different TRAIL receptors.

Apoptosis can be initiated by two different pathways, the intrinsic (also known as mitochondrial pathway) or the extrinsic pathway (Fulda and Debatin, 2006). Both pathways are modulated by the response of external stimuli, namely by the ligation of the ligand (CD95L, TRAIL) on the NK cell to their receptors (CD95, DR4/DR5) on the target cell. The process results in trimerization of the receptor, leading to the recruitment of Fas associated death domain (FADD), which interacts with the death domain (DD) of the death receptor. This interaction leads to the binding of the pro-Casp8/-10 to the adapter protein FADD and the formation of the so-called Death Inducing Signaling Complex (DISC) (Kischkel et al., 1995, Bodmer et al., 2000). In the DISC Casp8 is activated by proteolytic cleavage which cleaves and thereby activates executioner caspases, like Casp7, -3 and -6, resulting in the caspase cascade (Oberst et al., 2010). Different modulators are known for the regulation of this signaling cascade, an important inhibitor to suppress a caspase cascade is X chromosome-linked inhibitor apoptosis protein (XIAP), which can bind to Casp3, -7 or -9 through its IAP repeat domains (Deveraux et al., 1998,

Eckelman et al., 2006). The intrinsic pathway triggers apoptosis by two groups of molecules, anti-apoptotic Bcl-2 and pro-apoptotic Bax. In addition, Casp8 can also cleave cytosolic BH3-only proapoptotic Bcl-2 family member, Bid (BH3 interacting domain death agonist) to tBid (truncated Bid) (Li et al., 1998). tBid moves to the mitochondria to activate Bax and/or Bak (proapoptotic members of the BCL-2 family), resulting in the release of cytochrome c and Second Mitochondria-derived Activator of caspases (SMAC, also known as DIABLO), serine protease Omi/HtrA2, AIF and endonuclease G (Saelens et al., 2004). A well-described inhibitor to prevent the oligomerization of Bax/Bak is Bcl-2, which associated with Bax, or other pro-apoptotic proteins leading to an inactivation (Dlugosz et al., 2006, Westphal et al., 2014). Cytochrome c activates another adaptor protein, namely apoptotic protease-activating factor-1 (Apaf-1), resulting in a sequentially recruitment and activation of the initiator Casp9 and the effector Casp3 and Casp7 (Bratton et al., 2001). The complex of Casp9 and Apaf-1 is known as the apoptosome.

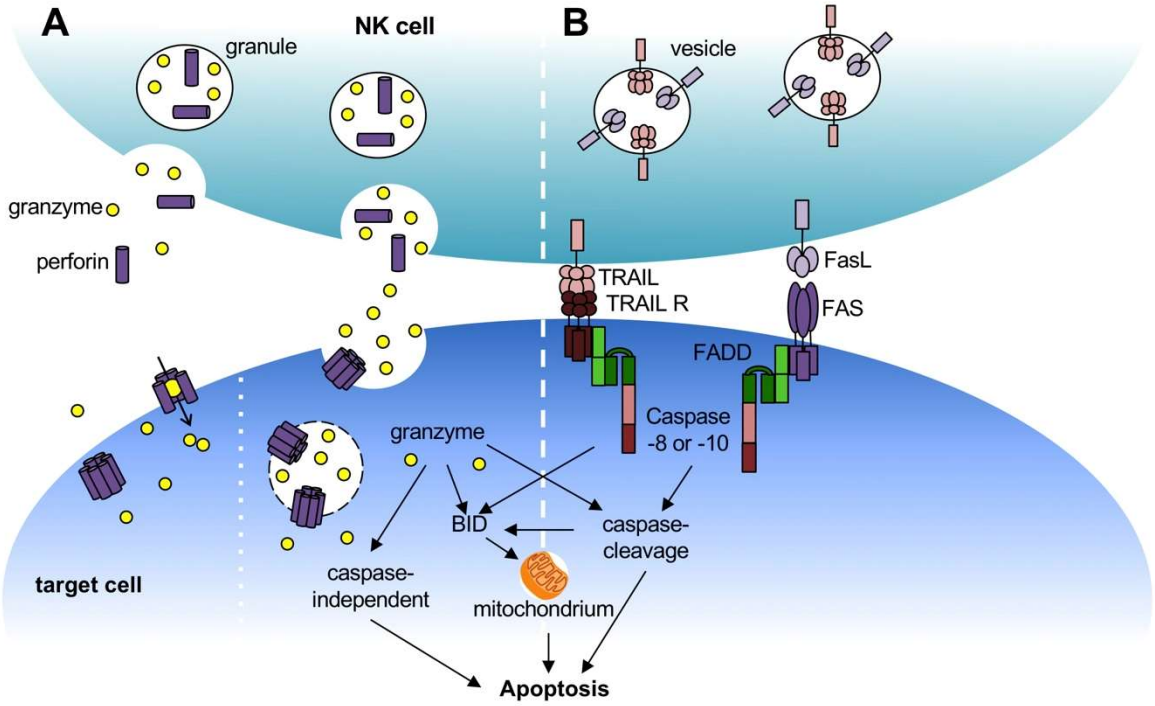

Figure 2: Two pathways to induce apoptosis. (A) Granule-mediated cytotoxicity is triggered by the release of lytic granules towards a locally attached target cell. Then, Grz can either enter the target cell by perforin-pores (left) or by endocytosis and perforin-assist escape from endosomes (right). In the next steps, Grzs can then induce caspase dependent or caspase-independent apoptosis. (B) Death receptor-mediated cytotoxicity is induced by surface expression of TRAIL or CD95L, which can trimerize and activated their cognate receptor. This results in caspase activation, caspase cascade, mitochondrial dysfunction, and apoptosis.

1.5 Production and storage of CD95L

The CD95L (FasL or Fas ligand) is a member of the TNF family of type II transmembrane proteins (40 kDa). CD95L consists of a cytoplasmic part (aa 1-81), which includes a casein kinase (CKI) substrate motive, a proline-rich domain (PRD) and a transmembrane region (aa 81-103). Activated NK and T cells can express CD95L on their cell surface (Suda et al., 1995, Montel et al., 1995), which contains of three putative sites for N-linked glycosylation (N184, N250 and N260). It is known that N-glycosylation acts as a protector for degradation and furthermore plays an important role in storage and stability (Lettau et al., 2008, Voss et al., 2008). Mutations in these glycosylation sites lead to reduced expression level of CD95L (Voss et al., 2008). The tight regulation of the expression of CD95L is essential to prevent non-specific killing. After synthesis in the ER, it is transported by the Golgi to the granules. For the sorting into the granules the PRD is necessary. The PRD interacts with SH3-domain containing proteins such as members of the Src family tyrosine kinases like Fgr, Src, Lyn, Lck, Hck, Abl as well as Src related kinases like Grb2, Gads, Nck (Lettau et al., 2011). In particular, Fgr binds to the PRD, resulting in a tyrosine phosphorylation (Y7, Y9 and Y13 within the N-terminus), which is required for trafficking of CD95L (Zuccato et al., 2007). Additionally, for the correct sorting a mono-ubiquitylation at the lysine residue K72, K73 flanking the PRD is essential (Zuccato et al., 2007). CD95L is stored in secretory granules/lysosomes and the expression on the surface depends on the degranulation. Even though the expression of CD95L has not been described in detail in NK cells, it is known for T cells that an acute stimulation through the TCR results in a biphasic surface expression of CD95L. The first surface expression of CD95L occurs within ten minutes (stored CD95L). Affected by a continuous stimulation of the T cell, *de novo* synthesized protein peaks after 2-4 h of stimulation (He and Ostergaard, 2007). The engagement of CD95 by CD95L results only in the induction of apoptosis if the CD95L forms homo-trimeric or even hexameric complexes (Holler et al., 2003). Membrane-bound CD95L contains a cleavage site (Ser126/127 in human) (Schneider et al., 1998) for matrix metalloproteinases (MMPs), MMP-7 or like A Distintegrin And Metalloproteinase domain, ADAM-10 in T cells (Kirkin et al., 2007). The protease-cleaved soluble complex (sCD95L, 26 kDa) allows mediation of both pro-apoptotic as well as anti-apoptotic effects and the local micromilieu seems to have an influence on this effect (Schneider et al., 1998, Chen et al., 1998).

1.6 Production and storage of TRAIL

TRAIL (Apo2L) is a type II transmembrane protein with homology to CD95L and TNF (Wiley et al., 1995). It is expressed on a variety of immune cells such as NK cells, T cells, dendritic cells and monocytes. The transcription of its mRNA can be induced by type-I-interferons (Almasan and Ashkenazi, 2003). On freshly isolated NK cells TRAIL is not generally detectable, while the stimulation by the cytokines IL-2 and/or IL-15 induces the potent TRAIL expression on human NK cells (Kayagaki et al., 1999b, Johnsen et al., 1999, Kashii et al., 1999). On the other side, TRAIL expression was also observed on peripheral blood T cells upon stimulation by IFN-α (Kayagaki et al., 1999a). TRAIL was discovered to have the ability to kill cancerous cells while sparing healthy cells, which has been shown to be also important for NK cell-mediated apoptosis (Walczak et al., 1999). Preformed TRAIL is stored in lysosomal-like compartments in human Jurkat T cell line or in human T cell blasts and co-localizes with CD107a/LAMP-1 (Monleon et al., 2001). However, it is still unknown how the secretory vesicle trafficking mechanism is regulated in terms of TRAIL and if it is stored in the same vesicles as CD95L. It is also uncertain, how target cell exposure can induce the surface expression of TRAIL within the synapse. Through the cytokine-induced expression, TRAIL is distributed on the whole surface and therefore not concentrated at any specific part of the NK cell surface. Hence, the question arises how this surface expression can induce direct target cell killing. TRAIL is a substrate of the metalloprotease MMP2 and it was shown in *in vitro* experiments with the recombinant protein that the proteases transform TRAIL to a soluble form of the ligand (24 kDa) (Secchiero et al., 2010). Soluble TRAIL still showed apoptotic activity, resulting in killing of target cells within immediate proximity of secreting NK cells. Furthermore, TRAIL is only bioactive as a homotrimer and a zinc ion associated to C230 is essential for proper folding, trimer association and biological activity (Walczak et al., 1999). It can bind to four cognate membrane receptors and one soluble receptor (von Karstedt et al., 2017). Binding of TRAIL to its receptors TRAIL-R1 (DR4, death receptors) and TRAIL-R2 (DR5) results in an intracellular formation of DISC, which finally leads to apoptosis. The induction of apoptosis is only possible because of the presence of the DD within their intracellular domain. In contrast, TRAIL-R3 (DcR1, decoy receptors, contain a truncated DD), TRAIL-R4 (DcR2, contain no DD, only a glycosyl-phosphatidyl inositol (GPI) anchor) and osteoprotegerin cannot induce apoptosis. These receptors as well as the soluble receptor mostly induce NF-*κ*B signaling, impeding the apoptotic pathway in cells (Chaudhary et al., 1997).

1.7 Serial killing of NK cells

While the mechanisms of cellular cytotoxicity for T cells and NK cells were well characterized over the last decades, the ability to kill multiple target cells in a serial fashion was initially only discovered for T cells (Zagury et al., 1975). The ability to initiate apoptosis in multiple target cells in a sequential manner is a mechanism called “serial killing”. Early studies revealed similar serial killing activity also for NK cells (Ullberg and Jondal, 1981). In light of this, it is noticeable that a high variability between individual NK cells regarding the number of killing events is described in different studies, and, remarkably, it was shown that the majority of killing events was performed by a minority of NK cells. To date it remains unclear what characteristics of NK cells are defining them as serial killers. Therefore, the aim of current NK cell research is to isolate this subpopulation of NK cells in order to characterize these cells. The killing of multiple target cells requires a strictly serial process, since the polarization of lytic granules is essential for efficient NK cell killing and to minimize bystander killing (Hsu et al., 2016). However, MTOC polarization is not mandatory for degranulation (Bertrand et al., 2013). Against this background, NK cells are supposed to form only one lytic synapse with one target cell at a time point. After a successful killing, the NK cell needs to detach from the killed target cell to establish a new cytotoxic contact with another target cell, so that the following killing process begins. However, the repetition of these killing events depends on the individual NK cell. Even though a recent study indicated that as little as two to four granules was sufficient for a successful target cell kill, the NK cells release 10 % of their granules in a single killing event. As a consequence, NK cells lose the majority of their GrzB and perforin content during serial killing, which may not be compensated completely by *de novo* biosynthesis or by re-cycling and re-internalization of these proteins (Li et al., 2010). Furthermore, it is described that NK cells lose activating receptors from their surface, which may result in attenuation of signaling pathways (Netter et al., 2017).

1.8 Fluorescence localization reporter

Although serial killing was discovered in early studies, it is unclear how the two distinct mechanisms to induce target cell death are coordinated and regulated during serial killing activity of NK cells. Both cytotoxic mechanisms are based on the activity of proteases, GrzB for granule-mediated apoptosis and Casp8 for the death receptor-mediated cytotoxicity. Recently, fluorescence localization reporters were developed to measure protease activity on a single cell level (Liesche et al., 2018) and were used in scope of this thesis. HeLa-CD48 target cells were stably transfected with a fluorescence localization reporter (NES-ELQTD-GFP-T2A-NES-VGPD-mCherry, T2A system). These vectors

encode two different fluorescent proteins (GFP or mCherry) fused to the localization domain NES (nuclear export signal) through a linker (cleavage site) containing the amino acid sequences VGPD or ELQTD. These sequences comply with the specific cleavage sites of substrates of GrzB (VGPD) or Casp8 (ELQTD), so that the reporter can be specifically cleaved by either GrzB or Casp8. Translation of this reporter sequence results in equal expression of two reporter proteins using the T2A self-cleaving peptide sequence, which allows a bicistronic transcription (**Fig. 3B**). The presence of the NES causes the localization of the reporter proteins in the cytosol of healthy living cells. Once the linker is cleaved by GrzB or Casp8 protein, the corresponding released fluorescence protein can enter the nucleus by passive diffusion, resulting in an increased fluorescence signal in the nucleus. An increased red fluorescence signal in the nucleus shows GrzB activity, whereas a green nucleus illustrates Casp8 activity (**Fig. 3A**). This allows the parallel quantification of GrzB and Casp8 activity in a single target cell induced by a single NK cell (Liesche et al., 2018).

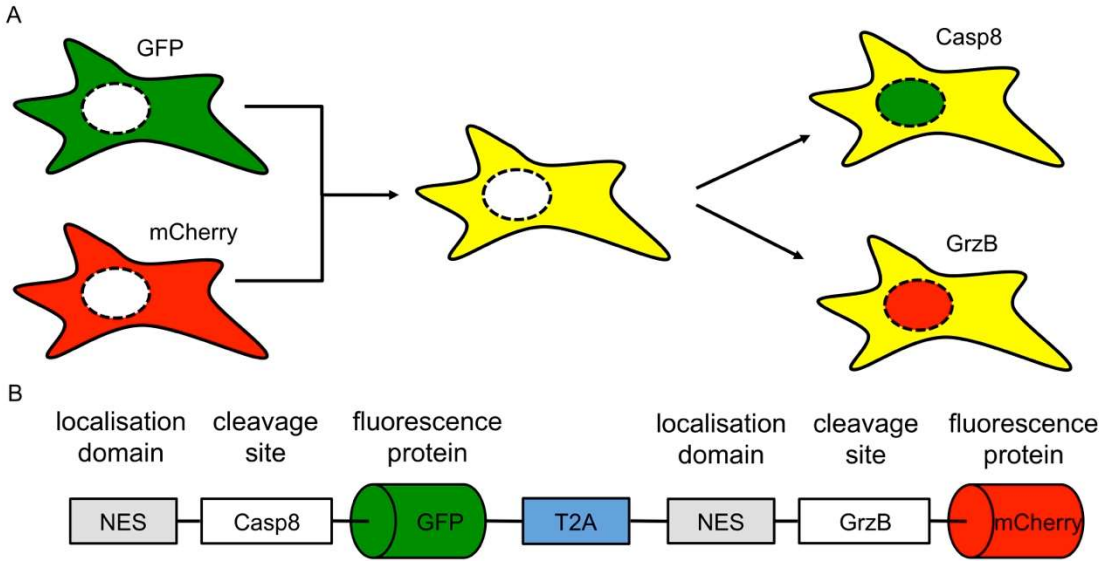

Figure 3: Schematic illustration of a fluorescence localization reporter (**3A**) and fluorescence distribution inside the cell when using a nuclear export signal (NES) as localization domain. In intact cells (**3A**, left) the fluorescent protein is almost exclusively localized in the cytoplasm. Upon cleavage of the reporter (**3A**, right), the fluorescent protein is equally distributed in the nucleus and cytoplasm. Schematic illustration of the mRNA of the reporter, which results in a translation into two proteins (**3B**) (Liesche et al., 2018).

2 Aim of the thesis

It is well established that NK cells possess two pathways to kill, however, their regulation during serial killing remains unclear. Open questions are if these pathways are simultaneously induced or separately and which pathway is important for efficient serial killing. Therefore the aim of the thesis was to investigate the regulation and the orchestrated interplay between both cell death pathways during NK cell serial killing. Understanding the regulation of this process is important for better insights into NK cell cytotoxicity.

To detect the two killing pathways we use fluorescent localization reporters to measure GrzB (granule-mediated pathway) and Casp8 (death receptor-mediated killing) activities simultaneously in single target cells upon their killing by NK cells. In particular, we want to track single NK cells during the serial killing in microchips via time lapse microscopy, to understand how serial killing operates. In order to find out what impact these two pathways have on serial killing, we will interfere either with the granule-mediated cytotoxicity or death receptor-mediated apoptosis using pharmacological or genetic approaches. By combining these methods, we are able to follow the killing series of every NK cell during the co-incubation with target cells that express our reporters and observe which killing pathway is used in every killing events. This will enable us to determine the contribution of each killing pathway to the serial killing activity of NK cells and provide novel targets for strategies to improve the cytotoxic activity of these important immune cells.

3 Material and Methods

3.1 Materials

3.1.1 Primary monoclonal antibodies

name (clone)	conjugate	source
CD107a (H4A3)	FITC	BioLegend, San Diego,California USA
CD107a (H4A3)	PE-Cy5	BioLegend, San Diego,California USA
CD45 (HI30)	AF700	BD, Franklin Lakes, New Jersey, USA
granzyme B (GB11)	Pacific Blue	BioLegend, San Diego,California USA
granzyme B (GB11)	AF647	BioLegend, San Diego,California USA
perforin (dG9)	FITC	BioLegend, San Diego,California USA
perforin (dG9)	BV510	BioLegend, San Diego,California USA
CD95L (NOK-1)	biotin	BioLegend, San Diego,California USA
TRAIL (RIK-2)	PE	BioLegend, San Diego,California USA
TRAIL-R1 (HS101)	biotin	Biomol, Hamburg, Germany
TRAIL-R2(HS201)	biotin	Biomol, Hamburg, Germany
CD95 (DX2)	PE-Cy7	BD, Franklin Lakes, New Jersey, USA
CD56 (MEM-188)	PE	BioLegend, San Diego,California US
perforin (Pf-344)	/	Mabtech, Hamburg, Germany
CD45 (HI30)	FITC	BD, Franklin Lakes, New Jersey, USA
CD56 (MEM-188)	PE-Cy5	BioLegend, San Diego,California USA
CD95L (D1N5E)	/	Cell Signaling Technology, MA, USA
CD3-ζ (6B10.2)	/	Santa Cruz Biotechnology, TX, USA
CD45 (RUO)	/	BD, Franklin Lakes, New Jersey, USA
IFN-γ (4S.B3)	FITC	BioLegend, San Diego,California US
XIAP (ab28151)	/	Abcam, Cambridge, UK
Bcl-2 (100/D5)	/	Thermo Fisher Scientific, Rockford, IL, USA
BID (3C5)	/	Thermo Fisher Scientific, Rockford, IL, USA
Serpinb9 (7D8)	/	Abcam, Cambridge, UK

3.1.2 Secondary labelling reagents

name	conjugate	source
Streptavidin	PE	Jackson ImmunoResearch, West Grove, PA, USA
Streptavidin	Cy5	
Goat anti Mouse IgG	HRPO	Cell Signaling Technology, MA, USA
Goat anti Rabbit IgG	HRPO	Jackson ImmunoResearch, West Grove, PA, USA

3.1.3 Buffers and Media

Media	
HeLa Medium	DMEM, 10 % FCS, 1 % penicillin/streptomycin
K562/CTL Medium	IMDM, 10 % FCS, 1 % penicillin/streptomycin
NK92 Medium	Alpha MEM, 12.5 % FCS, 12.5 % horse serum, 1 % P/S, 0.1 % 2-mercaptotethanol, 100 IU/ml IL-2
NK cell medium	IMDM,GlutaMAX™ ,10 % FCS, 1 % P/S
Buffer	
Triton X-100 lysis buffer	150 mM NaCl, 20 mM Tris-HCl,pH 7.4, 10 % Glyercol, 0.5 % Triton X-100, 2 mM EDTA, 10 mM NaF, 1 mM PMSF, 1 mM ortho-vanadate
PBS	137 mM NaCl, 8.1 mM Na_2HPO_4, 2.7 mM KCl, 1.5 mM KH_2PO_4
PBS-T	1x PBS, 0.05 % Tween 20
PBS-T/NaCl	1x PBS, 0.05 % Tween 20, 0.5M NaCl
Blocking buffer (WB)	1x PBS, 5 % non-fat dry milk powder
Transfer buffer (WB)	24 mM Tris, 129 mM Gylcin, 20 % MeOH
5x RSB	10 % SDS, 50 % Gylcerol, 25 % 2-Mercaptoethanol, 0.1 % Bromphenol Blue, 0.3125 Tris-HCL, pH= 6.8
4 % Paraformaldehyde (PFA)	PBS, 4 % PFA
FACS Buffer	PBS, 2 % FCS

3.1.4 Cells

name	Transfected with / Genom editing	Origin
Primary NK cells	untransfected	whole blood from healthy humans
Primary NK cells	perforin KO	whole blood from healthy humans
Primary NK cells	TRAIL KO	whole blood from healthy humans
HeLa	CD48	cervical cancer cell line
HeLa	CD48-NES-ELQTD-GFP-T2A-NES-VGPD-mCherry	cervical cancer cell line
HeLa	CD95 KO	cervical cancer cell line
HeLa	CD48-CD95 KO-NES-ELQTD-GFP-T2A-NES-VGPD-mCherry	cervical cancer cell line
K562	untransfected	CML
K562	mbIL15-41BBL	CML
NK92	untransfected	human NK cell line from malignant non-Hodgkin lymphoma
NK92	ADAP-KO	human NK cell line from malignant non-Hodgkin lymphoma
NK92	rescued ADAP-KO	human NK cell line from malignant non-Hodgkin lymphoma

3.1.5 Inhibitors

name (concentration)	source
Concanamycin A (50 nM)	Sigma-Aldrich, St. Louis, MO, US
Cycloheximide (10 mg/mL)	Sigma-Aldrich, St. Louis, MO, US
Brefeldin A (5 mg/mL)	Sigma-Aldrich, St. Louis, MO, US

3.1.6 Reagents

name	source
PBS	Thermo Fisher Scientific, Rockford, IL, USA
Lipofectamine 2000	Jackson ImmunoResearch, West Grove, PA, USA
Penicilin-Streptomycin	Thermo Fisher Scientific, Rockford, IL, USA
Fetal calf serum	Thermo Fisher Scientific, Rockford, IL, USA
Puromycin	Calbiochem/Merck Milipore, Billerica, MA, USA
G418 / Geneticin	Thermo Fisher Scientific, Rockford, IL, USA
Dimethyl sulfoxide (DMSO)	Avantor (J.T.Baker), Center Valley, PA, USA
IL-2	NIH Cytokine Repository, Frederick MD, USA
IL-15	Pan-Biotech, Aidenbach, Germany
IL-21	Miltenyi Biotech, Bergisch Gladbach, Germany
Paraformaldehyde (PFA)	Sigma-Aldrich, St. Louis, Missouri, USA
BD FACS Permeabilizing Solution 2	BD, Franklin Lakes, New Jersey, USA
EGTA	Sigma-Aldrich, St. Louis, Missouri, USA
IMDM	Thermo Fisher Scientific, Rockford, IL, US
RPMI1640	Thermo Fisher Scientific, Rockford, IL, US
Chromium-51	Hartmann Analytic, Braunschweig, Germany
Triton-X-100	Carl Roth, Karlsruhe, Germany
Zombie-NIR	
CellTracker™ Deep Red Dye	Thermo Fisher Scientific, Rockford, IL, US
LysoTracker™ Green DND-26	Thermo Fisher Scientific, Rockford, IL, US
SYTOX™ Blue Dead Cell Stain	Thermo Fisher Scientific, Rockford, IL, US
PBS	Thermo Fisher Scientific, Rockford, IL, USA
Lipofectamine 2000	Jackson ImmunoResearch, West Grove, PA, USA
Penicilin-Streptomycin	Thermo Fisher Scientific, Rockford, IL, USA
Fetal calf serum	Thermo Fisher Scientific, Rockford, IL, USA
Puromycin	Calbiochem/Merck Milipore, Billerica, MA, USA
G418 / Geneticin	Thermo Fisher Scientific, Rockford, IL, USA
Dimethyl sulfoxide (DMSO)	Avantor (J.T.Baker), Center Valley, PA, USA
IL-2	NIH Cytokine Repository, Frederick MD, USA
IL-15	Pan-Biotech, Aidenbach, Germany

name	source
IL-21	Miltenyi Biotech, Bergisch Gladbach, Germany
Paraformaldehyde (PFA)	Sigma-Aldrich, St. Louis, Missouri, USA
BD FACS Permeabilizing Solution 2	BD, Franklin Lakes, New Jersey, USA
EGTA	Sigma-Aldrich, St. Louis, Missouri, USA
IMDM	Thermo Fisher Scientific, Rockford, IL, US
RPMI1640	Thermo Fisher Scientific, Rockford, IL, US
Chromium-51	Hartmann Analytic, Braunschweig, Germany
Triton-X-100	Carl Roth, Karlsruhe, Germany
Zombie-NIR	BioLegend, San Diego, California, USA
CellTracker™ Deep Red Dye	Thermo Fisher Scientific, Rockford, IL, US
LysoTracker™ Green DND-26	Thermo Fisher Scientific, Rockford, IL, US
SYTOX™ Blue Dead Cell Stain	Thermo Fisher Scientific, Rockford, IL, US

3.1.7 Kits

name	source
Dynabeads untouched human NK kit	Invitrogen/LifeTechnologies, Darmstadt,Germany
SuperSignal™ West Dura Extended Duration Substrate	Thermo Fisher Scientific, Rockford, IL, USA
Luna® Universal qPCR Master Mix	NEB, Ipswich, MA, USA
Transcriptor First Strand cDNA Synthesis Kit	Roche, Basel, Switzerland

3.1.8 Software

name	source
FlowJo 10.5.3	*FlowJo*, LLC, Ashland ,USA
GraphPad PRISM v.8.1.1	GraphPad, La Jolla ,USA

3.1.9 Plasmids

Short name	Amino acid sequence
NES	MNLVDLQKKLEELELDEQQ, M=start codon
ELQTD	TGGG ELQTDGGGGGGR
VGPDF	SGGGVGPDFGRGGGG
mCherry	MVSKGEE...DELYK (Shaner et al., 2004)
mGFP	MVSKGEE...DELYK (Heim et al., 1995)
T2A	EGRGSLLTCGDVEENPGP

Fusion protein (reporter)	source
NES-ELQTD-mGFP-T2A-NES-VGPDF-mCherry	DNA was obtained by Dr. Clarissa Liesche/ Dr. Joël Beaudouin

3.1.10 sgRNA

target	sequence	source
perforin	CTGTGAAAATGCCCTACAGG	Invitrogen, Darmstadt, Germany
perforin	ATCCGCAACGACTGGAAGGT	Invitrogen, Darmstadt, Germany
CD95	GATCCAGATCTAACTTGGGG	Invitrogen, Darmstadt, Germany
CD95	TGCACTTGGTATTCTGGGTC	Invitrogen, Darmstadt, Germany
TRAIL	GGGTCAACCAGTCCTTGATG	Invitrogen, Darmstadt, Germany
TRAIL	GAAGATCACGATCAGCACGC	Invitrogen, Darmstadt, Germany
TRAIL	TACAAACACGGTGGTTGTCT	Invitrogen, Darmstadt, Germany
TRAIL	ATGGCTATGATGGAGGTCCA	Invitrogen, Darmstadt, Germany

3.1.11 Primer

Forward	Reverse	Gen
5'-GTCGGAGTCAACGGATTTGGT-3'	5'-CGTTCTCAGCCTTGACGGT-3'	GAPDH
5'-CCACTGAAAAAGATGAGTATGCCT-3'	5'-CCAATCCAAATGCGGCATCTTCA-3'	B2M
5'-ATTATGCTTCTCCCACCACA-3'	5'-CTAGGGAACCAATCACATGC-3'	IPO8
5'-CTGTTACTGCCAGGACCCAT-3'	5'-TCTGTCACTCTCCTCTTTCCAAT-3'	IFN-γ
5'-GTCTACCAGGCCAGATGCACAC-3'	5'-GGCATGGACCTTGAGTTGGA-3'	CD95L

3.2 Methods

3.2.1 Cell Biology

3.2.1.1 Cell culture of cell lines

Cell lines were grown in appropriate medium in cell culture flasks at 37 °C, 5 % CO_2. Sub culturing was performed three times per week. The stably transfected cells were treated with 1 µg/mL puromycin for CD48 selection and with 1 mg/mL G418 for the T2A system. Cells were frozen in FCS containing 10 % DMSO at -80 °C and for long-term stored at -170 °C in liquid nitrogen. Cell lines were thawed every three month.

3.2.1.2 Isolation of NK cells

Peripheral blood mononuclear cells (PBMC) were purified from the blood of healthy volunteers by density centrifugation over Lymphocyte Separation Medium (LSM). The gradient was set up starting with the LSM, which was covered by a layer of blood. After centrifugation (1025 x g for 25 min) the white interface containing the PBMC was harvested. Afterwards the NK cells were purified with the *Dynabeads® Untouched™ Human NK Cells Kit* (Thermo Fisher) according to the manufacturer's instructions. The isolated the NK cells had a purity of 90 % to 99 %, which was confirmed by flow cytometry (**4.1.4**).

3.2.1.3 NK cell culturing with feeder cells

To maintain the isolated NK cells in culture, the cells were resuspended in culture medium ($1x10^6$-$2x10^6$ cells/mL) in 96-U-well plates with 200 IU/mL recombinant human IL-2 and 100 ng/mL recombinant human IL-21, mixed with irradiated (30 gray) K562-mb15-41BBL feeder cells ($5x10^5$ -$1x10^6$ cells/mL). Cells were restimulated after 7 days with 100 IU/mL IL-2, mixed with irradiated K562-mb15-41BBL feeder cells ($5x10^5$ -$1x10^6$ cells/mL) and cells were subcultured at a 1:2 dilution after reaching a density of $3x10^6$ cells/mL. After 14 days in culture, 50 % of the medium was changed twice a week with 100 IU/mL IL-2 and 50 IU/mL IL-15.

3.2.1.4 Transfection

One day before transfection, $3.2x10^5$ HeLa cells were seeded in a 6-well plate. Cells were transfected with the respective amount of plasmid using Lipofectamine 2000 according to the manufacturer's manual (Tab 1.). To select stably transfected cells, the appropriate selection was applied the following day.

Tab. 1: Amount of Lipofectamine 2000 and DNA according to the manufacturer's manual.

Cell number	medium	Lipofectamine	DNA	Cell culture flask
$1.6x10^5$ HeLa	each 200 µL	8 µL	2 µg	Tissue culture plate (12 well)
$3.2x10^5$ HeLa	each 400 µL	16 µL	4 µg	6 well culture plate

3.2.1.5 Generation of stable transfected HeLa cells

To generate a stable transfected cell line, HeLa cells were transfected transiently as described in 3.2.1.4. After 3 days of maintaining the cells were sorted to enrich bright double positive cells (GFP^+RFP^+) with a *BD FACSJazz™.* Afterwards the cells were cultivated with 1 mg/ml G418. The cells were expanded and sorted again until the population was homogenously positive for the transfected reporter.

3.2.1.6 Knockout of perforin or TRAIL in primary human NK cells

To generate perforin or TRAIL deficient NK cells, the CRISPR-Cas9 System was used. $4x10^6$ NK cells per sample washed with 10 mL PBS and centrifuged with 100 x g, 10 min. Meanwhile 20 – 10 µg Cas9 nuclease and two or four different 3 – 1,5 nmol sgRNA were mixed and incubated at RT for 10 min. The cells were resuspended in the 100 µL P3 primary cell solution (AMAXA P3 primary cell 4D Nucleofector X Kit) containing Cas9 and two or four sgRNA, transferred to a cuvette and the program (DK-100) was applied (using the 4D Nucleofector X Kit 4D-Nucleofector™ X Unit). Immediately following the electroporation, 500 µL pre-warmed RPMI medium without supplements was added slowly and the cuvette was incubated for 10 min at 37 °C/5 % CO_2. The NK cells were transferred to a 96-U well plate with additional 500 µL NKpop medium. Additionally, as a control, NK cells were only incubated with P3 primary cell solution and treated the same way as described above. After seven days in culture the efficiency of the KO was tested by flow cytometry (3.2.2.1).

3.2.1.6 Generation of perforin KO clones

For the generation of perforin KO clones, two 96 U plates were prepared with 50 µL NKpop medium per well with 100 IU/ml IL-2, mixed with irradiated (30 Grey) $10x10^6$ K562-mb15-41BBL feeder cells. The KO NK cells were counted and the cells were diluted to final concentration of 1 cell in 100 µL per well when added into the prepared 96 U well plates. The plates were incubated at 37 °C in a humidified 5 % CO_2. After two days of incubation, 80 µL NKpop medium with 100 IU/mL fresh IL-2 was added. The incubation was continued for 5 days, then the cells were restimulated with 100 IU/ml IL-2 and $5x10^6$ irradiated (30 Grey) $5x10^5$ K562-mb15-41BBL feeder cells. Three times a week 80 µL/well was replaced with fresh NKpop medium with 100 IU/mL IL-2. After two weeks of

incubation, NK cell clones were picked from wells, which showed visible cell pellets and medium colour change to yellow (acidification of the medium). The selected clone from one well was subcultured in two wells of a fresh 96 U well plate and incubated. The clones were subcultured 1:2 after reaching a density of $3x10^6$ cells/mL. The purity of the perforin KO clones was determined by flow cytometry (3.2.2.1).

3.2.1.7 Knockout of CD95 in HeLa cells

To generate CD95 deficient HeLa cells, the CRISPR-Cas9 System was used. $4x10^6$ HeLa cells per sample were co-incubated with the respective amount of two different sgRNA and Cas9 (using the AMAXA SE cell solution 4D Nucleofector X Kit, program CN-114). HeLa cells were handled the same way as described above (3.2.1.6). Except for the variation of transferring the HeLa cells in a 12-well plate with 500 µL DMEM medium.

3.2.2 Flow cytometry staining/sorting and labelling of cells

3.2.2.1 Cell staining for flow cytometry

A minimum of $0.5x10^5$ cells was stained in 96 V-plates in 50 µL ice cold FACS buffer (PBS + 2 % FCS) containing a respective amount of antibody. The used antibodies were either directly conjugated to a fluorophore or unconjugated (ref. to chapter 3.1.1). Cells were incubated for 20 min on ice and washed afterwards. If necessary cells were stained with a secondary antibody. For intracellular staining, cells were fixed with 2 % PFA and permeabilized with BD FACS Permeabilizing Solution 2 buffer for 10 min at RT. After cell staining, the cells were resuspended in FACS buffer and examined with the BD LSR Fortessa™.

3.2.2.3 Sorting of degranulating NK cells

Target cells (HeLa-CD48) were cultivated overnight at a density of 3×10^5 cells/mL in DMEM containing 10 % FCS, 1 % penicillin/streptomycin in small tissue flask (T75). NK cells and HeLa cells (E:T; 1:2) were co-cultured for different time periods (1 h or 3 h) in the presence of an α-CD107a antibody at 37 °C in a humidified 5 % CO_2 incubator. The NK cells were collected as described in 3.2.3.1. Additionally the NK cells were stained with a NK cell marker CD56 and dead cell dye 7-AAD (3.2.2.1). To enrich the purity of degranulating NK cells ($CD56^+7\text{-}AAD^-$), FACS was performed and adjusted to Sort objective “Purify” and Sort mode “2.0 Drops Pure”. As a control, NK cells without co-incubation were only sorted by NK cell marker and dead cell dye.

3.2.2.4 Sorting regarding Lysotracker staining

$8x10^6$ NK cells were stained with Lysotracker Green DND-26 according to 3.2.2.2. For better sorting results Lysotracker was displayed on a linear axis. NK cells were sorted on the basis of Lysotracker^{dim} or Lysotracker^{bright}.

3.2.2.5 Labeling with Lysotracker

$8x10^6$ NK cells were stained with 50 nM LysoTracker Green DND-26 in 1 mL IMDM medium for 30 min (37 °C/5 % CO_2). Then the cells were washed with 1 mL IMDM medium and resuspended in 500 µL IMDM medium for sorting preparation.

3.2.2.6 Labeling NK92 with CellTracker DeepRed

1 $x10^6$ NK92 were stained with 0.2 µM CellTracker DeepRed in 1 mL PBS for 30 min (37 °C/5 % CO_2). After staining the cells were washed with NK92 medium and incubated for a time period of 10 min up to 30 min at 37 °C/5 % CO_2 in the incubator to allow unbound dye to leak out.

3.2.3 Functional assays

3.2.3.1 Degranulation assay in 6 well plates/ T75 flask

Target cells (HeLa-CD48) were cultivated overnight at a density of $3x10^5$ cells/per well (6 well-plate) of $4x10^6$ cells/flask (T75 tissue flask) well in DMEM. The next day NK cells were added to HeLa cells (E:T ; 1:3) and were co-cultured for four or two different time periods (1 h, 2 h, 3 h or 4 h (6-well plate), 1 h or 3 h (T75 flask)) in the presence of an α-CD107a antibody. To investigate the NK cells, the supernatant of each single well was transferred to 15 mL tubes and non adherent cells were washed off using 5 mL PBS. In order to detach more NK cells, 1.5 mL of dissociation buffer was added in the T75 tissue flask. After 5 min of incubation time, 3.5 mL PBS was added. Additional surface and intracellular stainings of these NK cells was carried out. Cells were analyzed with the BD LSR Fortessa™ immediately or the day after (stored in 150 µL FACS buffer + 2 % FA).

3.2.3.2 ^{51}Cr-release assay

For a ^{51}Cr-release assay, K562 or HeLa cells were used as target cells. $5x10^5$ cells were harvested and resuspended in 100 µL Dynal buffer. Cells were labeled with 100 µCi ^{51}Cr (3.7 MBq) for 1 h at 37 °C, washed twice with fresh CTL medium and resuspended at a density of $5x10^4$ cells/mL in CTL medium. 5000 target cells/well were used in all experiments. NK cells were harvested and serial dilutions (log2) starting with 1:1 (NK:target cell) were prepared in 100 µl CTL per well. Each condition was prepared in triplicates and incubated for 4 h at 37 °C. For a serial killing ^{51}Cr-release assay, the NK

cells were diluted from 0.6:1 to 0.075:1 (E:T) and incubated for 16 h at 37 °C with $5x10^3$ target cells/well. The maximum release was examined by incubation of target cells with 1 % Triton X-100. To determine the spontaneous release, target cells were incubated alone without effector cells, both parameters are needed to calculated the percent specific release ((experimental release - spontaneous release) / (maximum release - spontaneous release)) x 100.

3.2.4 Further Methods

3.2.4.1 SDS polyacrylamide gel eletrophoresis (SDS-PAGE)

After addition of 5x non-reducing sample buffer, samples were boiled for 5 min at 95 °C, cooled on ice and centrifuged for 1 min at 20000 x g. A maximal volume of 25 µL and 5 µL of Precision Plus Protein Standard (BioRad) were loaded on 12 % NuPage gels (Invitrogen) and separated for 1 h 15 min at 150 V in 1 x MOPS buffer.

3.2.4.2 Western Blot

Following SDS-PAGE, proteins were transferred to a polyvinylidene difluoride (PVDF) membrane (Millipore) (activated with methanol) for 1.5 h at 200 mA in western blot transfer buffer. After transfer, membranes were incubated for 1 h at room temperature in blocking buffer and washed for at least three times in PBST. Membranes were incubated with the primary antibody for 1 h at room temperature or overnight at 4°C. The membrane was washed at least three times with PBST/NaCl and incubated with the appropriate horseradish-peroxidase (HRPO)-conjugated secondary antibody (diluted 1:10.000 in blocking buffer) for 1 h at room temperature. After incubation with the secondary antibody, the membrane was extensively washed with PBST and developed using SuperSignal DURA kit and X-Ray films.

3.2.4.3 Recovery of GrzB and perforin in NK cells

Primary human NK cells were co-cultured with HeLa-CD48 cells (E:T=1) according to 3.2.3.2. Subsequently NK cells were sorted in $CD107a^+$ and $CD107a^-$. As a control, NK cells without target cell contact were sorted in the same manner (3.2.3.4). After sorting, the cells were subcultured with five different cytokine treatments. Cells were treated with IL-15,IL-2 or IL-21 alone or with the combinations IL-15/-2/-21 and IL-15/-2, (concentration in all treatments: 100 IU/mL IL-2, 50 IU/mL IL-15, 100 ng/mL IL-21). After 1 h, 24 h or 48 h the cells were stained intracellularly for GrzB and perforin (3.2.2.1) or used for a 4 h ^{51}Cr-release assay (3.2.4.1).

3.2.4.4 Microchip preparation

3.2.4.4.1 Cleaning and preparation of the microchip for microscopy

The microchip (**3, Fig. 4**) contain of 100 wells (10x10), which were centered in the middle of the microchip covering an area of 3.9 x 3.9 mm^2. 350 µm-wide wells are separated by four 100 µm thick walls. For cleaning the microchip, the chip was placed into water and degased. As following step the chip was treated with *FACS clean* for 15 min, followed by 30 min of sonication in water. Subsequently, the chip was placed into 70 % of aqueous ethanol for 60 min and afterwards into water for another 60 min. After cleaning, the chip was positioned in a clean petri dish for drying under sterile conditions.

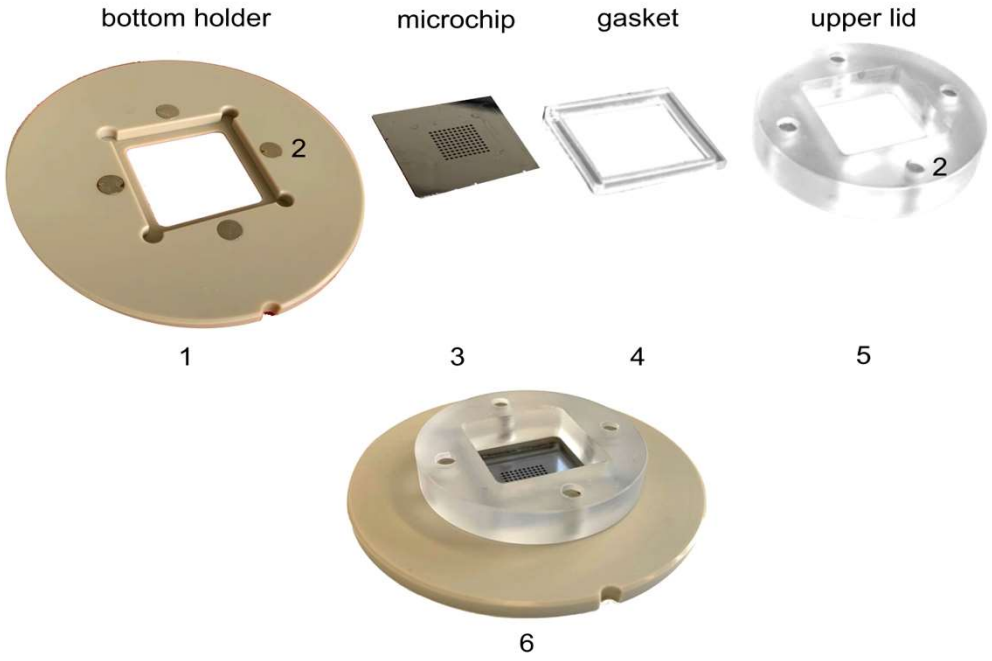

Figure 4: Microship components. (**1**) Bottom holder, (**2**) magnets, (**3**) microchip (10 x 10 wells), (**4**) PDMS gasket, (**5**) upper lid (plastic lid), (**6**) assembled microchip.

The gasket (**4, Fig.4**) is made of polydimethylsiloxane (PDMS) with a thickness of 1 mm. For cleaning of the PDMS gasket, it was placed into 100 % ethanol for 30 min, followed by two hours of incubation in water. The gasket was also positioned in a clean petri dish for drying. The bottom holder (**1, Fig. 4**) made of polyether ether ketone (PEEK) with a 0.2 mm thin flange. The upper lid (**5, Fig.4**) consists of the transparent material poly-methyl methacrylate (PMMA), which has a 20 x 20 mm hole in the center. During the experiment or before, this hole allows the addition of cells or other substances into the chip. For cleaning the bottom holder and the top lid, both parts were put into 100 % ethanol for

15 min. Subsequently, the holder and the lid were placed into water for 2 h. Finally, both parts were dried under sterile conditions.

3.2.4.4.2 Priming the microchip for experiments

For the priming of the microchip, a gasket (**4, Fig.4**) was placed on top of the microchip (**3, Fig.4**) and both parts were positioned between the bottom holder (**1, Fig.4**) and the upper lid (**5, Fig.4)** to prevent fluid leakage. For stabilization the holder and the lid contain magnets (**2, Fig.4**) to pinch the microchip and the gasket between the holder and the lid. The whole construct (**6, Fig.4**) was prepared for seeding the cells.

3.2.4.5 Seeding cells

3.2.4.5.1 Seeding cells into microchip

Before the cells were seeded into the microchip, the chip was covered with distilled water and degased to allow liquid to enter all wells. The water was replaced with 800 µL CTL medium. This replacement process was repeated with 800 µL CTL medium for five times to remove most of the water. The medium filled microchip was equilibrated for 1 h at 37 °C in a humidified atmosphere with 5 % CO_2. After 1 h equilibration the medium in the microchip was reduced to a volume of 400 µL. The cell seeding process in the microchip was performed by adding 1x 10^6 K562 or HeLa on top of the medium. Allowing the cells to sediment into the wells for minimum of 10 min (K562) or overnight (HeLa). The sedimentation process was tracked by Zeiss Primovert microscope (HeLa) or Zeiss ApoTome System (K562) and was terminated when 30-40 HeLa cells or 60-100 K562 cells settled in each well by replacing the supernatant containing the cells with fresh CTL medium. Afterwards, stained 1x10^6 /mL NK92 (CellTracker Deep Red, according to 3.2.2.3) cells or 1x10^6 primary NK cells were added to the microchip, resulting in a stochastic distribution of approximately 5-12 NK92/NK cells and 60-100 target cells per microwell. Supplements in the medium were IL-2 (100 IU/mL) and 1 μM dead cell dye SYTOX Blue added, in case of NK92.

3.2.4.5.2 Seeding cells into 8-well ibidi chambers

Before seeding the cells into the ibidi chamber, 100 µL CTL medium was added in each well. 3x10^4 HeLa CD48 cells stable expressed NES-ELQTD-GFP-T2A-NES-VGPD-mCherry were seeded into each 8 wells.

3.2.4.6 Microchip microscopy

HeLa CD48 cells or HeLa-CD48-CD95 KO with stable NES-ELQTD-GFP-T2A-NES-VGPD-mCherry expression were seeded onto microchips as described in 3.2.4.5.1. After overnight incubation, the NK cells (E:T=5) were added, and recorded for 13 h to 16 h at an

interval of 2-3 min. Images were obtained in three different microscopes (Zeiss LSM 880, Leica Microsystems CMS, ApoTome System) as described hereafter.

3.2.4.6.1 TCS SP5 confocal laser scanning microscope

Time-lapse live-cell images were performed by Hanna van Ooijen (KTH, Sweden) using a TCS SP5 confocal laser scanning microscope (Leica Microsystems CMS) with a 63x/1.4 OIL, HCX PL APO CS objective equipped with incubator chamber and environmental control system (37 °C, in a humidified atmosphere with 5 % CO_2). Fluorescence of mGFP and mCherry was acquired in line sequential mode. To visualize mCherry the helium–neon laser (561 nm), detection range 600–660 nm was used. For GFP the argon laser (488 nm), detection range 500–560 nm was used. All confocal images were analyzed using ImageJ software (Schneider et al., 2012).

3.2.4.6.2 Zeiss LSM 880 microscope

Time-lapse live-cell images were also performed with a LSM 880 laser scanning confocal microscope (Zeiss) with a 40x/1.1 W LD C-Aprochromat, equipped with incubator chamber and environmental control system (37 °C, in a humidified atmosphere with 5 % CO_2). Fluorescence of mGFP and mCherry was acquired in line sequential mode. To visualize mCherry the Argon Diode 405-30 in the laser line 561 nm was used, for GFP the DPSS 561-10 laser, in the laser line 488 with a beam splitter MBS 488/561 was used. Images were captured at a rate of one z-stack every 3 min and z-slices were spaced by 1 µm. Images were aquired at frame size of 512 x 512 pixels and a bit depth of 8 bits. All confocal images were analyzed using ImageJ software (Schneider et al., 2012).

3.2.4.6.3 Zeiss ApoTome microscope with HeLa or K562

Time-lapse microscopy was also performed with ApoTome System with Axio Observer 7 microscope (Zeiss) equipped with a 20×/0.8 Plan-Apochromat objective and an incubation chamber with environmental control (37 °C, 5% CO_2, humidity device PM S1). For the imaging of HeLa target cells fluorescence of mCherry and GFP was acquired in line sequential mode. mCherry was excited using the Colibri 7 LED-module 561 (filter set 64 HE LED) and for GFP the LED-module 488 (filter set 38 HE LED) and brightfield was acquired using the TL LED module. Images were acquired every 3 min for 16 h using an Axiocam 506 mono camera. For the live-cell imaging of K562 target cells, SYTOX Blue was excited using the Colibri 7 LED-module 475 (filter set 38 HE LED) and CellTracker Deep Red 555 (filter set 64 HE LED) and brightfield was acquired using the TL LED module. Images were acquired every 3 min for 16 h using an Axiocam 506 mono camera.

3.2.4.7 Well chamber microscopy

3.2.4.7.1 EVOS FL Auto microscopy

Time-lapse fluorescence microscopy were performed using an EVOS FL Auto Imaging System (ThermoFisher Scientific) equipped with a 60x/1.42 OIL in µ-Slide 8 Well ibidi slides, Plan Apochromat objective and an on stage incubator (37°C, in a humidified atmosphere with 5 % CO_2) and different EVOS LED light cubes (GFP, RFP) or with transmitted light. The resolution was 1280 x 960 pixels and images were recorded in 16-bit. Images were taken at a 2 min interval for 6 h – 8 h for each channel.

3.2.5 Molecular Biology

3.2.5.1 RNA Isolation

RNA was isolated from 1x10^6 primary human NK cells, which were co-cultured with 5x10^5 HeLa-CD48 cells for four different time periods (1 h, 2 h, 3 h or 4 h) in a 6 well plate, according to 3.2.3.1, but without α-CD107a. The RNA isolation method of *CHOMCZYNSKI* and *SACCHI* was used.

3.2.5.2 Reverse Transcription

1 ug RNA was transcribed to cDNA using the *Transcriptor First Strand cDNA Synthesis Kit* according to the manufacturer's manual.

3.2.5.3 Quantitative PCR (qPCR)

The qPCR was performed via the *Luna® Universal qPCR Master Mix* (NEB) according to the manufacturer's manual using the *CFX96 Touch Real-Time PCR Detection System* (*Bio-Rad*) with the correspoding software (BioRad CFX Manager™ V3.1).

3.2.6 Image Analysis and statistics

For the analysis of the fluorescence localization reporter experiments ImageJ (1.53d) was used (Schneider et al., 2012). Firstly, all time lapse images from one channel were combined in one stack (GFP, mCherry, bright field). Afterwards, the stacks were overlayed in order to generate one merge stack. For the measurement of the protease activity, three specific Regions of Interest (ROI) have been defined. The first ROI was placed in the background, to subtract the background of each image. The second ROI is set in the nucleus and the last ROI is placed in the cytosol. To examine the extent of substrate cleavage, the nuclear fluorescence signal intensity ($I_{nucleus}(t)$) is normalized to the cytosolic one ($I_{cytosol}(t)$).

In order to correct for potential photobleaching over the whole time, this normalization was performed for each time point (t):

$$I_{nucleus}^{normalized}(t) = \frac{I_{nucleus}(t)}{I_{cytosol}(t)}.$$

For the microchip experiments as well as the 8 well ibidi experiments, normalization was applied using the cytosolic signal of the target cells of three sequential time points before a NK cell attached, resulting in the normalized intensity $I_{nucle}^{normalized}(t)$. This kind of normalization is reasonable because only minor photobleaching was observed and was considered to be negligible.

ANOVA analysis and unpaired, two-tailed *t* tests were performed using GraphPad Prism software. When variances between groups differed significantly, the test was applied with Welch's correction. Data groups were considered not significantly different when $P > 0.05$. Otherwise they were considered significantly different with ****, $P \leq 0.0001$; ***, $P \leq 0.001$; **, $P \leq 0.01$; or *, $P \leq 0.05$.

4 Results

4.1 Establishment of the microscopic analysis of the target cell death

4.1.1. Measurement of reporter activity

NK cells are key players in efficiently recognizing and eliminating virus-infected and tumor cells. Individual NK cells can eliminate multiple target cells in a sequential manner in a process named serial killing. There are two major pathways to induce apoptosis, by releasing the content of the cytotoxic granules containing the serine protease granzyme B (GrzB) and the pore-forming protein perforin. On the other hand, apoptosis can be induced by the engagement of death receptors, which initiate caspase cascades. The complex interplay between both cell death processes remains poorly understood, therefore, investigating the regulation of this process is important for a better understanding of NK cell biology.

Therefore, we established fluorescence localization reporters in order to measure protease activity inside single cells. These reporters are fusion-proteins that consist of fluorescence proteins (GFP or mCherry) fused to the localization domain NES (nuclear export signal) through a linker that can be specifically cleaved by either GrzB or Casp8. The presence of the NES causes the constant export of the reporter proteins from the nucleus to the cytosol of healthy living cells. Once the linker is cleaved, the released small fluorescence protein distributes evenly in the cytosol and the nucleus by passive diffusion, resulting in an increased fluorescence signal in the nucleus. This process of increased signal in the nucleus can be visualized by microscopy. In contrast to other studies (Vrazo et al., 2015, Kanno et al., 2007, Li et al., 2014), (Packard et al., 2007), these reporters allow the parallel assessment of two different protease activities at once in single target cell upon NK cell-mediated killing.

We used live cell imaging of the fluorescent localization reporters to detect GrzB and Casp8 activities in single target cells upon their killing by NK cells (**Fig. 5**). Primary human NK cells were co-cultured with HeLa target cells expressing the Casp8 and GrzB reporters. These HeLa target cells also expressed CD48, the ligand for the activating NK cell receptor 2B4 (CD244), which increased sensitivity regarding killing by NK cells.

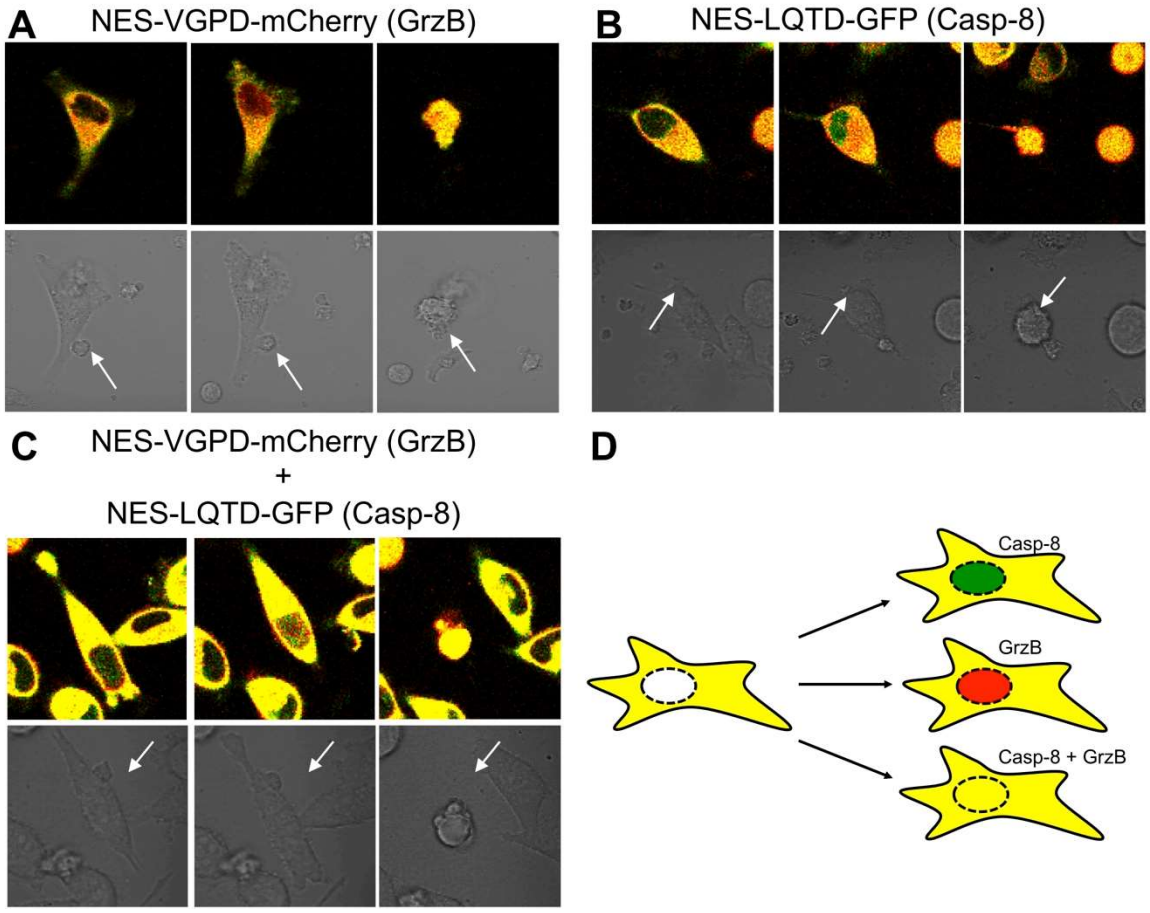

Figure 5: GrzB and Casp8 activity in target cells killed upon co-culture with primary human NK cells. Killing activity of primary human NK cells was determined against HeLa-CD48 stably expressing NES-LQTD-GFP-T2A-NES-VGPD-mCherry in a 16 h experiment. Three different HeLa cells reported different protease activities due to NK cell-induced cell death. NK cells are indicated with an arrowhead in the brightfield images (lower row) with the corresponding merged picture of the green and red fluorescence (upper row). (**A**) Example for GrzB activity, (**B**) example for Casp8 activity, (**C**) example for a similar activity of GrzB and Casp8. (**D**) Schematic illustration of the overlay of fluorescence localisation reporters in an intact HeLa cell (left), cleavage of the reporter corresponding in a red coloured nucleus (GrzB activity), in a green coloured nucleus (Casp8 activity) or in a yellow coloured nucleus (GrzB+Casp8 activity). Experiments were performed in EVOS FL Auto microscope.

Figure 5 depicts exemplarily three different HeLa cells that show reporter activity caused by the different proteases after NK cell-induced cell death. In the first image of every row, the three different cells are shown at the time point of the NK cell attachment. In the overlay of the GFP and mCherry channels, yellow fluorescence signal could be observed in the cytosol resulting from the merged green and red fluorescence of both reporters, whereas no fluorescence was visible in the nucleus. Subsequently, a change in the fluorescence distribution was induced. Because of the protease-specific cleavage site of the reporters, a red fluorescence signal in the nucleus is directly related to GrzB activity, whereas a green fluorescence signal in the nucleus is associated with Casp8 activity. When GrzB as well as Casp8 are active, a yellow fluorescence signal can be observed in the nucleus.

The last image in every row shows the time of death of each target cell resulting in cell shrinkage and formation of apoptotic bodies. At this time, nucleus and cytosol cannot be distinguished anymore.

4.1.2 Determination of the time of cell death

The first objective was to examine if the time of cell death observed with the fluorescence localisation reporters is comparable to conventional methods. Therefore, we used SYTOX Blue as an indicator of dead cells. This dead cell dye can only enter the cells once the membrane became permeable. As SYTOX Blue has positive charges at physiological pH, this may partially inhibit its entry into the intact cell but once inside the cell it shows a strong binding to DNA or RNA. For this purpose, we wanted to verify whether the starting point of cleavage of both reporters after the induction of apoptosis is comparable to the apoptosis induction reported by the dead cell dye SYTOX Blue. (**Fig. 6**)

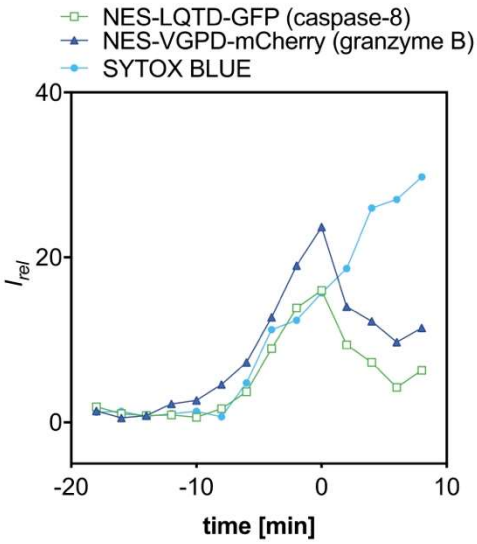

Figure 6: Examination of the time of death. Primary human NK cells were co-cultured with HeLa-CD48 stably expressing NES-LQTD-GFP-T2A-NES-VGPD-mCherry in a 6 h experiment in the presence of SYTOX BLUE as a dead cell marker. One example for a single cell with more GrzB-reporter cleavage compared to Casp8 cleavage is shown. The relative intensity of reporter fluorescence of GrzB, Casp8 and fluorescence of SYTOX Blue (I_{rel}) was plotted over time (min). Experiments were performed using an EVOS FL Auto microscope.

The measurement of the normalized intensity is calculated by dividing the measured signal in the nucleus by the signal measured in the cytosol. As outlined in figure 6, before the induction of apoptosis the two reporters to detect GrzB and Casp8 are not cleaved, which is shown as flattened curves (-20 min until -10 min). At the time point -10 min the GrzB and Casp8 fluorescence signal started to increase, which represented the start of the cleavage of the two reporters (NES-LQTD-GFP (Casp8) and NES-VGPD-mCherry

(GrzB)). The increased fluorescence was detected from the appearance of fluorescence inside the nucleus (ref to **Fig. 5**). The processes of apoptosis began. About 10 min later, the nucleus and cytosol collapsed (data not shown), which is defined as cell death and set to time point 0. At this time point, the maximum intensity of both fluorescence reporters is reached. After the time of death, it seems that the intensities of the fluorescence localization reporters decreased. This artefact was observed because of the cell shrinking, which made it impossible to distinguish between the nucleus and the cytosol. In further analysis, we used the defined cell death time point 0 as the endpoint of all performed analysis and showed the cleavage of GrzB and Casp8 before the cell death.

Additionally, SYTOX Blue was present in the experiment. SYTOX Blue was not able to bind to the DNA before the induction of apoptosis, which is seen in the flattened curve (-20 min until -10 min). At time point -10 min, the dye was able to enter the nucleus due to loss of membrane integrity. The dye bound to the DNA/RNA, which resulted in an increased SYTOX Blue staining. At the defined cell death point 0 the intensity of the dead cell dye increased further, as SYTOX BLUE is still able to bind to the easily accessible DNA/RNA after the collapse of the nucleus and cytosol. The parallel increase of the intensity of the dead cell dye and of both reporters (GrzB and Casp8) shows that the time of death observed with the reporters correlates to conventional measurements of cell death.

4.1.3 Specific induction of apoptosis by the death receptor

We investigated if GrzB and Casp8 activity can be distinguished within the same cell using the fluorescence localization reporters, because it was described that Casp8 can get activated through cleavage by GrzB (Medema et al., 1997). To address this issue, we tried to induce apoptosis in the target via one mechanism only and measured both reporter proteins in parallel. Soluble cross-linked CD95L (IZsCD95L) was used to specifically trigger apoptosis via the death receptor CD95 and EGTA to inhibit the killing via perforin and granzymes.

To investigate if Casp8 and GrB activity can be distinguished within the same cell, primary human NK cells were co-cultured with HeLa cells stably expressing the Casp8 and GrzB reporters in presence or absence of EGTA (**Fig. 7**). Untreated NK cells showed mainly GrzB activity in their initial killing event (35 % reporter cleavage, **Fig 7B**). EGTA binds Ca^{2+}, which leads to an inhibition of calcium-dependent perforin polymerization. Upon addition of EGTA to the cells, we observed efficient cleavage of Casp8 in the initial kill (**Fig. 7A**). In the same cell, the GrzB activity was low with up to 12 % reporter cleavage.

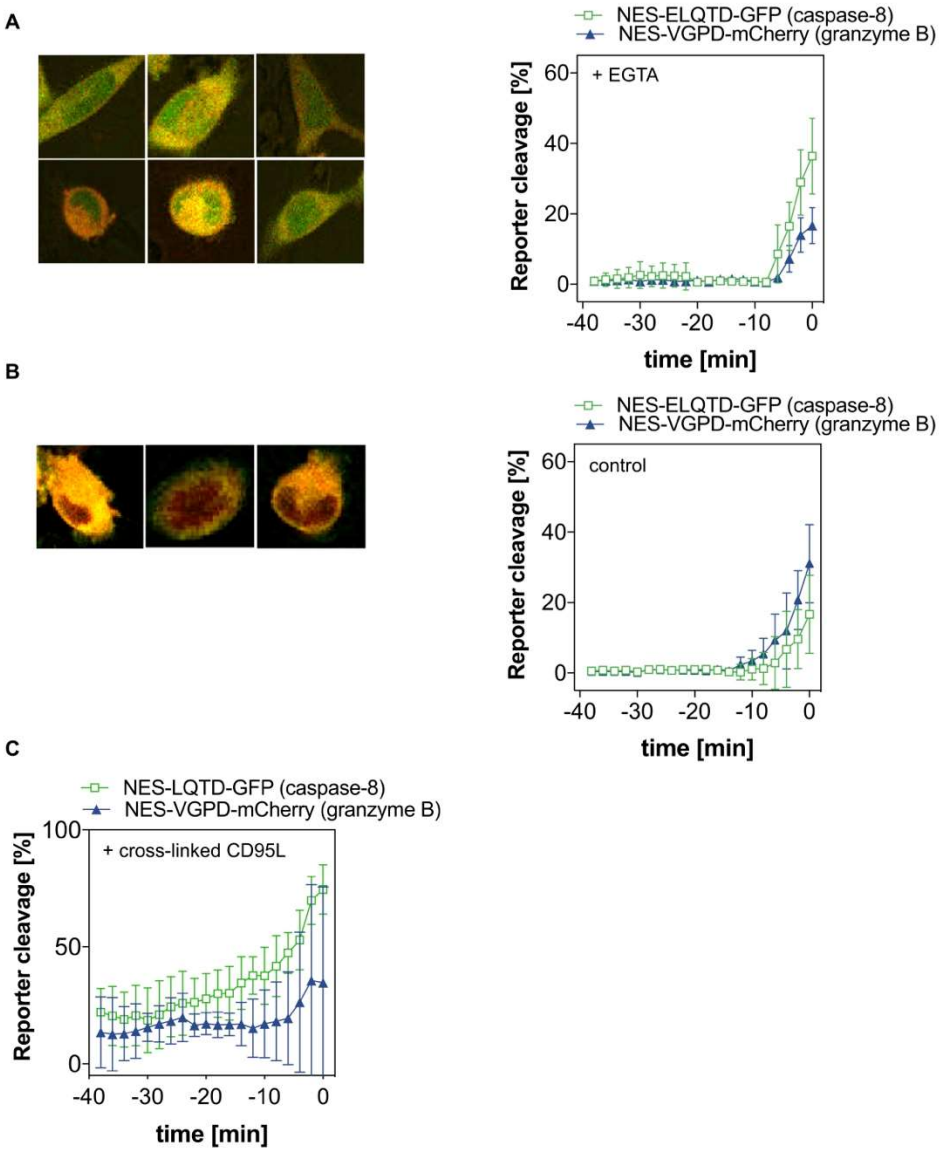

Figure 7: Specific induction of apoptosis by the death receptor by CD95L or calcium depletion with EGTA. HeLa-CD48 cells stably expressing NES-ELQTD-GFP-T2A-NES-VGPD-mCherry were incubated with activated primary human NK cells in the presence (**A**), the absense (**B**) of 0.5 mM EGTA or in the presence of cross-linked CD95L without NK cells (**C**). The average mean with standard deviation of reporter cleavage is plotted over time and examples of dying cells with GrzB activity (red nucleus) and Casp8 activity (green nucleus) are shown. Experiments were performed using an EVOS FL Auto microscope.

Another experiment to analyze if Casp8 and GrzB activity could be clearly distinguished within the same cell was performed using soluble CD95L. Soluble CD95L is able to bind CD95 but cannot efficiently induce apoptotic signaling. To induce apoptosis by the soluble CD95L, crosslinking of the ligand is needed. The soluble cross-linked trimerized CD95L binds to CD95, which leads to clustering of CD95 resulting in Casp8 dependent apoptosis (80 % reporter cleavage). By the addition of cross-linked CD95L in the absence of NK cells, a predominate increase of Casp8 activity was observed. In the same cell, the GrzB reporter was cleaved only up to 22 %. Several other controls had been included in recent

publications (Liesche et al., 2018). In all performed experiments the death of the cell leads to an increase of both reporters in the nucleus, but when the cell is killed via CD95/death receptors the Casp8 reporter increases first and higher. This leads to the conclusion that the two reporter proteins can be measured in parallel to distinguish the mechanisms through which the cell was killed.

4.2 Serial killing in microchips

In our first experiments (**Fig. 5**, **Fig. 6** and **Fig. 7**) we used the commercially available 8-well ibidi microscopy slides. With this slides it was possible to create time lapse videos to measure the protease activity in one HeLa cell induced by one NK cell, but the NK cells were able to leave or enter the field of view at any time during the experiment. Therefore, it was not possible to follow individual NK cells over a long period of time in those standard microscopy slides. In order to solve this problem, the following experiments were performed using a microchip that enables long-term tracking of individual NK cells (Guldevall et al., 2016, Frisk et al., 2011). For these experiments up to 100 target cells were seeded into the microchip and co-cultured with 2-10 NK cells. The size of the used microchips was 350-μm-wide, so one well could be observed within one imaging field of view. This allowed the measurement of the killing sequence of all NK cells in individual microwells because each cell could be tracked over the whole experiment. These microchip experiments were performed in collaboration with the laboratory of Björn Önfelt (KTH, Sweden) (**Fig. 8**).

Figure 8A gives an example for a single NK cell that killed five targets in succession. The first four killing events showed a predominant GrzB-induced cell death, the last killing event was mostly Casp8 activity-mediated. It was noticeable that the time span between NK cell commitment (time point when NK cell signaling arose and the killing process began) until target cell death was significantly shorter for GrzB-mediated killing events in comparison to Casp8-mediated killing. During our cooperation, Hanna van Ooijen could analyze 270 killing events of NK cells from three different healthy donors. In nearly all cases the first killing event was indicated by strong GrzB activity (**Fig. 8B**). Further in almost all cases the observed NK cells made no non-cytotoxic interaction before their first kill. While for 56 NK cells only one killing event was observable, 214 NK cells showed a second killing event in the course of the experiment. During the second kill a small part of target cells exhibited a dominant Casp8 activity. In the following series of cell cytotoxic contacts, the proportion of cells mediating apoptosis via Casp8 activity was increased in comparison to a decreasing number of cells with dominant GrzB activity. Finally, the sixth

kill was dominated by Casp8 activity. Remarkably, after the sixth killing event another cytotoxic contact was rarely observed, however, further target cell contacts of NK cells occurred that were non-cytotoxic. This aspect indicated that the observation time did not limit the number of the observed killing events. Furthermore, the total amount of NK cells tracked was 347 of which only 270 NK cells showed any cytotoxic activity. Out of this fraction a small part of 15 NK cells were able to kill six targets in succession. Since the utilized NK cells were activated via the stimulation with IL-2, the experiments were repeated with non-activated freshly isolated NK cells from three healthy donors. These experiments were performed to exclude that the interferences of the *in vitro* activation lead to an influence of NK cells. In these experiments up to 4 target cell killings were observed by one NK cells in a serial fashion. Because of the lower cytotoxicity of these NK cells, a lower number of targets killed was expected. Nonetheless, the same protease activity trend was observable. The first killing event was mediated mostly by GrzB activity, whereas the last target was eliminated via Casp8 activity. This suggests that the NK cells used at first GrzB-mediated killing and then switch to the Casp8-mediated killing in a serial fashion, independently of whether the NK cells were activated or freshly isolated.

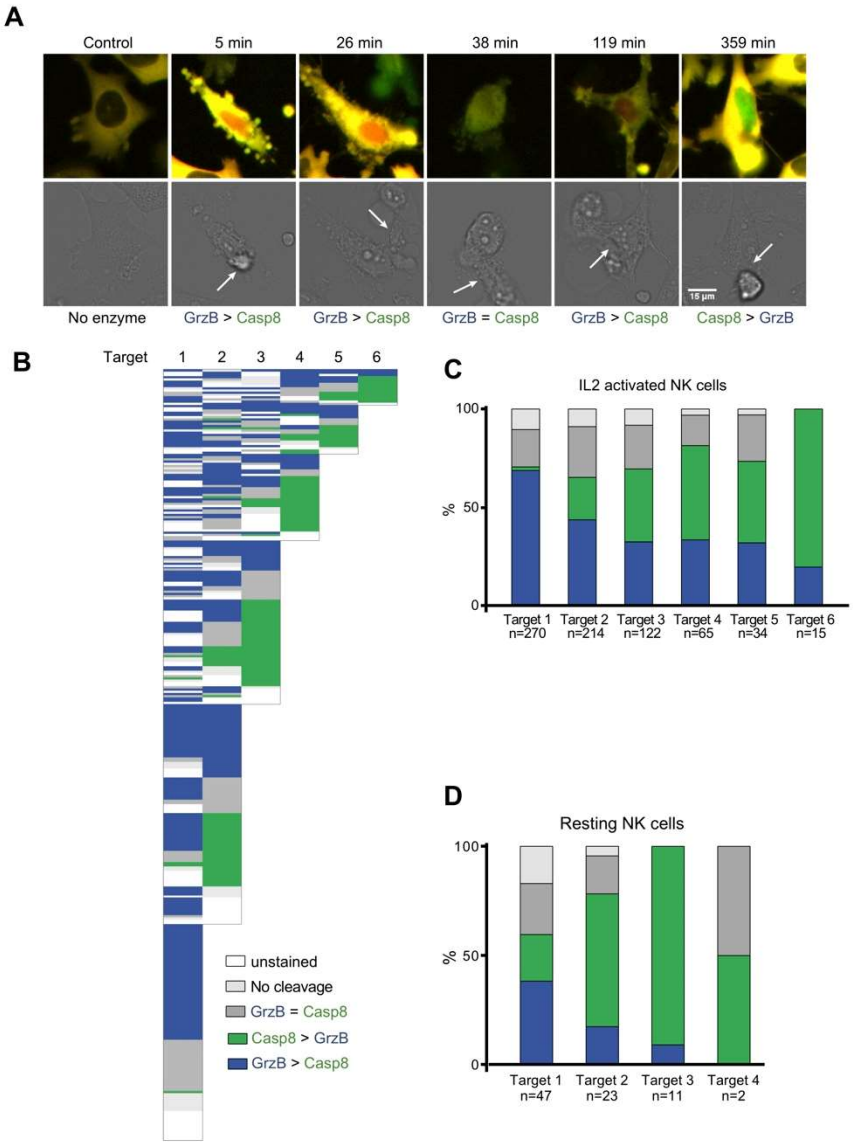

Figure 8 NK cells initially kill via GrzB and switch afterwards to the Casp8-mediated killing. Serial killing activity of primary human NK cells was analyzed against HeLa-CD48 cells stably expressing NES-ELQTD-GFP-T2A-NES-VGPD-mCherry. IL-2-treated NK cells from three donors were used in three independent experiments (**A-C**), additionally resting, fresh isolated NK cells from three different donors were used in three independent experiments (**D**). A total number of 347 IL-2 activated and 63 resting NK cells was tracked over 15-17 h. Each killing event of each NK cell was labeled with regard to GrzB (blue) and Casp8 (green) activity. (**A**) One Example for five sequential killing events by one serial killer NK cell with according enzymatic activity (red nuclear signal indicated GrzB activity and green nuclear signal declared Casp8 activity. The NK cell was visualized via brightfield (lower row) and marked with white arrowheads. (**B**) The activity for each NK cell is shown in a row with sequential killing events as columns, GrzB activity is display in blue, Casp8 acitivity is shown in green, equal activity of GrzB and Casp8 is displayed in dark grey, whereas target cells, which do not express the reporter, are presented in white and no cleavage of the reporter is exhibited (no reliable measurement possible) in light grey. (**C-D**) Target cell death was defined in terms of their respective number in the corresponding NK cell killing sequence. Both histograms illustrated the proportion of target cell deaths visualizing the three different reporter activities (blue: GrzB > Casp8, green: Casp8 > GrzB, grey: GrzB = Casp8, white: HeLa target cells, which do not express NES-ELQTD-GFP-T2A-NES-VGPD-mCherr, named unstained) or no cleavage (light grey). Experiments were performed using a TCSSP5 confocal laser scanning microscope.

Furthermore, the initial granule-mediated killing event was more likely associated with non-apoptotic phenotype, which showed more of a necrotic, cell rupture phenotype. In contrast, the last Casp8-mediated killing event was more likely of the apoptotic phenotype. These phenotypes were seen in all performed experiments but only systematically analyzed from our collaboration partner (Prager et al., 2019).

To exclude that heterogeneities within the target cells affect the mechanisms of apoptosis induction, the levels of different prominent proteins playing important roles during apoptosis were measured (**Fig. 9**).

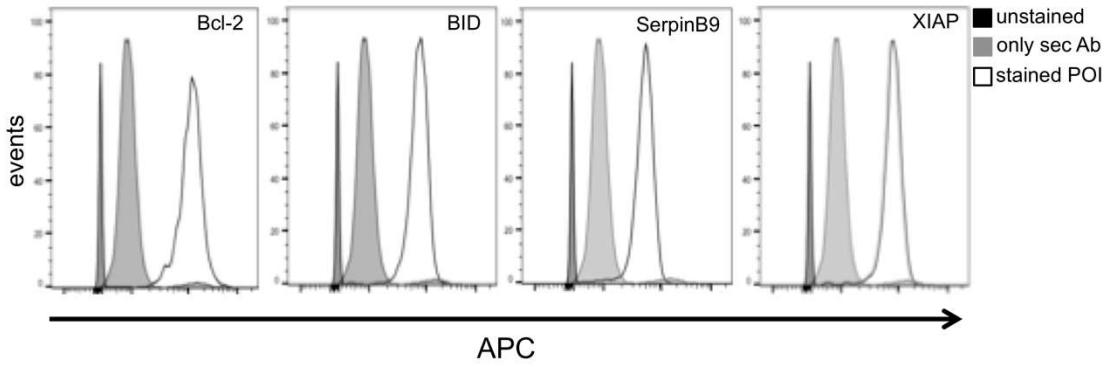

Figure 9: Homogenous expression of Bcl-2, Bid, Serpin B9 and XIAP in HeLa target cells. HeLa-CD48 cells stably expressing NES-ELQTD-GFP-T2A-NES-VGPD-mCherry were fixed with 4 % PFA, permeabilized and stained with secondary antibody only (only sec Ab, grey histogram), with antibodies specific for the indicated proteins (stained POI, transparent histogram) or unstained (unstained, black histogram).

The apoptosis-regulating proteins Bcl-2, BID, SerpinB9, XIAP were stained intracellularly and analyzed via flow cytometry. Bcl-2 is an important anti-apoptotic factor, having been detected in a variety of different tumor types (Campbell and Tait, 2018). BID represents a pro-apoptotic factor of the Bcl-2 family playing a crucial role for death receptor-mediated apoptosis in many cell systems (Esposti, 2002). Furthermore, SerpinB9 is a serine protease inhibitor showing inhibitory activity against cytosolic GrzB (Sun et al., 1996). Lastly, XIAP is a key member of the intrinsic inhibitors of apoptosis (IAP) proteins and blocks cell death by inhibition of distinct caspases (Holcik et al., 2001). All of these pro- or anti-apoptotic factors may directly influence the GrzB or Casp8 induced apoptosis, thus a high variability in the expression levels of these factors could influence the apoptosis mechanism. Figure 9 shows the expression level of these four different proteins within HeLa cells stably expressing NES-ELQTD-GFP-T2A-NES-VGPD-mCherry. The cell line exhibited a very homogenous expression of all these proteins. Due to the high homogeneity of the HeLa cells, we can exclude heterogeneity in their cell death resistance.

4.3 GrzB, perforin, CD95L and TRAIL expression after degranulation

It is known that NK cell killing is mediated by exocytosis of lytic granules, which contain GrzB and perforin or induced by death receptors, like CD95L and TRAIL. To ascertain why NK cells switch their killing mechanism during serial killing, staining of these four proteins (GrzB, perforin, CD95L and TRAIL) was examined in the course of NK cell activation. For this assay the activated primary human NK cells were incubated with the HeLa cells for different time periods (1 h - 4 h). CD45 was used as a NK cell marker to exclude HeLa cells from the analysis. Additionally, the degranulation marker CD107a was present to distinguish between NK cells, that had killed or not (**Fig. 10**). The NK cells were divided in $CD107a^+$, having degranulated and $CD107a^-$, exhibiting no degranulation.

The figures showed the expression of CD95L, TRAIL, GrzB and perforin of NK cells after 1 h, 2 h, 3 h, 4 h co-incubation with HeLa cells. The activated primary human NK cells already showed TRAIL expression on the surface even in the absence of target cell contact. These cells were stimulated with IL-2 and IL-15 in the process of cultivation, which leads to an increased expression of TRAIL (Johnsen et al., 1999). The $CD107a^+$ NK cells exhibited within 1 h of target cell contact a reduction of intracellular GrzB and perforin. After 4 h of co-incubation with HeLa cells, the $CD107a^+$, degranulating NK cells had lost most of their GrzB and perforin. As expected, the non-degranulating NK cells ($CD107a^-$ NK cells) did not lose a significant amount of GrzB and perforin. Therefore, CD107a staining is strongly correlated to a reduction of GrzB and perforin. The expression of CD95L was detectable on the surface of $CD107a^+$ NK cells within 1 h of co-incubation and increased during the complete time of co-incubation. In contrast, NK cells that did not degranulate did not possess any surface CD95L expression over the whole incubation time. On the other hand, TRAIL was decreased over 4 h of co-cultivation, which was detectable equally on $CD107a^+$ and $CD107a^-$ NK cells. This demonstrated a mechanism by which NK cells use first the fast GrzB-mediated apoptosis to kill their target cell, which can be concluded by a reduction of the amount of perforin and GrzB during each degranulation event as well as the absence of CD95L during the first contact (ref to 4.2). During this event, target cell contact as well as the degranulation event seems to result in the high surface expression of CD95L. Therefore, during the serial killing process, both granule- and receptor-mediated cytotoxicity may be functional, which would result in a mix of GrzB and Casp8 activity in the target cell. If a high CD95L surface expression in combination with low granule content is present, the last killing event would be preferably induced via death receptor signalling, leading to a strong Casp8 activity.

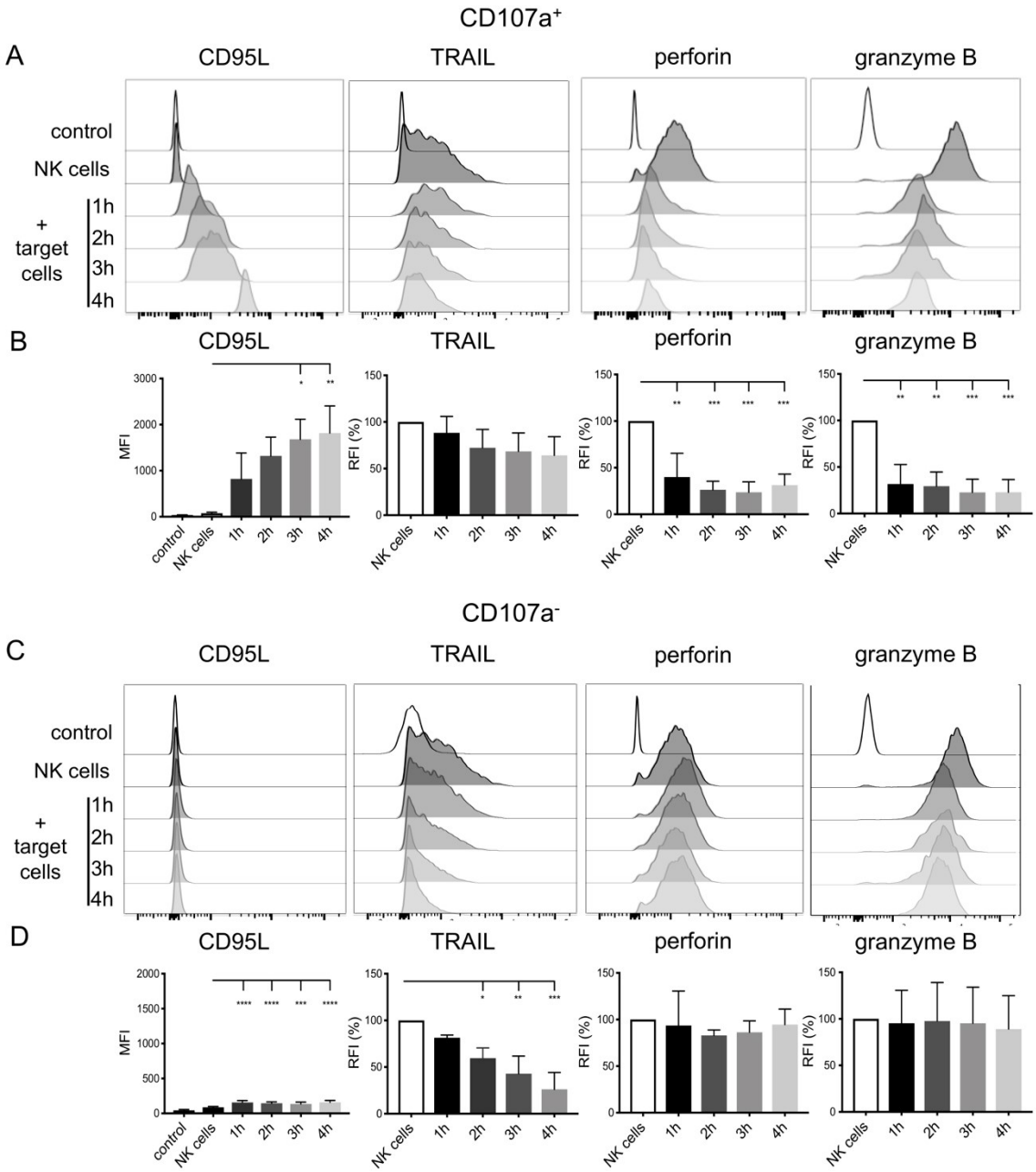

Figure 10: Reduced granule content and induction of surface expression of CD95 on NK cells during serial killing. Primary human NK cells were co-cultured at an E/T ratio of 1 with HeLa-CD48 with presence of an anti-CD107a antibody. After different time periods (1 h, 2 h, 3 h or 4 h), NK cells were collected and stained on the surface for CD45, CD95L or TRAIL, which was followed by an intracellular staining for perforin and GrzB. As a control, unstained NK cells and stained NK cells with no co-cultivation (NK cells) were used. (A and C) NK cells were identified by gating on their size and granularity in the FSC/SSC dot plot, single cells and by the NK cells marker CD45. Histograms illustrated the staining for CD95L, TRAIL, perforin, GrzB on CD107a+ (A) and CD107a- (C) NK cells. (B and D) The bar graph shows the mean fluorescence staining intensity (MFI) of three independent experiment for CD95L or the relative fluorescence staining intensity (RFI normalized to the NK cell only control) for TRAIL, perforin and GrzB after the different co-culture periods for CD107a+ (B) and CD107a- (D) NK cells. Values shown are the mean ± SD; *, P < 0.05; **, P < 0.01; ***, P < 0.001; ****, P < 0.0001 (one-way ANOVA).

4.4 Serial killing activity of NK cells without functional perforin

For a precise identification of the contribution of both pathways to the serial killing activity of NK cells, different experiments were performed to interfere with the GrzB-mediated pathway. These cells then were used for time lapse microscopy in microchips. It is not entirely clear how GrzB enters the target cell, but it is assumed that GrzB seems to utilize two pathways to enter the target cell, both of which require perforin.

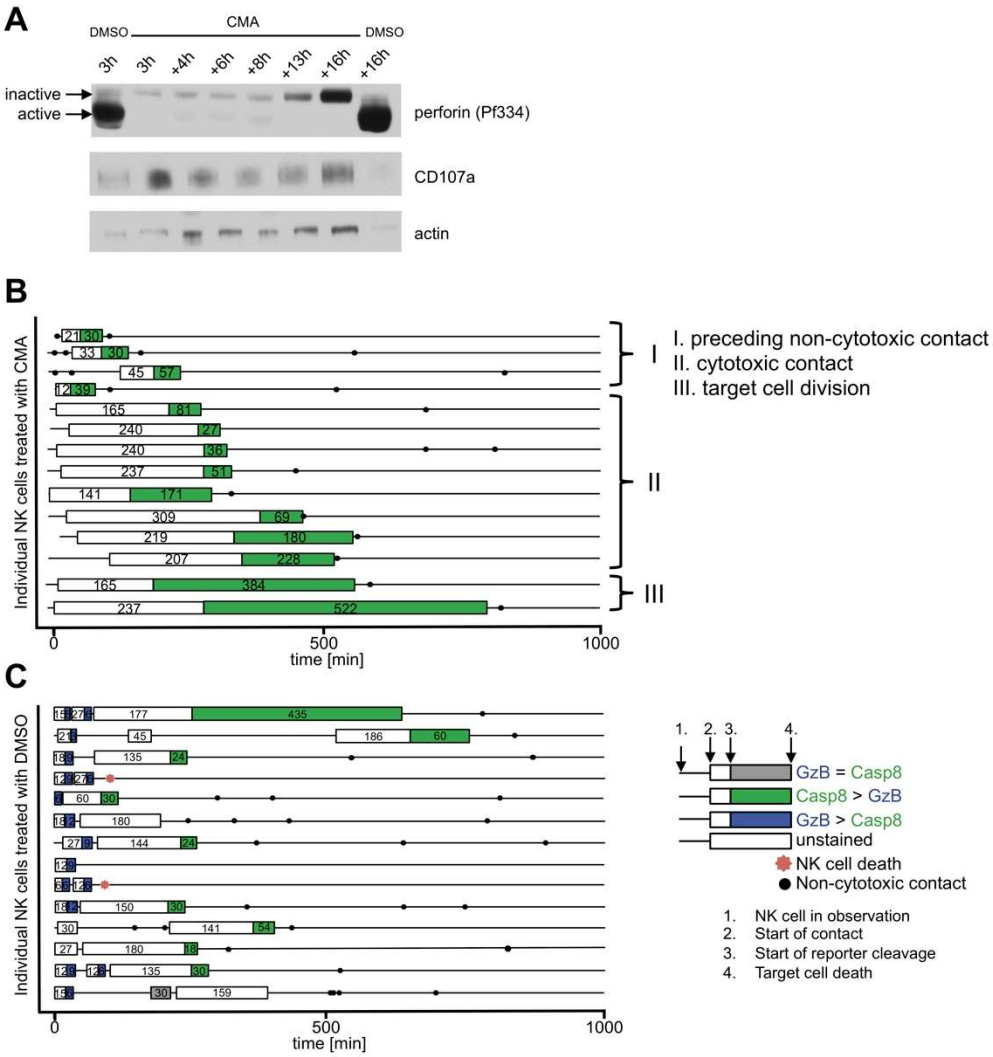

Figure 11: Perforin is crucial for NK cell serial killing. Serial killing activity of CMA-treated or DMSO-treated NK cells was analyzed against HeLa-CD48 cells stably expressing NES-ELQTD-GFP-T2A-NES-VGPD-mCherry (**B-C**). Depletion of active perforin was achieved by 50 nM CMA treatment **(A)** Western Blot analysis of perforin, CD107a and actin in CMA-treated and DMSO-treated NK cells after 3 h of treatment and up to 16 h post treatment. **(B, C)** CMA-treated **(B)** and DMSO-treated **(C)** NK cells was analyzed. Treated NK cells were tracked over 16 h, each line represents one NK cell. Every box visualized NK cell target cell contact. While the length of the boxes displays the duration of the cellular contact, the reporter cleavage is visualized by color (blue: GrzB > Casp8, green: Casp8 > GrzB, grey: GrzB = Casp8, white: HeLa target cells, which do not express NES-ELQTD-GFP-T2A-NES-VGPD-mCherry, named unstained). Non-cytotoxic contacts were represented by black dots and NK cell death by a red star. Experiments were performed using a Zeiss LSM 880 microscope.

GrzB is able to invade the target cell either directly through perforin pores or via endocytosis. Therefore, an assay with concanamycin A (CMA) was performed.. CMA is established as inhibitor of vacuolar type H^+-ATPase (V-ATPase). This ATPase is a proton pump, which is responsible for controlling the pH of cellular compartments (Pamarthy et al., 2018). V-ATPases are located to a variety of cellular membranes of eukaryotic cells, like endosomes, lysosomes, Golgi-derived vesicles and secretory vesicles (Forgac, 2007, Kane, 2006, Wagner et al., 2004). CMA belongs to a class of pleomacrolides (macrolide antibiotic) that target the V_o sector, which is responsible for the translocation of protons across the membrane. This leads to a full but reversible inhibition of the V-ATPase (Pamarthy et al., 2018). The treatment with CMA leads to an increased pH of the lytic granules, which impaired the maturation of perforin. Primary human NK cells were pretreated with CMA or DMSO, as a control, for 3 h. The expression of perforin was investigated by western blot and the cytotoxic activity was tested by time-lapse imaging using a microchip platform. (**Fig. 11**)

As noted in figure 11 two forms of perforin can be distinguished by western blot, the inactive, immature form at 66 kDa and the mature, active form at 60 kDa. Furthermore, in the DMSO-treated NK cells, the 60 kDa mature, active form of perforin showed a stronger signal intensity as the inactive, immature perforin form (66 kDa), indicating a high number of cleaved perforin, which was seen in lane DMSO 3 h and DMSO 16 h. The 60 kDa mature perforin protein was almost undetectable after 3 h of treatment with 50 nM CMA. To further assess if the effect of CMA is reversible within a time frame relevant for our experiments, the cells were washed after the treatment and afterwards incubated for another 4 h to 16 h without any treatment. In CMA-treated NK cells no mature perforin was detectable, whereas immature perforin accumulated in a time-dependent manner. This result demonstrated that CMA leads to a complete inhibition of mature perforin for at least 16 h after 3 h pretreatment. These pretreated NK cells were also used for measuring serial killing activity via time-lapse microscopy. Figure 11C shows 14 individual NK cells, which were treated with DMSO. Every line displays one NK cell over the whole 16 h experiment. The boxes indicate a target cell contact with cytotoxic activity of the NK cell, GrzB-mediated killing is represented in blue and Casp8-mediated killing in green. A non-cytotoxic contact is marked by a dark dot. As already shown for untreated NK cells, also DMSO-treated NK cells induce apoptosis first by the GrzB-mediated pathway and afterwards switch to a Casp8-mediated pathway. The GrzB-mediated killing always took around 20 min from contact to target cell death, irrespective of if it is the first or subsequent killing event. In contrast to the GrzB-mediated killing, the average Casp8-mediated kills appeared within 150 min. It seems that the differences in the death kinetics

are intrinsic to the killing pathway and not influenced by differences between individual NK cells. Predictably, the CMA-treated NK cells in figure 11B induced apoptosis by using Casp8 activity. They only performed one single Casp8-mediated kill, which also showed slow kinetics. However, it was observable that the average time from contact to death in these Casp8-mediated kills took 100 min much longer than the Casp8 mediated killing in DMSO-treated NK cells. Additional contacts after the first kill were observed but no second Casp8-mediated kill occurred. Noteworthy, there were three differences seen in the Casp8-mediated killing. Three NK cell clones (**Fig. 11B**, **I**) had some non-cytotoxic contacts before their killed their target cell. Another nine NK cell clones (**Fig. 11B**, **II**) killed their target cell via Cas8-mediated kill by the first attachment. Two NK cell clones (**Fig. 11B**, **III**) showed NK:target cell killing during the target cell division, which took much longer to kill the target cell.

To confirm that these effects caused by CMA treatment are not due to off-target effects of the inhibitor, it was of high interest to generate perforin knockout in primary human NK cells (perforin KO) for further investigations. To achieve this, the CRISPR/Cas9-System with two different sgRNA in various combinations was used. Investigation of the KO cells was performed after 7 days via flow cytometry. (**Fig. 12**)

The efficiency of the KO was only around 30 % (**Fig. 12A**). To further assess primary human NK cells without perforin a purity of 100 % KO NK cells would be necessary. Since sorting in the case of intracellular proteins is not feasible, clones were generated and some clones were expanded that had no perforin (KO clone, **Fig. 12B**) and some had the wildtype perforin level (WT clone, **Fig. 12B**). Finally, the killing of the HeLa cells by these clones was tested similar to the inhibitor experiments by time-lapse imaging using the microchip platform. This microchip assay with perforin KO NK cell clones was in good agreement to the experiments using CMA, supporting that the phenotype observed was caused by the lack of active perforin. While the WT clones showed the previously described switch of GrzB- to Casp8-mediated kills, the perforin KO clones performed only one single killing event initiated by Casp8 activity, even though subsequent target cell contacts occurred which were non-cytotoxic. The inhibitor as well as the perforin KO studies demonstrated the necessity of perforin for the serial killing activity of NK cells.

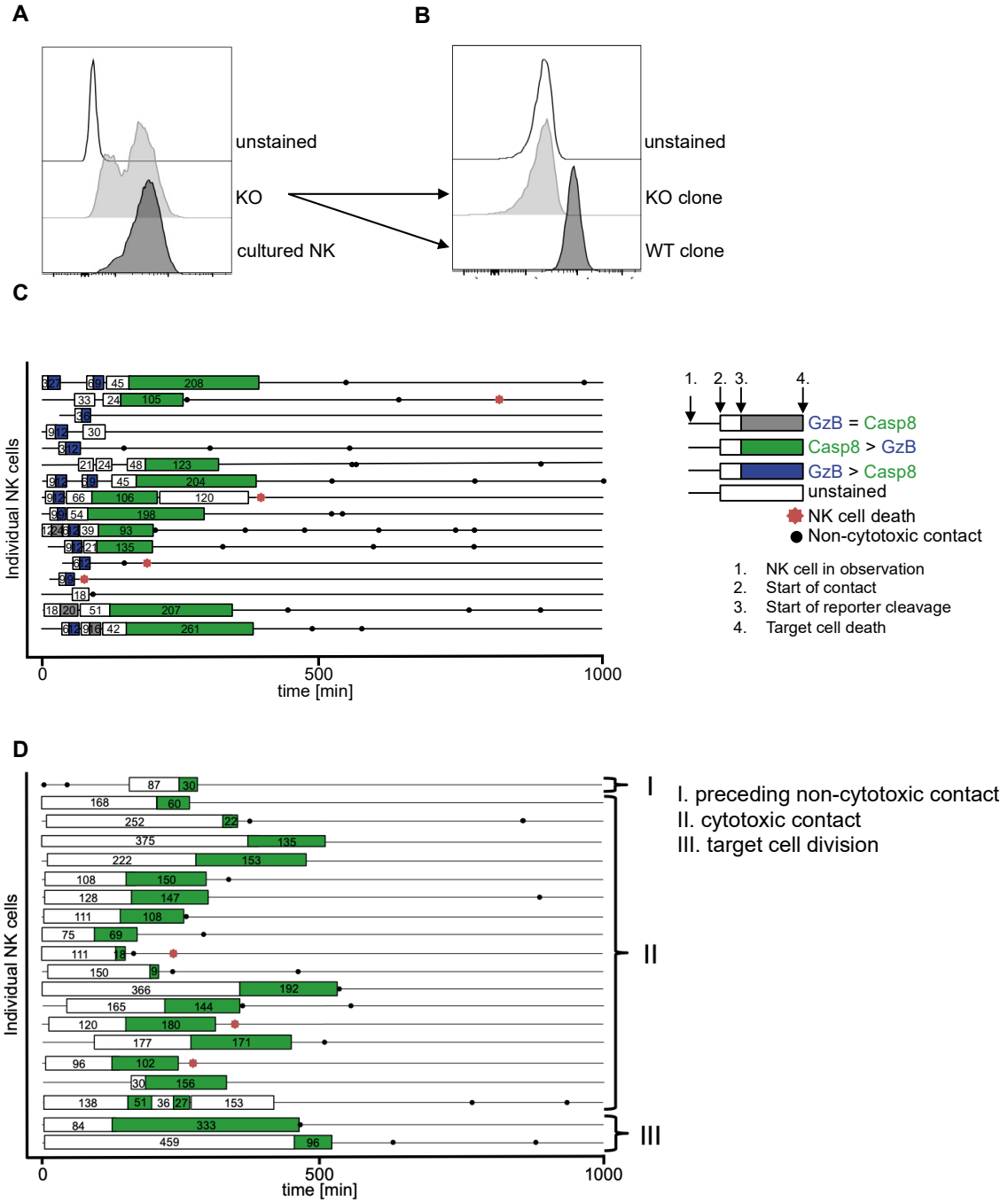

Figure 12: No serial killing activity via Casp8-mediated pathway. Serial killing activity of generated perforin KO or WT clones was analyzed against HeLa-CD48 cells stably expressing NES-ELQTD-GFP-T2A-NES-VGPD-mCherry. (A) Intracellular flow cytometry staining of perforin in NK cells before (cultured NK) and after CRISPR-Cas9-mediated KO. (B) Exemplary illustration of intracellular staining of generated KO and WT clones. (C,D) Perforin WT (C) and perforin KO (D) NK cell clones (each experiment was performed with two independent clones) were analyzed against HeLa-CD48 cells stably expressing NES-ELQTD-GFP-T2A-NES-VGPD-mCherry. Clones were tracked over 15-17 h, each line represents one NK cell. Every box visualized NK cell target cell contact. While the length of the boxes displays the duration of the cellular contact, the reporter cleavage is visualized by color (blue: GrzB > Casp8, green: Casp8 > GrzB, grey: GrzB = Casp8, white: HeLa target cells, which do not express NES-ELQTD-GFP-T2A-NES-VGPD-mCherry, named unstained). Non-cytotoxic contacts were represented by black dots and NK cell death via a red star. Experiments were performed using a Zeiss LSM 880 microscope.

Interestingly, we observed some kinetic differences of the reporter cleavage in GrzB-mediated kills to the Casp8-mediated killing, but also within the Casp8-mediated apoptosis.

We wanted to determine the time point from NK cell contact to reporter cleavage. The time from contact to reporter cleavage in the control NK cells was very short for GrzB-mediated kills (7 min), whereas it took an average 87 min for the Casp8 kills. The CMA and perforin KO NK cells were separated into three groups. The first group contained of three CMA-treated NK cells (**Fig. 11B**, **I**) and one perforin deficient NK clone (**Fig.12 B**, **I**) that had some non-cytotoxic contacts before their killed their target cell. It took only an average 51 min for Casp8-mediated kills. This time span (51 min) was comparable to the control NK cells, which took an average 87 min for Casp8-mediated kills. Also these NK cells had contacts beforehand. This leads to the assumption that the CMA-treated or perforin deficient NK cells were primed in theses non-cytotoxic contact beforehand. The second group consisted of eight CMA-treated NK cells (**Fig. 11B**, **II**) and 17 perforin KO NK cell clones (**Fig. 12B**, **II**), which killed their target cell via Casp8-mediated kill by the first attachment. We determined also here the time span from NK cell engagement to the reporter cleavage, which took 188 min. The third group contained of two CMA-treated NKs (**Fig. 11B**, **III**) and two perforin deficient NK cell clones (**Fig. 12B**, **III**), which showed NK:target cell killing during the target cell division. The time span for these cells took 236 min.

4.5 Detachment of CMA-treated and perforin KO NK cells

During further investigation, the regulation of NK cell detachment as a key factor for serial killing was considered more closely. For cytotoxic contacts, it is known that NK cells do not detach from their target until this cell is dead. For serial killing events, the detachment process after killing of a target cell is essential in order to attach to a subsequent target cell. Previous studies pointed out that NK cells treated with CMA showed an unaltered formation of conjugates and no differences in degranulation, but a prolonged conjugation time (Anft et al., 2020). These experiments were only performed with CMA-treated NK cells. To confirm these FACS-based data, we analyzed the CMA-treated NK cells with HeLa target cells and analyzed the killing sequence by time-lapse microscopy. In order to exclude off-targets effects we used in addition the recently generated perforin deficient NK cell clones. Therefore, the experiments with perforin KO, CMA-treated or control NK cells were reanalyzed with the focus of the first killing event and detachment.

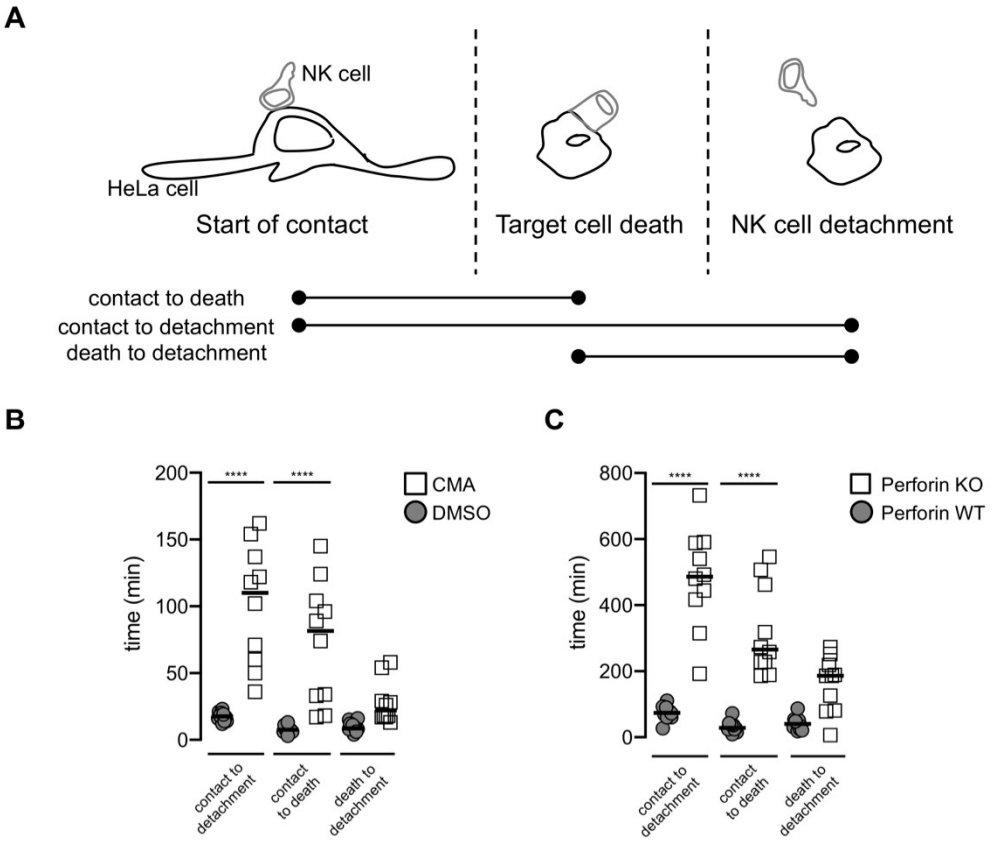

Figure 13: Prolonged contact duration can be attributed to slower target cell death not to impaired detachment. (A) Every first killing event shown in B and C was analyzed for the time period from contact to detachment and the time period from contact to death as well as the time period from death to detachment. **(B)** Primary human NK cells were pretreated with 50 nM CMA or DMSO as a control for 3 h. NK cells were washed incubated with HeLa cells and analyzed by video microscopy for 16 h. **(C)** NK cell clones (WT/KO perforin) were generated as explained in 4.4, only the first killing event was analyzed by confocal time-lapse microscopy. Experiments were performed using a Zeiss LSM 880 microscope.

For all killing events, different time periods regarding the killing process were investigated. In detail, we determined the time period between contact (NK cell to target cell) and detachment, period from contact to death or period of death to detachment (**Fig. 13A**). In NK cells treated with CMA (**Fig. 13B**) as well as in perforin KO NK cells (**Fig. 13C**) a significant increase of the time period from contact to detachment becomes apparent for cells without functional perforin, which was in line with the previous results obtained by flow cytometry (Anft et al., 2020). The increased time interval from contact to target cell death was seen in both CMA or CRISPR/Cas9-treated, perforin depleted NK cells. In detail, CMA-treated NK cells needed an average time of 73 min and the perforin KO cells needed an average time of 319 min from contact to death, whereas the DMSO-treated NK cells needed an average time of 10 min (perforin WT: 30 min). As described before, this delay was caused by a slower receptor-mediated killing of the target cell, because the CMA-treated as well as the perforin KO cells only induced receptor-mediated killing. Additionally, in the time from death to detachment no significant difference was

observable between CMA-treated or perforin KO and control NK cells. The data demonstrated that without perforin a slower death receptor-mediated kill of the HeLa target cells occurred. This could be explained by the increased killing time. The CMA-treated cells as well as the perforin KO cells showed unchanged detachment after death receptor mediated killing, which confirmed that detachment is regulated by target cell death.

4.6 Serial killing activity of ADAP KO NK92 cells

Adhesion and degranulation are of utmost importance for apoptosis induction of NK cells. Adhesion of immune cells is based on complex mechanisms. A crucial player within the formation of immune signaling complexes is the adhesion and degranulation-promoting adapter protein (ADAP). Next to its well-characterized role in T cells, ADAP is also expressed in many other cells, in particular in NK cells. However, the function of ADAP in NK cells has been controversially discussed in past studies (Fostel et al., 2006). Recently, BÖNING et al. illustrated that during bacterial infection in mice ADAP is required for efficient cytotoxic capacity and migration of NK cells (Boning et al., 2019). In addition, the group of Lothar Jänsch could show that ADAP KO NK cells exhibit a decreased specific lysis of K562 target cells in comparison to WT NK cells (unpublished data). For a more detailed understanding, if this impaired cytotoxicity of ADAP KO NK cells is also seen in a serial killing manner, we analyzed ADAP deficient NK cells regarding their serial killing on a single cell level. Therefore, three modified NK cell lines (NK92 WT, NK92 ADAP KO, NK92 ADAP rescued) were obtained by Wenjie Bi (HZI, Germany). The NK92 WT cells were used to generate the NK92 ADAP KO by using the CRISPR/Cas9 system. In addition, these ADAP deficient NK92 cells were retransfected with ADAP-GFP (NK92 ADAP rescued). These three cell lines were co-cultured with K562 cells and the killing events were analyzed via time-lapse video microscopy. K562 cells were used as target cells in these experiments in order to create comparable data to the results from the Jänsch group.

These NK92 cell lines were tracked using Celltracker Deep Red, and cell death was detected by the uptake of SYTOX Blue. The CellTracker staining allowed us to distinguish between NK cells and K562 target cells as NK92 and K562 cells have a similar cell size. In addition, IL-2 was present during the experiment, because NK92 cells require IL-2 to maintain optimal cytotoxic activity. NK cell cytotoxicity was observed by the uptake of SYTOX Blue in the target cells. Data are shown in **figure 14**, every box represents one NK-K562 cell contact. The coloring of the box illustrated if the contact was cytotoxic (dark

blue or light blue) or non-cytotoxic (white). The cytotoxic events can be divided in a group where SYTOX Blue was seen immediately after induction of apoptosis in the target cell (cytotoxic contact labeled in dark blue in **Fig. 14 A/B/C**, example shown in **Fig. 14D** t = 45 min) or in another group where SYTOX Blue was seen after formation of apoptotic bodies (called cytotoxic contact with late SYTOX Blue staining, see in **Fig. 14D** t = 408 min). After 16 h of co-cultivation, 28 out of 38 analyzed WT NK92 cells killed 79 target cells (40.0 % of all contacts). WT NK92 cells were able to kill up to six targets in a serial fashion. Interestingly, only the last killing event of an individual cell showed late SYTOX Blue staining. However, after multiple killing events some NK92 cells established non-cytotoxic contacts. In contrast to WT NK92, a lower cytotoxic activity was detectable in NK92 ADAP KO cells. Only 17 out of 43 analyzed NK92 cells exhibited cytotoxic activity (12.8 % of all contacts), and a maximum of three target cells was killed in a serial fashion. While comparing the overall number of contacts of WT NK92 and ADAP KO NK92 cells to targets, it was notable that the average amount of cell contacts were similar (WT: 5.0 contacts/cell, ADAP KO: 4.7 contacts/cell). In figure 14C rescued NK92 cells were analyzed on a single cell level. The rescue was performed by the reintroduction of ADAP into NK92 ADAP-KO cells. The results using ADAP rescued cells were comparable to the WT NK92 cells, as 32 out of 43 cells killed 90 target cells (40.0 % of all contacts). Also the average number of cell contacts was similar (rescued ADAP-KO: 5.2 contacts/cell). Taken together, the experiment with ADAP-KO NK92 cells illustrated that ADAP seems to play an important role for the cytotoxic function of NK cells. However, this effect was not a result of reduced ability to establish target cell contacts but rather an effect of decreased cytotoxic activity of the ADAP KO NK92 cells.

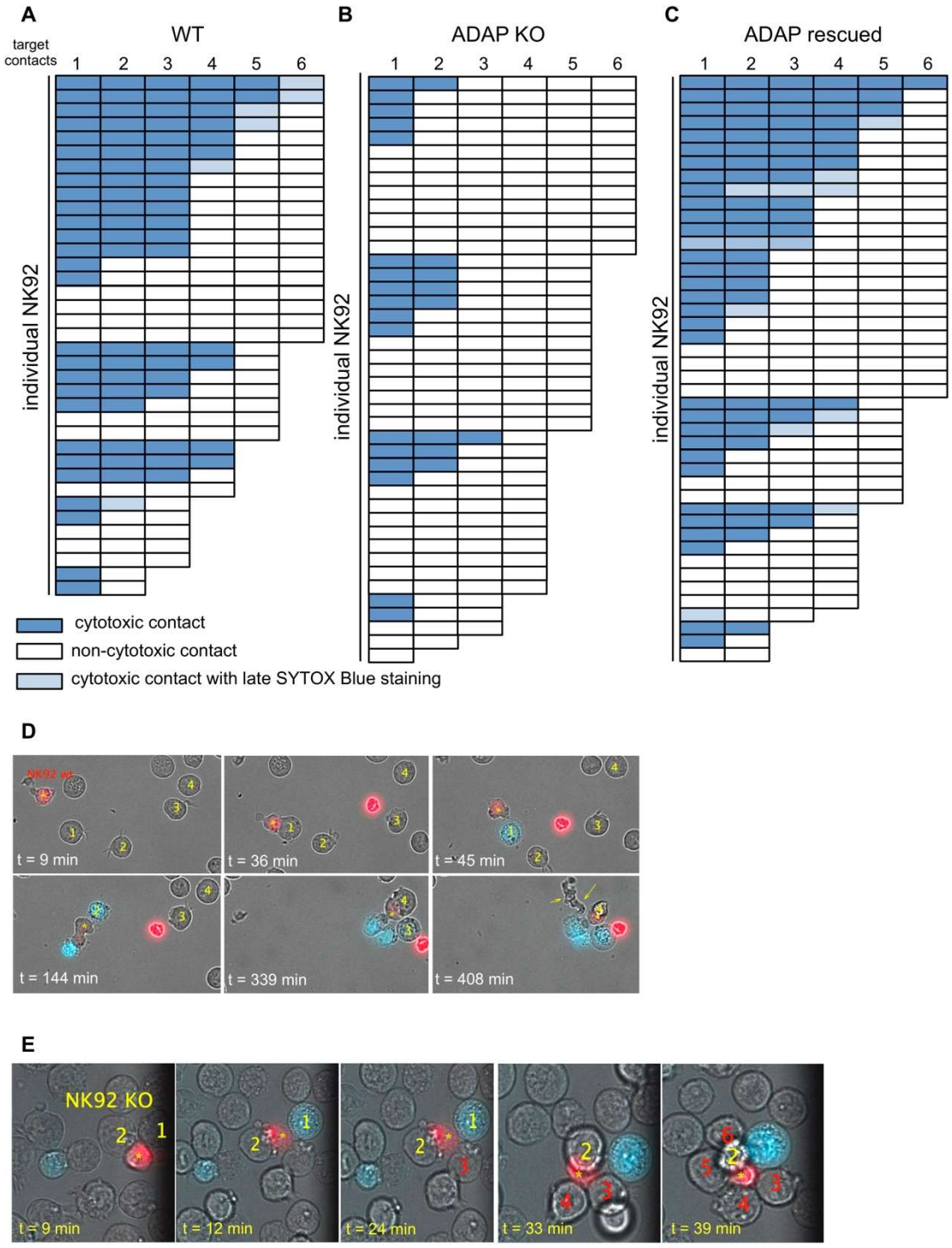

Figure 14: Reduced serial killing by ADAP KO NK92 cells. Serial killing activity of CellTracker™ Deep Red stained NK cells was examined against K562 target cells in the presence of SYTOX Blue. IL-2 treated NK92 cell lines (WT (A), ADAP KO (B), ADAP rescued (C)) were tracked over 16 h. Each row represents one individual NK92 cell that made contact with up to six K562 target cells. Each box represents one target cell contact of this NK92 cell. Killing events are displayed in blue (dark blue: cytotoxic contact, light blue: cytotoxic contact with late SYTOX Blue staining), non-cytotoxic contacts are illustrated in white. (D) One example for four sequential killing events by one WT NK92 cell, last kill showed at t = 408 min. (E) One example of one representative ADAP KO NK92 cell, making many non-cytotoxic contacts. The tracked NK cell is marked with a yellow star. Target cell contacts were numbered consecutively, yellow number for cytotoxic or red number for non-cytotoxic contacts. Experiments were performed using a Zeiss ApoTome microscope.

4.7 Influence of granule content on cytotoxic activity

As previously discussed, some NK cells are able to kill multiple target cells in a serial fashion, and are an essential part of the granula-mediated pathway during this serial killing process. About one third of the cells were able to kill a minimum of three cells in a row, but some cells did not show any cytotoxic activity. Therefore the question arose what features distinguishes serial killers from the non-serial killers. Recent studies investigated the features of serial killer NK cells and demonstrated a relation between the ability of cells for serial killing and the cell size, as serial killers exhibited a larger cell size (Vanherberghen et al., 2013, Choi et al., 2019). Taking into account that expanded IL-2/IL-15/IL-21 NK cells are larger and possess more GrzB and perforin stored in the granules as freshly isolated NK cells (Zhang et al., 2008), it has been defined that the larger cell size of the serial killers could be a result of a higher amount of granules. To analyze if a higher amount of granules can be combined with more serial killing activity, we wanted to separate NK cells with low amount of granule content from NK cells with a high amount of granule content. In previous experiment to stain components of the granules, we permeabilized the cells, which leads to holes in the membrane and killed the cells. However, for the analysis of this hypothesis, living cells are needed. The Lysotracker Green® is a dye to visualize acidic organelles in living cells. The probe is a fluorophore linked to a base (unprotonated at neutral pH), which can freely enter the cell. It accumulates in acidic organelles, lead to a protonation, which results in an increased fluorescence intensity. Therefore, the NK cells were stained with LysoTracker Green® and sorted regarding to LysoTracker^{dim} (low granule content) and LysoTracker^{bright} (high granule content). Cells were sorted into LysoTracker^{bright} NK cells that consisted of the 20 % with the highest LysoTracker intensity or LysoTracker^{dim} NK cells with a low staining of LysoTracker **(Fig. 15B)**.

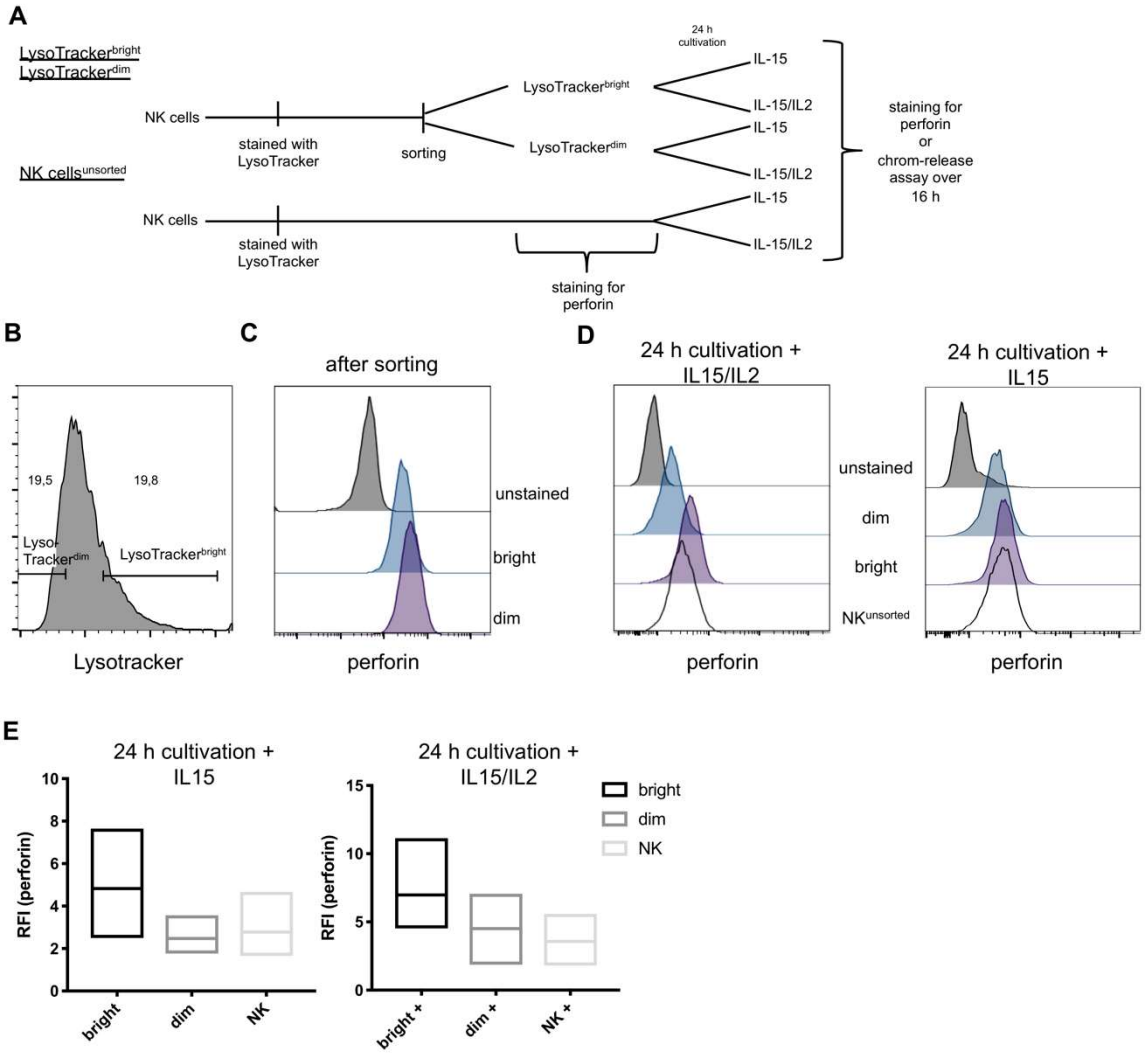

Figure 15: More granules seem to accompany with more perforin expression. (A) Schematic timeline for the experiments with LysoTracker^{bright}, LysoTracker^{dim} sorted primary human NK cells or control NK cells (NK cells^{unsorted}). (**B**) Representation of the Lysotracker stained NK cells and the sorting gates. (**C**) Histogram of perforin staining from one representative experiment for after sorting is shown. (**D**) Sorted (dim,bright) or unsorted NK (NK^{unsorted}) cells incubated for 24 h with IL-2/IL-15 (left histogram) or low dose IL-15 (right histogram) were stained for perforin. (**E**) The quantification of perforin expression from LysoTracker^{bright}, LysoTracker^{dim} and NK cells^{unsorted} from three independent donors after 24 h cultivation with low dose IL-15 (right) or IL-15/IL-2 (left).

Staining the cells after the sorting process confirmed that LysoTracker^{bright} NK cells possess more perforin as LysoTracker^{dim} NK cells **(Fig. 15C)**. After the sorting step, some of these cells were cultured either with low dose of IL-15 or with IL-2 and IL-15 (marked by + **Fig. 15E/D**) and stained for perforin. Even after the incubation the difference in perforin levels between LysoTracker^{bright} and LysoTracker^{dim} was still detectable **(Fig. 15D)**. To investigate, whether the hypothesis regarding the correlation between serial killer size and granule amount could be validated, a killing assay with a pretty low E/T was performed over 16 h to monitor serial killing **(Fig. 16)**.

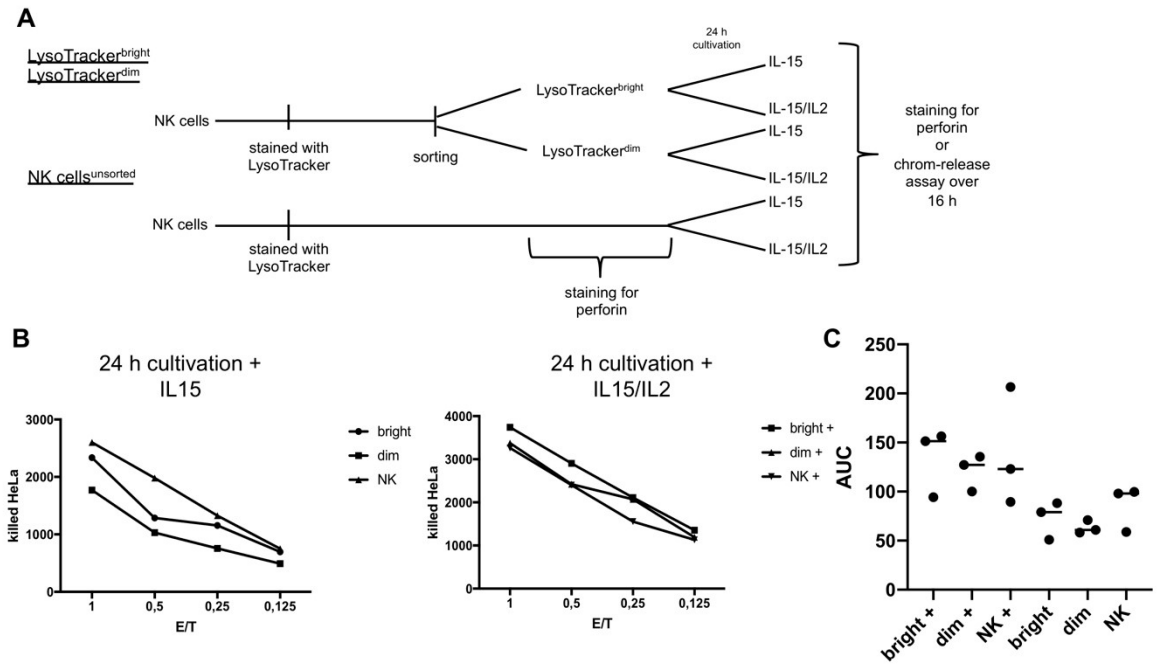

Figure 16: More granules seem to have a small influence on killing activity. (A) Schematic timeline for LysoTracker^{bright}, LysoTracker^{dim} sorted primary human NK cells or control NK cells (NK cells^{unsorted}). NK cells prepared as described in **Fig. 15A** were used in a 16 h chromium-51 release assay against specific lysis [%], NK cells were treated 24 h either with low dose IL-15 or with IL-15/2 (marked with +). (**B**) One representative experiment out of three independent experiments is shown. (**C**) The quantification of three independent experiments with NK cells from three different donors is shown. To summarize all data the area under curve (AUC) was calculated from the diagrams as displayed in 16B.

IL-15 activated LysoTracker^{bright} NK cells exerted a higher lytic function against K562 target cells when compared to the IL-15 activated LysoTracker^{dim} NK cells (**Fig. 16B**). Both Lysotracker$^{dim/bright}$ NK cells showed a slightly reduced specific lysis in comparison to NK cells^{unsorted}. The same trend was observable with IL-15/2 stimulation. To summarize all ^{51}Cr-release assays from three independent donors, the area under curve was calculated from the diagrams as displayed in 16B. In conclusion, 16 h ^{51}Cr-release assays with stimulated IL-15/2 NK cells revealed an increased specific lysis in comparison to the low dose stimulated IL-15 NK cells. In addition, also the differences of cytotoxic lysis between LysoTracker^{bright}, LysoTracker^{dim} and NK cells^{unstorted} seem to getting smaller in the stimulated IL15/2 NK cells compared to low dose IL-15 stimulated NK cells. In conclusion, the data illustrated that IL15/2 or IL15 activated LysoTracker^{bright} NK cells had a slightly increased cytotoxicity compared to the IL15/2 or IL15 activated LysoTracker^{dim} NK cells.

During the process of CRISPR/Cas9 to generate perforin KO clones, we generated a clone, which possessed more perforin (perf^{high}) than the control (perf^{WT}). This generated perf^{high} NK cell clone allows the investigation of this hypothesis with another experimental system (**Fig. 17**).

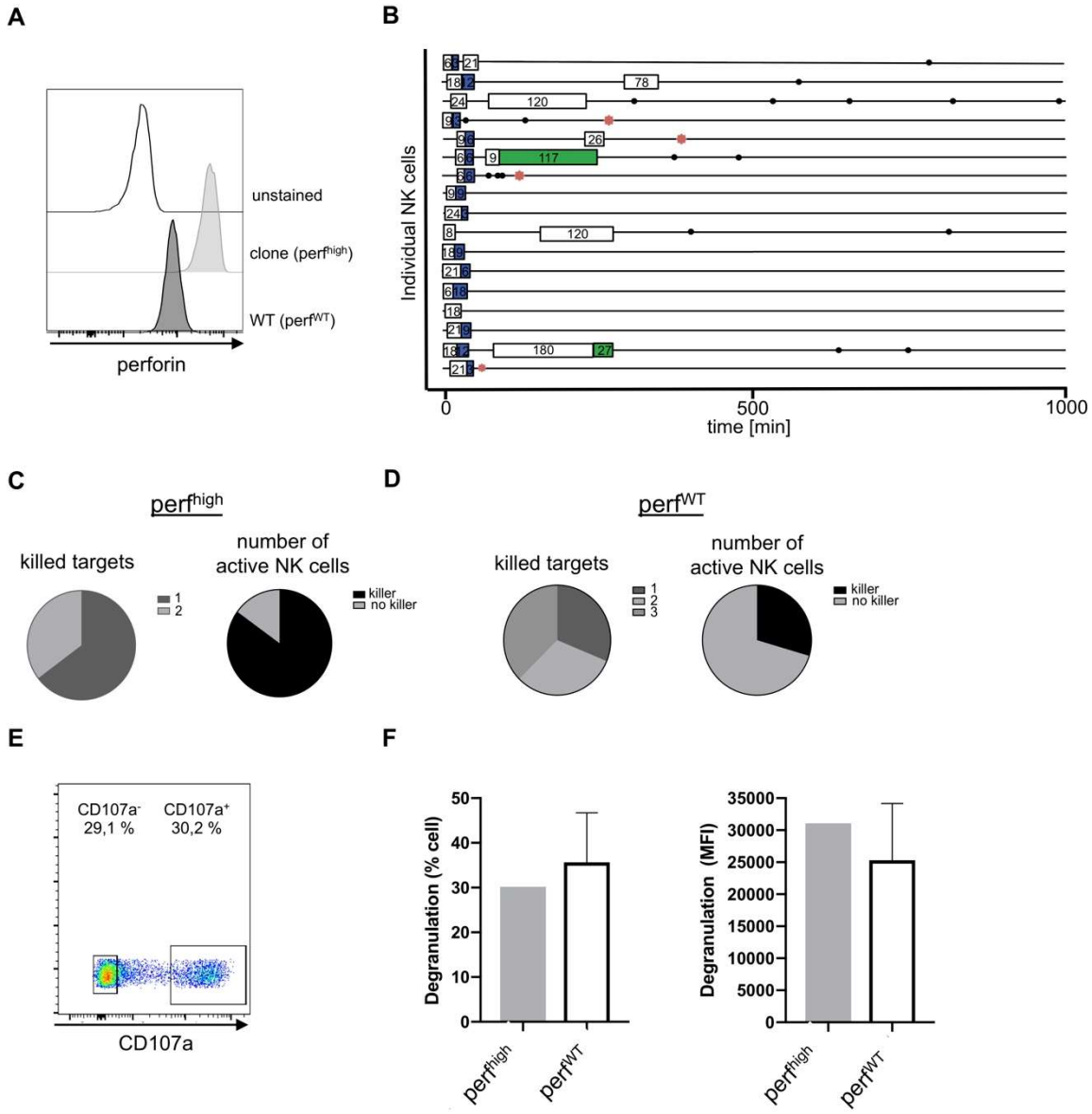

Figure 17: More perforin expression seems to have slight influence on killing activity. (**A**) Intracellular FACS staining of perforin in human NK cells after expansion of single cell clones, example for a clone with high level of perforin expression (perf^{high}) and WT clones with normal level of perforin expression (perf^{WT}). (**B**) perf^{high} NK cell clones were analyzed against HeLa-CD48 cells stably expressing NES-ELQTD-GFP-T2A-NES-VGPD-mCherry. Clone were tracked over 16 h, each line represents one NK cell. Every box visualized NK cell target cell contact. While the length of the boxes displays the duration of the cellular contact, the reporter cleavage is visualized by color (blue: GrzB > Casp8, green: Casp8 > GrzB, grey: GrzB = Casp8, white: HeLa target cells, which do not express NES-ELQTD-GFP-T2A-NES-VGPD-mCherry, named unstained. Non-cytotoxic contacts were represented by black dots and NK cell death via a red star. (**C-D**) Pie charts show the proportion of killed targets by one active NK cell or percentage of active NK cells of clone (perf^{high}) (**C**) or WT NK cells (perf^{WT}) (**D**). (**E**) Degranulation was analyzed after 4 h co-incubated with HeLa-CD48 target and stained for CD107a^{-} and CD107a^{+} in perf^{high} cells. (**F**) After 4 h co-incubated with HeLa-CD48 target cells % CD107a^{+} of perf^{high} or perf^{WT} NK cells (left) or MFI (right) of % CD107a^{+} cells for perf^{high} or perf^{WT} NK cells is quantified. Experiments were performed using a Zeiss ApoTome microscope.

The selected NK cell clone was also co-cultured with HeLa-CD48 cells stably expressing NES-ELQTD-GFP-T2A-NES-VGPD-mCherry and the killing events were analyzed via

time-lapse video microscopy (**Fig. 17B**). Within NK cell clone (perf^{high}) the proportion of cells showing cytotoxic activity was increased in comparison to WT NK cell clone (perf^{WT}) (**Fig. 17C/D and Fig.12C**). However, those cytotoxic cells (perf^{high}) had less ability for serial killing (**Fig. 17C/D**). This demonstrates that at least for perf^{high} clone the amount of granules seems to have no direct influence on the serial killing behavior of an NK cell. The clone exhibit lower frequencies of CD107a^{+} NK cells (**Fig. 17F**), but the cells that did degranulate showed a higher surface level of CD107a (**Fig. 17D**). In addition the degranulation capacity of the NK cell clone seems to be slightly affected. This perf^{high} NK cell clone shows an altered cytotoxic behaviour, but similar to the Lysotracker sorted NK cells, its higher perforin level is not associated with higher serial killing activity.

4.8 Serial killing activity in CD95 KO HeLa target cell

In the previous results the main focus was on the GrzB-mediated pathway, which seems to take an important part in serial killing. But after inducing fast GrzB-mediated killing the NK cell switch to the slow death receptor-mediated killing. So, an interesting part was to inference with the death receptor-mediated pathway. To take a closer look on the contribution of the death receptor-mediated killing, experiments were performed after depleting the gene CD95, also known as Fas from HeLa target cells using the CRISPR/Cas9 method (**Fig. 18**).

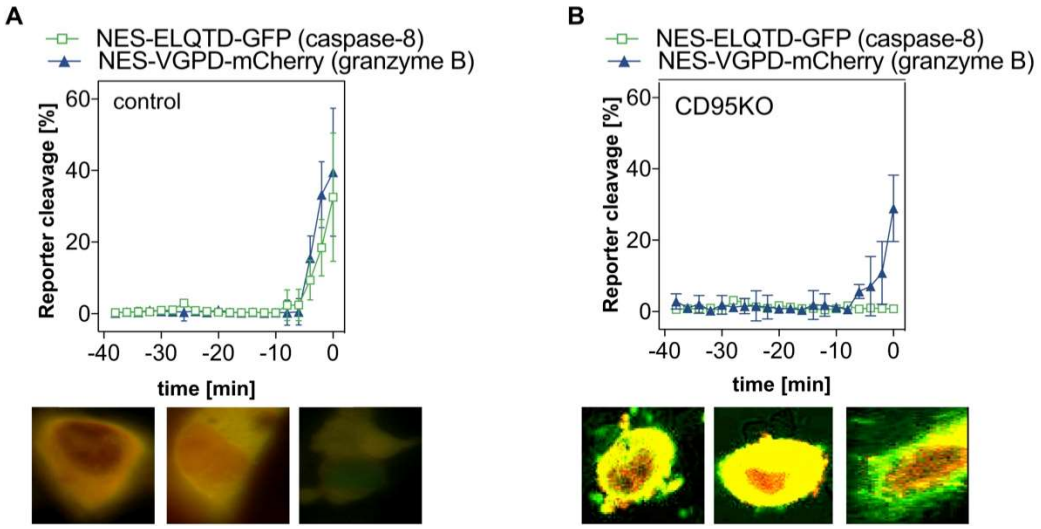

Figure 18: Lack of GrzB reporter cleavage in CD95 KO HeLa target cells (**A-B**) Initial killing activity of primary human NK cells of single cells (mean ± SD, time point 0 set to time of cell death) with more GrzB than Casp8 reporter cleavage was illustrated, in HeLa-CD48 (**A**, control) or HeLa-CD48-CD95 KO (**B**, CD95 KO) target cells stably expression NES-ELQTD-GFP-T2A-NES-VGPD-mCherry. **(A-B)** Examples for every initial killing event induced by different NK cells (lower row). Experiments were performed using a Zeiss ApoTome microscope.

Interestingly, no cleavage of Casp8 (death receptor) was detectable in the CD95 KO (**Fig. 18B**) cell line, whereas in the control HeLa-CD48 target cells (**Fig. 18A**) cleavage by both proteases was visible in all cases.

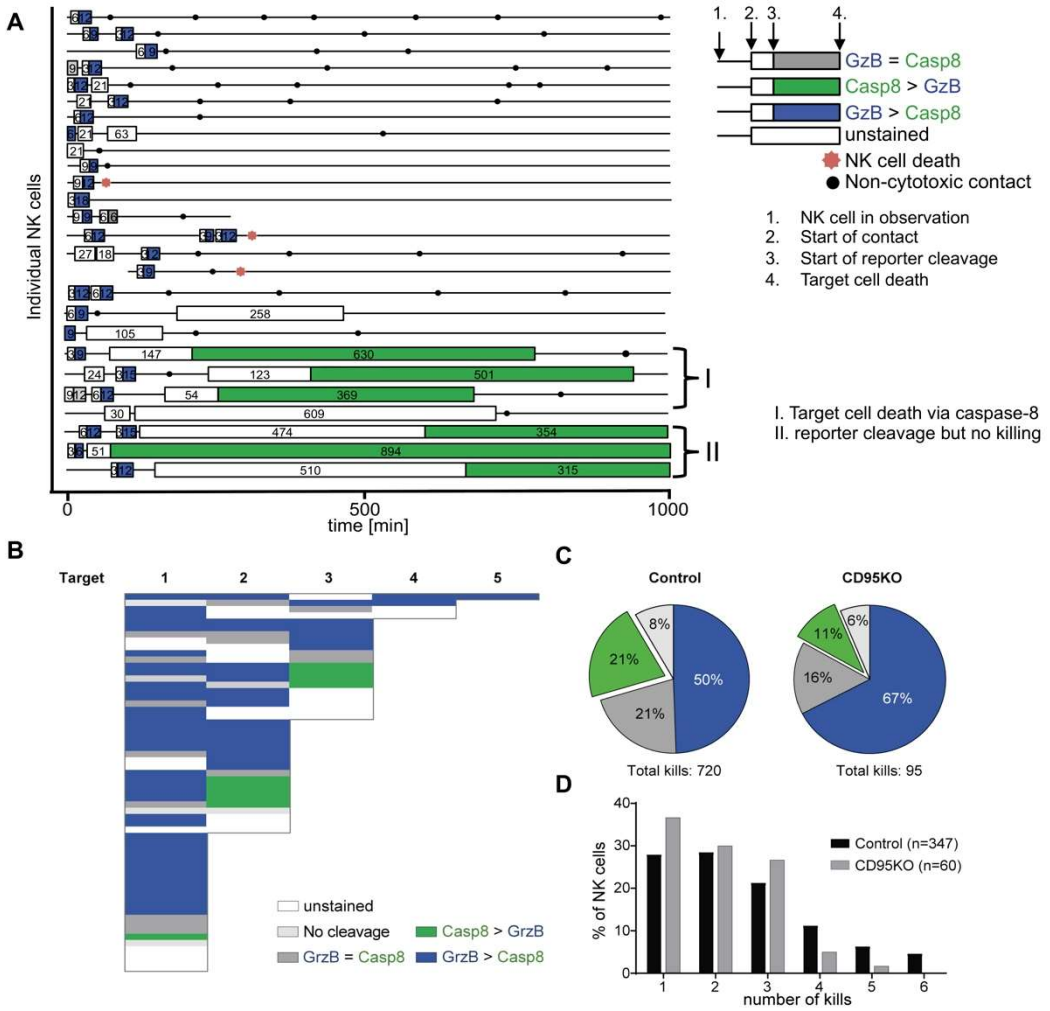

Figure 19: Reduced Casp8 mediated killing. (**A**) Primary human NK cells were analyzed against HeLa-CD48 cells stably expressing NES-ELQTD-GFP-T2A-NES-VGPD-mCherry. Clones were tracked over 16 h, each line represents one NK cell. Every box visualized NK cell target cell contact. While the length of the boxes displays the duration of the cellular contact, the reporter cleavage is visualized by color (blue: GrzB > Casp8, green: Casp8 > GrzB, grey: GrzB = Casp8, white: HeLa target cells, which do not express NES-ELQTD-GFP-T2A-NES-VGPD-mCherry, named unstained). Non-cytotoxic contacts were represented by black dots and NK cell death via a red star. (**B**) Diagram summarize all prepared experiments of the contribution of GrzB and Casp8 activity. (**C**) Relative distribution of reporter cleavage of all killing events for control CD95KO HeLa target cells. (**D**) Relative distribution of killed target cells one to six different control or CD95KO killed target cells induced by single NK cells Experiments were performed using a the Zeiss ApoTome microscope and a TCS SP5 confocal laser scanning microscope.

Testing these CD95 KO cell lines by time-lapse imaging using a microchip platform, serial killing was still observable (**Fig. 19A**). As expected, these kills were predominantly induced by GrzB-mediated pathway. Nevertheless, also Casp8-dependent kills were detectable, possibly due to the fact that the HeLa target cells also expressed low level of

TRAIL-R2 (**Fig. 20**). By combining the findings of all experiments, it was possible to observe a clear reduction of Casp8-mediated kills in CD95 KO target cells (21 % to 11 %) compared to control target cells (**Fig. 19B**, **Fig. 19C**). However, in absence of CD95 the serial killing activity of NK cells was reduced (from an average of 2.53 to 2.05 kills/NK cell). This reduction was consistent with the fact that a final CD95-dependent kill was no longer possible. This demonstrates that serial killing is reduced in the absence of CD95, which was mainly due to the lack of the final Casp8-mediated kill.

In addition, these observed CD95KO Casp8-mediated killing events seemed to be prolonged compared to the control Casp8-mediated kills. The control Casp8-mediated kills took around 160 min (Prager et al., 2019), whereas the CD95KO Casp8-mediated kills last around 737 min. This effect leads to the assumption that the control Casp8-mediated kills are mainly induced by CD95L, whereas the CD95KO Casp8-mediated kills are TRAIL mediated.

4.9 Serial killing activity of TRAIL KO NK cells in HeLa CD95 KO target cells

As shown above, there was still some Casp8-mediated killing detectable, but possessed a different kinetics. In CD95 KO HeLa target cells also other members of the TNF receptor family could account for a relevant share in Casp8-mediated killing, such as TRAIL. To further investigate whether CD95 KO HeLa target cells have the ability to be killed via TRAIL despite the fact that previous experiments showed a reduction of TRAIL expression on NK cells during co-cultivation with HeLa cells, the surface expression of TRAIL death receptors, like TRAIL-R1/R2, were examined by flow cytometry (**Fig. 20**).

In fact, HeLa target cells expressed low levels of TRAIL-R2, which could induce Casp8-meditated killing (**Fig. 20A**). To exclude TRAIL/TRAIL-R2-mediated killing, the CRISPR/Cas9 method was used to delete TRAIL in primary human NK cells.

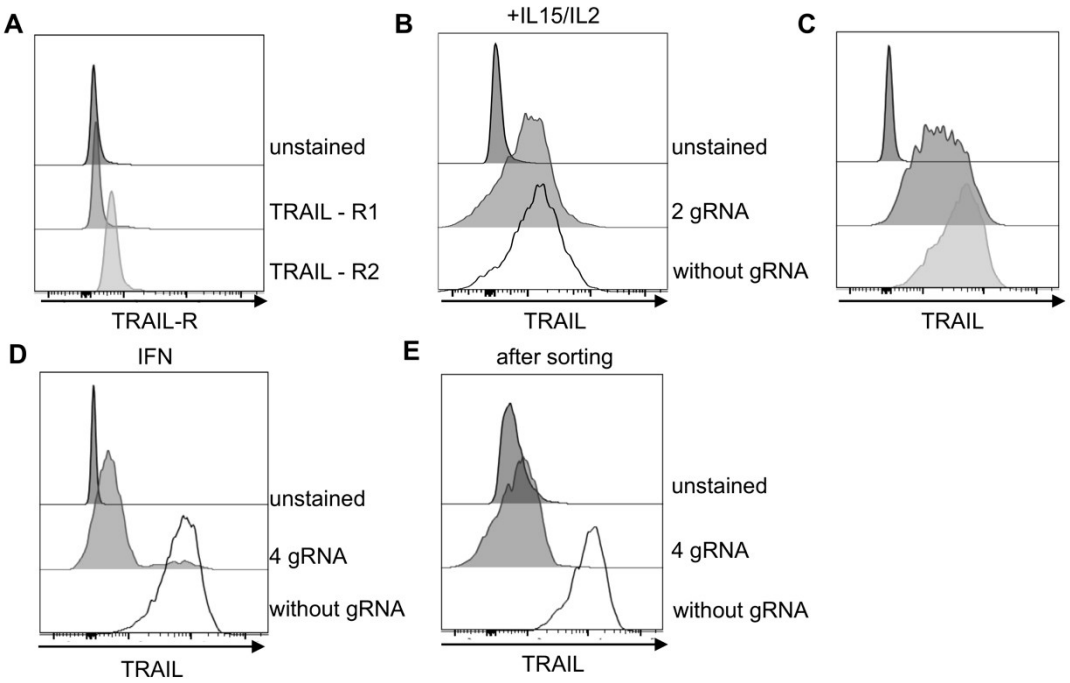

Figure 20 Different NK cell treatments to visualize generated TRAIL knockout. (A**)** HeLa-CD48-CD95 KO cells stably expressing NES-ELQTD-GFP-T2A-NES-VGPD-mCherry were stained with α-TRAIL-R1 or α-TRAIL-R2. **(**B-E**)** Cultured primary human NK cells were stained with a-TRAIL. **(**B**)** NK cells were cultivated with 100 U/mL IL-2 and 10 ng/mL IL-15 alone. **(**C**)** Cultured NK cells were incubated with 100 U/mL IL-2 and 10 ng/mL IL-15 (middle row) or with additionally 10 U/mL uni-IFN-α overnight. **(**D**)** CRISPR-Cas9-mediated or control NK cells (without sgRNA) were cultured for 7 days (100 U/mL IL-2 and 10 ng/mL IL-15) and after day six treated wit uni-IFN-α overnight. **(**E**)** NK cells were stained with α-TRAIL immediately after sorting.

To increase the expression of TRAIL on the NK cell surface, NK cells were stimulated with IL-15 and IL-2. This increased expression of TRAIL should help to distinguish after the CRISPR/Cas9 knockout between $TRAIL^+$ and $TRAIL^-$ NK cells. During the first knockout experiment, there was no KO visible, which was either due to that no efficient knockout was performed or a very low-level expression of TRAIL (**Fig. 20B**). It is known that TRAIL could be highly induced by IFN-α in fresh isolated NK cells (Papageorgiou et al., 2007). So, to overcome this issue of no detection, a treatment was performed with 100 U/mL universal IFN-α overnight, which led to an up-regulation of TRAIL on the surface of activated NK cells (**Fig. 20C**). Another experiment was performed to generate TRAIL-deficient NK cells using multiple sgRNA and after seven days of cultivation 100 U/mL IFN-α was added overnight. In the presence of IFN-α (**Fig. 20D**), the $TRAIL^+$ NK cells reached a high level of TRAIL, which allowed to distinguish them from the $TRAIL^-$ NK cells. The efficiency of the KO was 90 %. To generate 100 % TRAIL-KO NK cells, the 90 % deficient TRAIL NK cells were sorted on $TRAIL^-$. Also NK cells without sgRNA treatment were sorted on $TRAIL^+$ as a comparable control. Killing of HeLa target CD95 KO cells by the deficient-TRAIL NK cells as well as the control cells (control $TRAIL^+$ NK cells) were analyzed by time-lapse imaging using microchip platform.

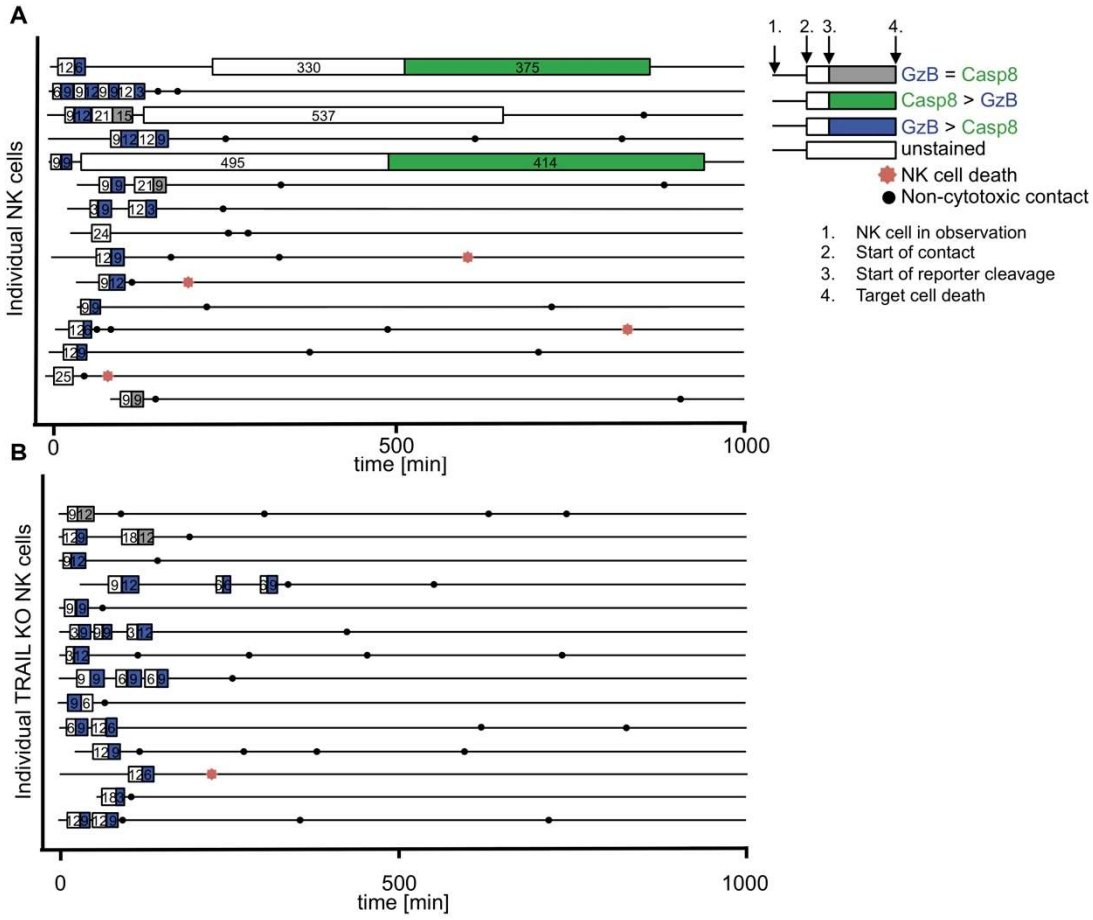

Figure 21: Lack of Casp8-mediated killing by application of TRAIL KO NK cells. (**A,B**) Serial killing activity of generated TRAIL WT (**A**) or TRAIL KO (**B**) NK cells (each experiment was performed with three independent donors) was analysed against HeLa-CD48-CD95 KO cells stably expressing NES-ELQTD-GFP-T2A-NES-VGPD-mCherry. Individual NK cells were tracked over 16 h, each line represents one NK cell. Every box visualized NK cell target cell contact. While the length of the boxes displays the duration of the cellular contact, the reporter cleavage is visualized by color (blue: GrzB > Casp8, green: Casp8 > GrzB, grey: GrzB = Casp8, white: HeLa target cells, which do not express NES-ELQTD-GFP-T2A-NES-VGPD-mCherry, named unstained). Non-cytotoxic contacts were represented by black dots and NK cell death is illustrated via a red star.

The analysis of the control TRAIL$^+$ NK cells showed serial killing, with first fast GrzB-mediated death and afterwards switch to a slower Casp8-mediated killing for the last kill (**Fig. 21A**). This switch to the slower Casp8-mediated killing was also reduced in this experiment. However, in the absence of TRAIL on the NK cell surface, serial killing of CD95 KO HeLa target cells via GrzB were still detectable, whereas the Casp8-mediated killing was lacking. Nevertheless, the serial killing activity of TRAIL KO NK cells mediated by GrzB was only detected during the initial 200 min. NK cells established multiple sequential contacts after the killing events, some made short-lasting noncytotoxic contacts, whereas other made long-lasting noncytotoxic interactions. These findings suggest functional exhaustion of NK cells after 200 min, which was not recovered in the last 760 min of the experiment.

Furthermore, in comparison with other single cell analysis (e.g. **Fig. 13** or **Fig. 15**), the mortality of the NK cells (control or TRAIL KO, data not shown) was increased.

As previously observed for CD95KO HeLa target cells (**Fig. 19**), the TRAIL$^+$ NK cells showed an extended Casp8-mediated kill compared to the control NK cells (Prager et al., 2019). However, as mentioned above, in co-cultivation of TRAIL KO NK cells with CD95 KO HeLa target cells no Casp8-mediated kill was detectable. This leads to the assumption that the Casp8-mediated kills could exclusively be initiated by either CD95L- or TRAIL-mediated signaling. Therefore, the observed Casp8-mediated killing events for TRAIL$^+$ NK cells (**Fig. 21**) as well as for unsorted NK cells (**Fig.19**) co-cultured with CD95 KO HeLa target cells seemed to be induced by TRAIL signaling.

4.10 Recovery of GrzB and perforin in NK cells after co-cultivation with HeLa target cells

As shown in the previous experiments a reduction in the amount of perforin and GrzB in CD107a$^+$ NK cells was detectable. The NK cells were able to release the majority of the cytotoxic granules, which resulted in an initial fast GrzB-mediated killing. After serial killing events the NK cells made multiple but non-cytotoxic contacts, which suggest that the NK cells were functionally exhausted. Nevertheless, the NK cells survived the process of serial killing, but never recovered their functional exhaustion. Based on the lost of the cytotoxic granules, we wanted to investigate if the replenishment of granules, especially of GrzB and perforin, can be performed with the stimulation of different cytokines.

Therefore, NK cells were incubated for 3 h or 1 h with HeLa target cells or without targets (as control). Afterwards, we sorted CD56$^+$7AAD$^-$CD107a$^+$ NK cells or CD56$^+$7AAD$^-$ NK cells for the control. Subsequently, the cells were treated for 1 h, 24 h or 48 h with various combinations of cytokines (IL-15/2, IL-15/2/21,IL-15, IL-2, IL-21) and stained for GrzB or perforin (**Fig. 22A**). The expression level of GrzB and perforin was still reduced after 1 h stimulation with various combinations of cytokines in degranulated NK cells compared to the control NK cells, when the NK cells were 1 h pre-activated with HeLa target cells (**Fig. 22B**). After 24 h and 48 h of cytokine stimulation with IL-15, IL-2 or IL-21 the mean GrzB signal (MFI) in degranulated NK cells was twofold elevated compared to control NK cells. The stimulation with the combination of IL15/2 or IL15/2/21 leads to an additive effect of the expression of GrzB after 24 h or 48 h in the degranulated NK cells as well as in the control NK cells. Interestingly, compared to the control NK cells, the IL-21 stimulated, degranulated NK cells had a minimal elevated perforin level after 24 h or 48 h.

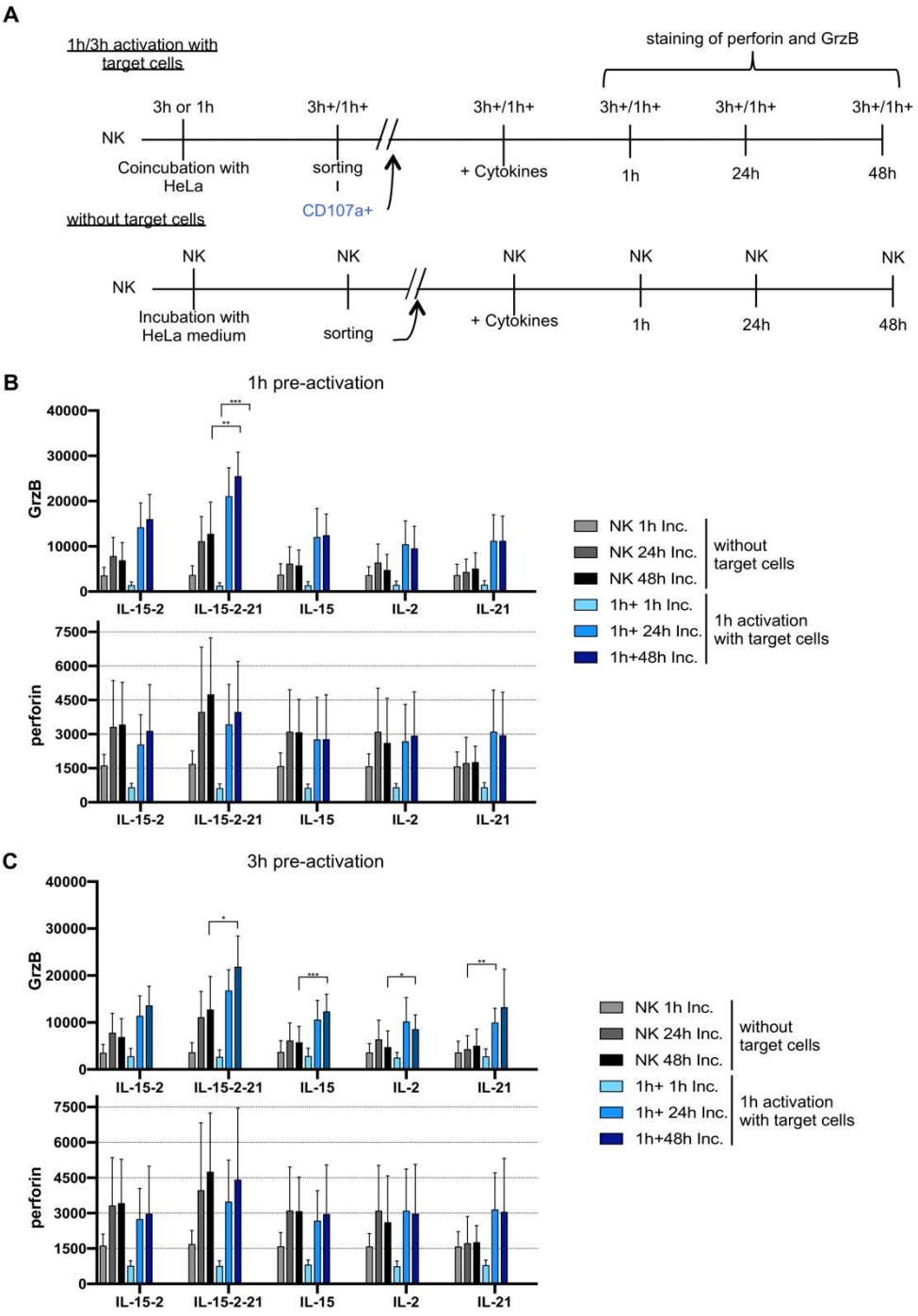

Figure 22: IL-15/2/21 restored GrzB expression whereas IL-21 alone restore perforin expression in NK cells. (**A**) Summary of experimental timeline of 1 h/3 h activated NK cells (1h/3h activation with target cells, upper row) or control NK cells (without target cells, lower row). (**B,C**) NK cells were co-cultured for 1 h (**B**) or 3 h (**C**) with HeLa-CD48 cells (E:T;1:2, bluish colour) or same donor NK cells were cultivated for 1 h (**B**) or 3 h (**C**) with HeLa-medium alone (grey colour). Afterwards, NK cells were re-isolated by sorting on $CD56^+7AAD^-CD107a^+$ (marked with +) or control NK cells were sorted on $CD56^+7AAD^-$ (marked with NK). NK cells were cultivated with various combinations of cytokines (IL-15/2/21, IL-15/2, IL-15, IL-2 or IL-21) and stained for GrzB (upper row, **B/C**) or perforin (lower row, **B/C**) after 1 h (light blue), 24 h (medium blue) or 48 h (dark blue).

Nevertheless, also the degranulated NK cells (after 24 h or 48 h) stimulated with other cytokines reached a constant basis level of perforin like the control NK cells. The data demonstrated that after 24 h in all different combination of cytokines the GrzB and perforin content in NK cells was recovered. We also observed comparable effects for GrzB and perforin in 3 h pre-activated NK cells (**Fig. 22C**). To summarize all data, the level of GrzB is elevated in IL-2, IL-15, IL-21 and with the combinations of IL15/2 and IL15/2/21, but perforin was only increased if the cells were singly stimulated with IL-21.

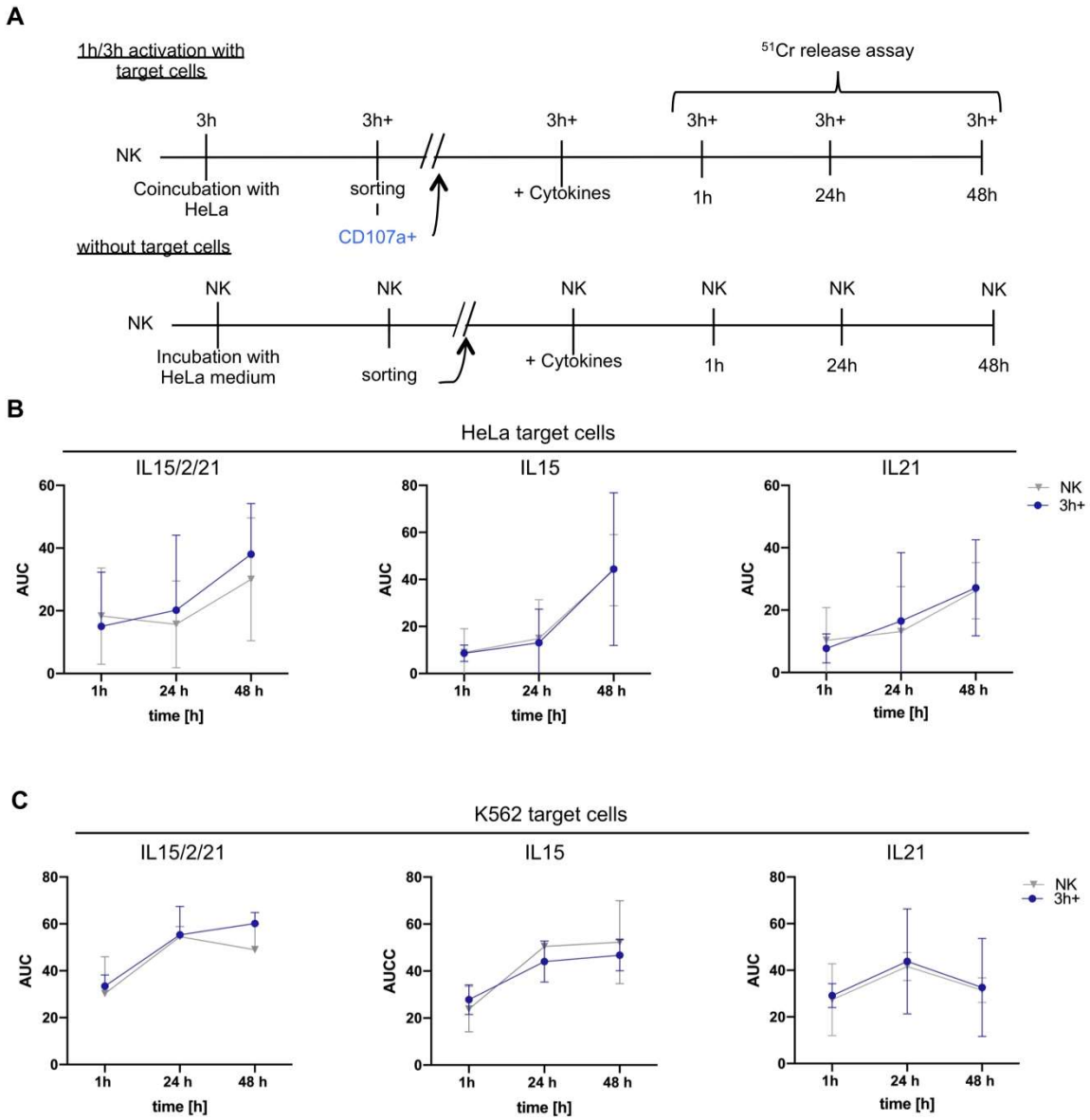

Figure 23: Cultivation with different cytokines showed no differences in killing ability of NK cells. (A) Summary of experimental timeline of 1 h/3 h activated NK cells (1h/3h activation with target cells, upper row) or control NK cells (without target cells, lower row). NK cells were co-cultured 3 h with HeLa-CD48 (E:T;1:2) or same donor NK cells were cultivated for 3 h with HeLa-medium alone. Afterwards, NK cells were re-isolated by sorting on $CD56^{+}7AAD^{-}CD107a^{+}$ or control NK cells were sorted on $CD56^{+}7AAD^{-}$ NK cells were cultivated with various combinations of cytokines (IL-15/2/21, IL-15 or IL-21). Thereafter cultivated NK cells were co-incubated with HeLa (**B**) or K562 (**C**) target cells for 4 h at an E:T of 1:1. The killing ability of the NK cells was tested after 1 h, 24 h or 48 h of cultivation.

Next, it was tested if these increased GrzB or perforin expression levels leads to an enhanced killing frequency. Therefore, NK cells were treated as described above and the killing activity was measured by a ^{51}Cr-release assay.

The ^{51}Cr-release assays were performed to account the overall killing efficiency of the differently stimulated degranulated and non-degranulated NK cells. For more efficient evaluation, the area under the curve (AUC) was calculated for each single time point. Additionally, in these experiments, HeLa cells (**Fig. 23B**) and also K562 cells (**Fig. 23C**) were used as target cell lines. However, almost all of the degranulated and control NK cells showed an increased killing activity in a time-dependent manner (1 h, 24 h, 48 h), whereas the IL-21 stimulated degranulated NK cells ($CD56^+7AAD^-CD107a^+$) and the control NK cells ($CD56^+7AAD^-$) against K562 exhibited a reduced killing efficiency. Stimulation with IL-15/2/21 or IL-15 lead to equal increasing of the cytolytic ability of NK cells, regardless of degranulated or control NK cells. In all experiments the degranulating compared to the control NK cells were found to be equally effective. However, the higher level of GrzB or perforin content of the degranulated NK cells compared to the non-degranulated NK cells showed no significant difference in NK cell cytotoxicity.

4.11 CD95L mRNA and protein expression in NK cells

It was illustrated in **Fig. 10** that NK cell surface protein expression of CD95L rose after one hour co-incubation with HeLa target cells, so the NK cells respond quickly upon activation by the HeLa target cell. Thus, this is leading to the question whether this effect is related to pre-formed mRNA or pre-formed protein stored in the primary human NK cells (**Fig. 24**)[*]

Western Blotting and real time RT-PCR were used to determine the relative CD95L protein and mRNA expression in primary activated NK cells (**Fig. 24A/B**). For the RT-PCR, the NK cells were co-incubated with HeLa cells for different time periods (1 h-4 h) and the mRNA level was analyzed afterwards. The mRNA expression of CD95L is not changed over the time. As housekeeping genes IPO8, B2M and GAPDH were used. As a positive control, IFN-γ was used, which showed an increased mRNA level at 2 h, which dropped after 3 h. To investigate if CD95L is stored as a pre-formed protein in primary human NK cells, the cells were treated with cycloheximide (CHX) which interferes with protein biosynthesis and thereby prevents regeneration of the protein level. Also in this

[*] "Analyse der stimulationsabhängigen Expression von CD95L und TRAIL auf NK-Zellen" generated by Markus Gilles in frame of his master thesis.

experiment, IFN-γ was measured in NK cells as a positive control. To measure IFN-γ intracellular in the NK cells, the IFN-γ-secretion have to be inhibited. To do so, the NK cells were treated with brefeldin A to interrupt the vesicle transport from ER to Golgi, which prevents the exocytosis of the vesicle.. The co-cultured NK cells with HeLa target cells showed a strong expression of CD95L on their surface after 4 h (4 h, **Fig. 24C**). This effect was not influenced by the addition of DMSO or CHX (CHX, DMSO, **Fig. 24C**). The expression of IFN-γ was also measured in the presence of IL-12/18 and brefeldin A, which did not inhibit the expression of IFN-γ in NK cells. Nevertheless, with the addition of CHX IFN-γ was not detectable anymore. Therefore, it was confirmed that the inhibition induced by CHX was effective. As an additional confirmation, we used the western blot technology, the expression level of CD95L protein in primary activated NK cells was monitored. This showed that CD95L seems to be stored in primary human NK cells as pre-formed protein.

In the next step the CD95L expression stability was investigated. For this assay, the activated primary human NK cells were co-cultured with HeLa cells for different time periods (1 h, 3 h). CD45 acted as NK cell marker to exclude HeLa cells from the flow cytometry analysis. Additionally, to distinguish between active or inactive NK cells, experiments including the degranulation marker CD107a, were performed. Afterwards the cells were sorted on $CD107a^{+}$. After the sorting process the NK cells were stimulated with IL-2/15 and incubated for different time periods without HeLa target cells. The expression of CD95L was detectable on the surface of NK cells after 1 h of co-incubation. During the incubation time of 3 h there was a further increase of CD95L. After the sorting process and additional 2 h incubation time with IL-2/15 a minor reduction of CD95L was detectable. This effect was observed regardless of 1 h (1 h + 2 h) or 3 h (3 h + 2 h) pre-activation by HeLa target cells. During 18 h of incubation a further decrease was noticed, however even after 18 h of incubation a significant level of CD95L was still present on the cell surface of both pre-activated NK cells (1 h + 18 h, 3 h + 18 h, **Fig. 24D**).

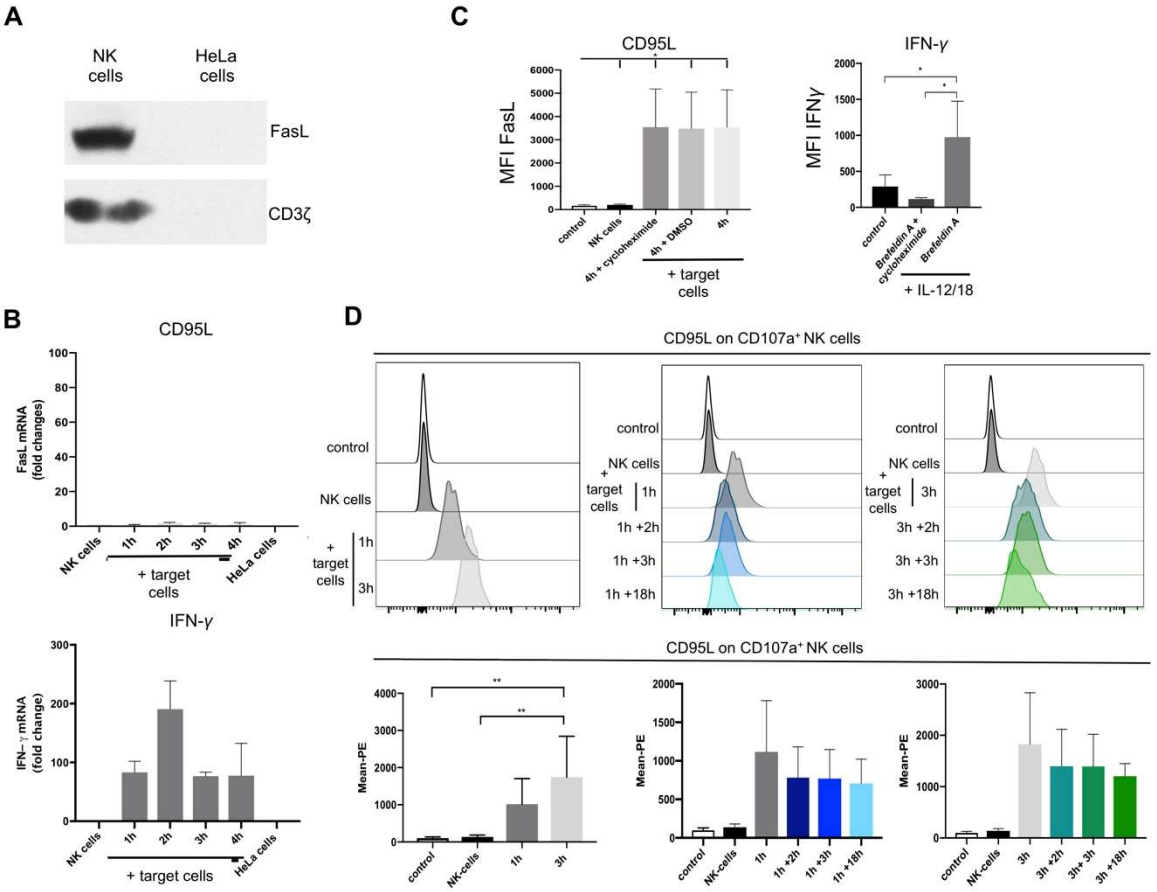

Figure 24: CD95L is stored in NK cells. (**A**) IL15 and IL-2 activated NK cells and HeLa cells were blotted for CD95L and CD3-ζ. NK cells were co-cultured with HeLa-CD48 for a time period from 1 h until 4 h. (**B**) After co-cultivation a RT-PCR analysis for CD95L, IFN-γ mRNA is depicted, which were first normalized to NK cells without co-cultivation, secondly set to the three different housekeeping genes (IPO8, GAPDH and B2M). (**C**) NK cells were pre-treated with cycloheximide (CHX) or DMSO for 30 min. Thereafter, NK cells were co-cultured with HeLa-CD48 for 4 h and stained for CD95L on CD107a$^+$ NK cells. For IFN-γ staining, NK cells were pre-treated with brefeldin A and CHX or brefeldin A alone for 30 min and afterwards cultivated with IL-12/18. (D Left histogram illustrated the staining for CD95L on CD107a$^+$ NK cells, beforehand NK cells were co-cultured with HeLa-CD48 for 1 h and 3 h. Middle histogram represented the staining for CD95L after sorting process (CD56$^+$CD107a$^+$) and cultivation for 2 h, 3 h or 18 h (+2 h, +3 h or +18h) for the pre-cultivated NK cells of 1 h. Right histogram illustrated the same results as the middle one just for 3 h. In the lower row Diagrams exhibited the mean fluorescence staining intensity (MFI) of three independent experiments for CD95L.

4.12 Serial killing activity of ILC3

Innate lymphoid cells (ILC) can be classified into five subsets NK cells, ILC1s, ILC2s, ILC3s and LTi cells. ILC3 can be discriminated in two subsets by the expression of NKp44. The NKp44^{neg} ILC3 cells are typically characterized by the secretion of IL-17A and express T-bet, RORγt and the surface marker CD117 (c-kit).(Lo et al., 2016) NKp44^{neg} ILC3s can eventually develop into NKp44^{pos} ILC3s with IL-1β and IL-23 stimulation (Teunissen et al., 2014). However, NK cells and ILCs are functionally different. ILC3s are devoid of perforin and GrzB and they are unable to kill via the granule-dependent mechanism (Hazenberg and Spits, 2014). Noteworthy, ILC3s have a high level of TRAIL expression in human tonsils (Nagasawa et al., 2019). Taking these aspects into consideration, ILC3s are natural generated cells, which lack perforin and have a high level of TRAIL expression. It is little known about the killing ability of ILC3. To acquire deeper insights into the killing ability of these cells, ILC3 cells were obtained in collaboration with Jana Götz (UMM, Germany) to perform single cell analysis with microchips. Therefore, ILC3 cells were co-cultured with HeLa target cells and the killing events were analyzed via time-lapse video microscopy. Beforehand, ILCs were isolated from blood and sorted by Jana Götz (UMM, Germany) on CD45^{+}, NKp44^{-}, Aqua Zombie-, Lin^{-} (CD3^{-}, CD19^{-}, CD14^{-}, CD34^{-}, CD94^{-}, CD123^{-}, TCR α/β^{-}, TCR γ/δ^{-}, FCεR1α^{-}), CD127^{+}, c-Kit^{+} and CRTH2^{-} and cultured with 10 U/ml IL-2, 100 ng/mL IL1β and 100 ng/mL IL-23 in GlutaMAX (RPMI medium with 1 % P/S, 10 % human serum) overnight (**Fig. 25**).

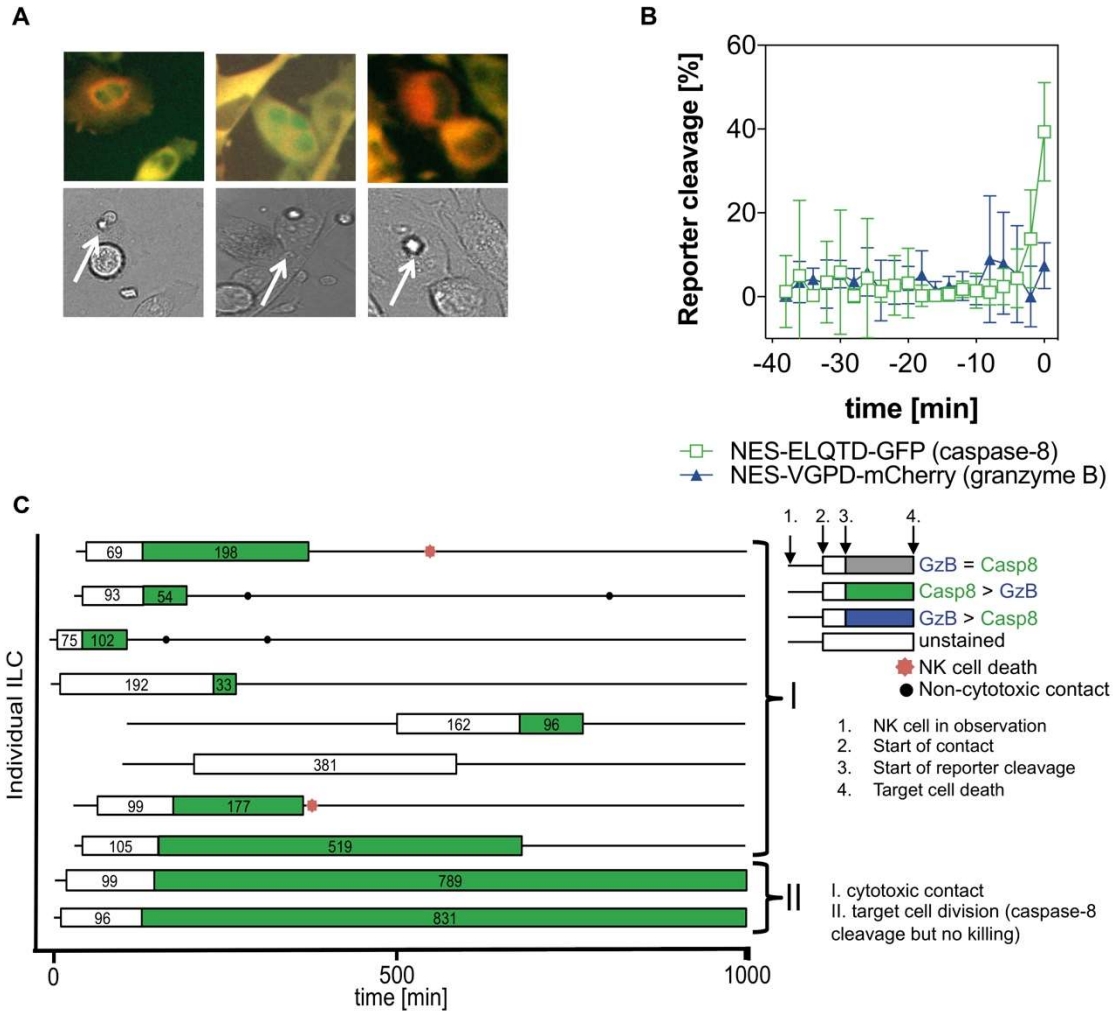

Figure 25: Lack of GrzB reporter cleavage by application of ILCs. Blood ILC3s were sorted on CD45$^+$, NKp44$^-$, Aqua Zombie-, Lin$^-$ (CD3$^-$, CD19$^-$, CD14$^-$, CD34$^-$, CD94$^-$, CD123$^-$, TCR α/β$^-$, TCR γ/δ$^-$, FCεR1α$^-$), CD127$^+$, c-Kit$^+$ and CRTH2$^-$ and cultured with 10 U/ml IL-2, 100 ng/mL IL1𝛽 and 100 ng/mL IL-23 in GlutaMAX overnight. Serial killing activity of ILCs was analyzed against HeLa-CD48-CD95 KO cells stably expressing NES-ELQTD-GFP-T2A-NES-VGPD-mCherry, IL-2 was permanent presence in the experiment. (**A**) Three examples for the initial killing events of three individual killer ILCs with according enzymatic activity (green nuclear signal declared Casp8 activity). ILCs were visualized via brightfield (lower row) and marked with white arrowheads. (**B**) Initial killing activity of primary human ILCs of single cells (mean ± SD, time point 0 set to time of cell death) with more Casp8 than GrzB reporter cleavage was illustrated in HeLa-CD48-CD95KO target cells stably expression NES-ELQTD-GFP-T2A-NES-VGPD-mCherry with 100 IU/mL IL-2. (**C)** Individual ILCs were tracked over 16 h, each line represents one ILC. Every box visualized ILC-target cell contact. While the length of the boxes displays the duration of the cellular contact, the reporter cleavage is visualized by colour (blue: GrzB > Casp8, green: Casp8 > GrzB, grey: GrzB = Casp8). Non-cytotoxic contacts were represented by black dots and ILC cell death is illustrated via a red star.

Figure 25A gives three examples for the initial killing activity of three single ILCs that showed cleavage of the Casp8 reporter. As expected, these kills were dominated by Casp8 activity. The 10 individual ILC cells showed different death kinetics, whereas some Casp8 kills took around 247 min (first seven ILC cells) other Casp8-mediated kills took much longer (820 min, **Fig. 25C**). Additional contacts after the first kill were observed but no second Casp8-mediated kill occurred. This suggests that the ILC3 cells used the Casp8-mediated killing once, similar to the perforin KO or the CMA-treated NK cells.

Therefore, this experiment illustrated that the Casp8 activity was due to activation of the death receptor-mediated pathway by ILC3 cells.

In addition, we also observed within these ILC3 cells prolonged Casp8-mediated kills. ILC3 cells are described to lack GrzB as well as perforin and in addition they express a high level of TRAIL on their surface. This leads to the assumption that these Casp8-mediated kills seemed to be induced by TRAIL signaling.

5 Discussion

In previous studies, specific protease bionsensors based on luciferase-dependent bioluminescence (Vrazo et al., 2015, Kanno et al., 2007, Li et al., 2014), fluorophore quenching (Packard et al., 2007), FRET imaging (Choi and Mitchison, 2013) or subcellular localization of a fluorophore were used to study the killing mechanism of NK cells. However, these protease biosensors do not easily allow multiplexing for the quantification of two protease activities in a single cell. The parallel assessment and quantitative monitoring of two protease activities (GrzB and Casp8) within the same target cell was only possible through the development of our specific reporter.

An early study by LIESCHE et al. and our data revealed that the GrzB reporter with the amino acid sequence VGPDF is specific for granule-mediated cytotoxicity, while at the same time it was not activated during death receptor-mediated apoptosis (ref to **Fig. 21**). In addition, also the Casp8 reporter with the amino acid sequence ELQTD is specific for death receptor signalling and not influenced by cytotoxic granules (also refer to **Fig. 7, Fig. 11, Fig. 12, Fig. 23**). For the granule-mediated pathway, GrzB cleavage was used as readout. Noteworthy, also other Grz activities like GrzA, GrzM, GrzK and GrzH contribute to this killing mechanism, but GrzB showed the prominent activity in our experiments (Liesche et al., 2018). If GrzB is inhibited or GrzB KO is performed, GrzA may provide a "back-up" system for GrzB (Shresta et al., 1999), but further research is required to prove this theory.

Different kinetics of cytotoxicity for granule- and death receptor-mediated cytotoxicity were observable. By extensively studying the different kinetics of cytotoxicity, we showed that there was no difference in the time span from contact to NK cell commitment for both killing pathway. Nevertheless, the time from NK cell contact to reporter cleavage and cell death was much longer for Casp8-mediated kills, which is consistent with previous studies (also refer to **Fig. 8**, **Fig. 11**, **Fig. 12**). The longer time period until cell death in Casp8-mediated kills may be explained by receptor activation including receptor clustering and recruitment of FADD. Additionally, the binding of pro-Casp8 to FADD, resulting in the formation of active Casp8 heterotetramer, takes around 10 min after the stimulation with CD95L or 30 min after the stimulation with TRAIL (Hoffmann et al., 2009). This activation of Casp8 activates other caspases, which results in a caspase cascade. All these recruitments and activation take time until the cell undergoes apoptosis. In contrast, granule-mediated killing is initiated by the efficient and focused release of activated GrzB to the cytosolic compartment of the target cell. In addition, GrzB can induce apoptosis caspase-dependent but also -independent in contrast to the death receptor-mediated

pathway. So, even if Casp8 is activated, the time to initiate cell death via the death receptors takes much longer to induce apoptosis compared GrzB-mediated killing. Noteworthy, the different kinetics of GrzB-mediated cell death was not dependent on the time point of the cell death during serial killing (ref. to **Fig. 11**, **Fig. 12**, **Fig. 19** (Prager et al., 2019) or related to impaired expression of proapoptotic or antiapoptotic regulators in the target cell (ref. to **Fig 8**). Consequently, the results of this study provide evidence that fundamental kinetic differences are inherent to the individual cell death pathway.

Interestingly, we also observed some death kinetic differences within the Casp8-mediated kills. Perforin deficient NK cells that had non-cytotoxic contacts before they killed the target cell via death receptor-mediated apoptosis showed a reduced time span of NK cell contact to reporter cleavage in comparison to the perforin KO and CMA-treated NK cells that killed their first target cell (ref to **Fig. 11** and **Fig.12**). This reduced time span suggests a faster Casp8 cleavage. A possible explanation for this observation may be that NK cells get primed in these non-cytotoxic contacts for a quicker successive kill. This effect was also observed in control NK cells, which initially killed via GrzB-mediated killing. In this step, the NK cells seem to get primed. For their last killing event, these cells used the Casp8-mediated pathway to induce apoptosis, which showed a comparable time span to the perforin deficient NK cells.

It was described that only a very small fraction of all NK cells represent a serial killer (Vanherberghen et al., 2013). In comparison with our results (ref. to **Fig. 8**), 270 NK cells out of 347 tracked NK cells killed one target, whereas 214 NK cells out of these 270 NK cells killed two targets. Furthermore, only a small fraction of 15 NK cells was able to kill six targets in a row. In conclusion, only 5 % of all tracked NK cells killed six targets in a sequent manner, confirming the previously described observations.

Different cell death phenotypes between death receptor and granule-mediated cytotoxicity were discovered (ref. to **Fig. 8**(Prager et al., 2019)). Casp8-mediated killing was clearly associated with typical programmed cell death, apoptosis, which was visible by the characteristic apoptotic morphologic changes, like blebbing, cell shrinking and cell condensation (Saraste and Pulkki, 2000). GrzB activation was correlated with a non-apoptotic-like behaviour with membrane rupture and necrotic phenotype (Prager et al., 2019). Also an intermediate phenotype (mixed form of apoptosis and necrosis) induced by GrzB was observed, which was also described by other groups (Backes et al., 2018). The observation of the necrotic phenotype could be related to granule release process. It was previously shown that for the granule-mediated killing just two to four granules are sufficient to induce cell death, nonetheless NK cells release around 10 % of their total

granules (YTS and NK92 contain an average of 194 and 206 lytic granules) in a single event (Gwalani and Orange, 2018). In fact, the NK cells release more granule content, maybe to ensure target cell killing. The necrotic phenotype (non-apoptotic like phenotype) could be related to high concentrations of perforin due to the high amount of granule content released by the NK cells. KEEFE et al. illustrated that the sublytic concentration of perforin to induce apoptosis with GrzB is between 50 and 500 ng/mL, which is dependent on the target cell (Keefe et al., 2005). If the sublytic concentration of perforin is exceeded, the cells die via the necrotic pathway. Furthermore, the nonapoptotic cell death was much more likely in the initial killing event for activated serial-killing NK cells compared with activated NK cells which only killed one or two targets, or in comparison with resting NK cells. This result implies that serial killers may release comparatively more GrzB and perforin per killing event (Vanherberghen et al., 2013). Alternatively, this necrotic phenotype could be caused by the induction of pyroptosis triggered by the activation of Casp3 (Rogers et al., 2019, Wang et al., 2017) or GrzB (Zhang et al., 2020). Pyroptosis is a necrotic form (highly inflammatory form) of programmed cell death driven by different members of the gasdermin superfamily, like gasdermin E (GSDME) (D'Arcy, 2019). GSDME consists of two0 domains, gasdermin-N and -C, and cleavage between these two domains by Casp3 or GrzB leads to the translocation and oligomerization of gasdermin-N in the plasma membrane and in the mitochondria (Rogers et al., 2019). GSDME is able to form pores like perforin in the plasma membrane as well as the mitochondria membrane. Taken together, it seems to be more likely that necrosis is responsible for the necrotic phenotype than the pyroptosis, because necrosis is faster than pyroptosis. A closer look on the necrotic phenotype reveals that there do exist at least two possible explanations for it, either more released granules per killing event or higher granule content in serial killer NK cells. GOODRIDGE et al. could show that there is a correlation between increased dense-core secretory granules and better NK cell effector functions in educated NK cells (Goodridge et al., 2019). These dense-core secretory granules could also be responsible for the functionality of serial killer NK cells.

The data demonstrates that NK cells could switch their killing mechanism during serial killing. Within the early phase, the cells showed a very low Casp8 activity. Therefore, it seems likely that the death receptor signaling and GrzB activation was initiated simultaneously (Kajino et al., 1998). Nevertheless, the fast granule-mediated pathway dominates over the slower death receptor mediated cell death. After intense exocytosis, the majority of the granule content was released and the concentration of surface CD95L was increased (ref. to **Fig. 10**). Thus, the death receptor mediated pathway became more dominant and the final kill was often induced by the death receptor-mediated apoptosis.

The death receptor mediated signaling seems to be a cytolytic back-up system for the gradual depletion of GrzB and perforin to ensure efficient killing. Interestingly, GrzB and perforin were still detectable inside the NK cell, even after multiple killing events. This is in line with the finding that NK cells release about 10 % of their total amount of lytic granules per killing (Gwalani and Orange, 2018), and a maximum of six kills in a row was detectable (ref. to **Fig. 8**).

We assume that these Casp8-mediated kills were CD95L induced, but also the membrane bound TRAIL seems to play a role in the Casp8-mediated pathway. TRAIL seems to be distributed on the whole surface and therefore not concentrated at any specific part of the NK cell surface and it is reduced in a time dependent manner (ref. to **Fig. 10**). However, if we knockout the CD95 pathway, we still observed some Casp8-mediated killing, which showed prolonged Casp8-mediated kills in comparison to the control HeLa target cells. These Casp8-mediated apoptosis could be induced by two different ligands TNF or TRAIL. After knockout of TRAIL on the NK cell surface, no Casp8-mediated kill was observable. This demonstrates that these extended Casp8-mediated kills in the CD95 KO HeLa target cells in comparison to the control HeLa target cells are indeed TRAIL induced.

Based on the observation that residual amount of GrzB and perforin is still stored inside the NK cells after extensive killing, the question arises why the NK cells stop using this stored GrzB and perforin. Therefore, other factors might impact the serial killing process that limits the GrzB-mediated apoptosis. One potential limitation factor is the down-regulation or shedding of activating receptors, like 2B4, DNAM-1, NKG2D (Netter et al., 2017) or CD16 (Srpan et al., 2018). From target cell point of view, also a reduced expression of the activating ligands MICB, Nectin-2 and B7-H6 on the target cell after apoptosis was shown (Anft et al., 2020). This loss of activating ligands on the target cell surface could be induced by shedding or by internalization. The shed ligand could bind to the activating receptor, which leads to a reduced activation signaling for the subsequent kills. In addition, experiments with NK cells incubated with antibody-conjugated surfaces showed that switching the activating receptor could replenish perforin secretion (Srpan et al., 2018). This leads to the assumption that if the NK cells are continuously stimulated by same activating receptor, the cells stop inducing GrzB-mediated apoptosis after multiple kills. Once the NK cells are stimulated with a different activating receptor, the NK cells restart to release GrzB and perforin.

Furthermore, after depletion of GrzB and perforin due to intense exocytosis, the recovery of both could be demonstrated by treatment with different cytokines (ref. to **Fig. 22**). This

is in line with previously shown data, where a replenishment of GrzB and perforin was shown within 2 days by IL-2 or IL-15 treatment after loss of the granules during serial killing (Bhat and Watzl, 2007). However, during this study it could be observed that GrzB or perforin concentration within the degranulated NK cells was not only recovered but even up-regulated after 1 day, and further increased over time compared to the control NK cells (ref. to **Fig. 22**). The stimulation with IL-2, IL-15 or IL-21 seems to be very potent to induce the recovery of GrzB, whereas the combination of IL-2 and IL-15 or IL-2, IL-15 and IL-21 did not lead to a synergistic effect. The recovery of perforin was only observed, if the NK cells were stimulated with IL-21. This suggests that IL-2, IL-15 and IL-21 are not only important for survival and maintenance of NK cells but also necessary for the regeneration of exhausted NK cells. IL-2, IL-15 or IL-21 were described to increase the protein expression level of GrzB and perforin on freshly isolated NK cells (Janas et al., 2005, Zhang et al., 2018, Skak et al., 2008). However, this effect of upregulation was not observed for perforin with the stimulation IL-2 and IL-15. This suggests that there may be a difference in stimulation between freshly isolated NK cells and pre-activated NK cells that had degranulated.

From the ^{51}Cr release data we conclude that the stimulation with IL-2, IL-15, IL-21 or the combination of cytokines, degranulated NK cells as well as the stimulated control NK cells showed a comparable cytotoxicity (ref. to **Fig. 23**). However, it must be considered that the results from the ^{51}Cr release assay only illustrated average killing frequencies as bulk cell measurement and not the NK cell activity on a single cell level. Furthermore, TOMESCU et al. performed similar experiments and described that cytotoxic capacity of the degranulated and the non-degranulated NK cells were comparable (Tomescu et al., 2009), which is in line with our results. In conclusion, the data showed that up-regulation of either GrzB or perforin in comparison to the control cells do not lead to an increased cytotoxicity of the NK cells. This complies with the assumption that both GrzB and perforin in combination are required for efficient granule mediated killing *in vitro*. In addition, this effect could also be observed in *in vivo* experiments (Fehniger et al., 2007).

The recovery of GrzB and perforin could be observed for NK cells separated from the target cells (ref. to **Fig. 22**). Moreover, it is well-known from the literature that the dissociation of the NK cells from target cells may be the crucial step for the regeneration of the degranulated, exhausted NK cells. It was described that, if the NK cells were separated from their conjugates, the cytotoxic activity of exhausted NK cells could be increased by IL-2 stimulation (Jewett and Bonavida, 1996). However, if the NK cells were treated the same but not dissociated from the target cells, no recovered cytotoxic activity could be detected. This aspect is in line with the results that after switching from GrzB-

mediated pathway to the Casp8-mediated kill, a granule-mediated kill did not occur again during the 16 hours microscopy experiments (ref. to **Fig. 8**).

For an efficient serial killing process, a regulation of detachment is necessary. In the absence of perforin, NK cells showed a delayed detachment from target cells (Jenkins et al., 2015, Anft et al., 2020). In untreated cells, the acidic pH in the granules seems to be necessary for perforin to stay inactivated within the granules, the polymerization of perforin is pH and Ca^{2+}-dependent. As illustrated above (ref. to **Fig. 11**, **Fig. 12**), NK cells were treated with CMA to prevent maturation of perforin. In detail, CMA treatment results in proteolytic degradation and inactivation of perforin, as CMA interferes with the vacuolar type H^{+}-ATPase, which leads to an increased pH in the lytic granules (pH 5.7 $\pm$ 0.2 to pH 6.8 $\pm$ 0.2 in CTL) (Kataoka et al., 1996). As mentioned above, for the polymerization of perforin neutral pH is needed, which is achieved by the treatment with CMA. This leads to an ideal environment for the generation of perforin polymers, but perforin fails to induce autolysis due to the fact that a neutral pH is not sufficient for perforin polymerization, as this step is also Ca^{2+}-dependent. The Ca^{2+} levels within the resting lytic granule are very low (69 $\pm$15 μM), but the pore formation of perforin requires a minimum of 0.2 mM Ca^{2+} concentration (Dickson et al., 2012). In conclusion, the treatment with CMA leads to a neutral pH, but the Ca^{2+} concentration is too low, that perforin can form pores. Nevertheless, after only one hour incubation after CMA treatment a full degradation of perforin was visible, which was still gone after subsequent 16 hours (ref. to **Fig. 11**). This might be due to the fact that perforin is preformed as a protein in the granules and no preformed RNA is stored (Kataoka et al., 1997). However, the proteolytic degradation of perforin is not fully understood and needs to be investigated further. In addition, it was also observed that perforin stayed 16 h in their immature form (ref. to **Fig. 11**). An explanation for this effect could be that immature perforin is bound to calreticulin (Fraser et al., 2000) or CD107a (Cohnen et al., 2013), which keeps it quiescent. Otherwise this could be caused by the inhibition of cathepsin, which is only active in slightly acidic conditions (Barrett and Kirschke, 1981). Therefore, it is likely that there exists a kind of back-up system to prevent autolysis if the acidic environment of the lytic granules is lost. The CMA treated NK cells showed a delayed detachment, which could be caused by the decreased NK cell cytotoxicity as a sufficient kill is required for the detachment (Anft et al., 2020).

Another approach we used to interfere with proteins that are indispensible for NK cell cytotoxicity was the knockout using the CRISPR Cas9 system. The main difference between the CRISPR Cas9 knockout and the treatment with inhibitors is that a knock out removes target genes from the cell. In contrast, the pharmacological inhibition only blocks

the function of the protein, but the protein is still present. If the protein is drug-inhibited, it may lack a specific activity but is likely to interact with different binding partners. Noteworthy, the pharmacological inhibition takes place immediately, while the effect of the KO is delayed by days to observe the effect depending on the turnover rate of the protein. To exclude off-target effects from CMA, perforin KO NK cells were generated, however, the results with perforin KO NK cells were in line with the previous results of the CMA treatment. In combination with the data from ANFT et al. it was demonstrated that there is a clear correlation between detachment and successful cytotoxicity (Anft et al., 2020). For CMA-treated or perforin KO NK cells we observed a significant increase in the time from contact to detachment. It can be assumed that there could be a correlation between the delayed detachment and the cell death pathway CMA treated or perforin KO NK cells used to kill their target cells (ref. to **Fig. 11**, **Fig. 12**). It can be hypothesized that the delayed detachment is a consequence of the Casp8-mediated killing mechanism, which was shown to take much longer time than the GrzB-mediated pathway. Interestingly, it could be observed that the time from target cell death to detachment was not significantly different between perforin depleted NK cells and control NK cells, confirming that detachment is regulated by target cell death.

GrzB and CD95L are stored in different vesicular compartments inside CTLs and human NK cells (Schmidt et al., 2011, Schmidt et al., 2008). GrzB is localized in vesicles that contain additionally CD107a (LAMP-1), whereas CD95L is more co-localized in granules with CD63 (LAMP-3) (Lee et al., 2018). Interestingly, our data (ref. to **Fig. 10**) showed that the $CD107a^+$-degranulating NK cells lost their GrzB and perforin but in parallel expressed CD95L on their surface. So, the surface expression of CD95L was confined to $CD107a^+$-degranulating NK cells. It seems that these vesicles were both released though the stimulation with the HeLa target cell. However, our results do not allow a statement if there is a connection within the regulation of these distinct vesicular compartments. Other studies revealed that the CD63 vesicles are different to lytic granules regarding their regulation of degranulation (Kassahn et al., 2009). This data additionally supports the theory that GrzB- and perforin-exhausted NK cells seem to use the death receptor signaling as a back-up mechanism to maintain cytotoxicity. The results of the CD95KO HeLa target cells underlined this thesis additionally, as they showed a decreased serial killing activity of NK cells, which could be correlated to the missing back-up mechanism by CD95L. Additionally, using the CD95KO HeLa target cell in co-cultivation with TRAIL KO NK cells, the serial killing activity was even more decreased.

In general, after a Casp8-mediated kill there was hardly another kill induced by the NK cell. This could not be a consequence of NK cell exhaustion, because perforin

depleted NK cells induced also only one Casp8-mediated kill (ref to **Fig. 11**, **Fig. 12**). However, the question arises why the NK cells are unable to induce serial killing using the death receptors. This effect may be explained by different theories. On the one hand the accumulation of CD95L on the NK cells surface is induced by activation as explained above. After every induced degranulation, stored CD95L seems to be released and accumulated at the IS. For the last kill, which is predominantly Casp8-mediated, it seems that the majority of stored CD95L is released at the IS and induces Casp8-mediated apoptosis. So, the kill induced by Casp8 is possible because of the extremely focused accumulation of CD95L, which is preformed as a protein but not as mRNA, similar to perforin. It can be assumed that this focused distribution of CD95L on the NK cells surface plays a major role in perforin deficient NK cells as well as serial killers.

The question arises, why there is no exhaustion of CD95L during the serial killing process if the NK cells delivers CD95L to the IS during every degranulation. Other studies showed that CD95L was polarized at the IS after target cell recognition but less effective as perforin (Lee et al., 2018). Therefore, it can be concluded that CD95L is polarized to each degranulation process, but the majority of CD95L is only be delivered during the last killing event, as this step needs more time.

On the other hand, shedding of the CD95 ligand could reduce its concentration at the NK cell surface. One publication revealed that CD95L could be cleaved by metalloproteinases (ADAM10) (Ebsen et al., 2015), which was seen in different human T lymphocyte cell lines (Mariani et al., 1995), but is unknown for NK cells. So, this effect is only described for T cells but $CD8^+$-T cells and NK cells develop from the same common lymphoid precursor and share multiple features like effector cytokine secretion and cytotoxicity. In light of their common function, the assumption appears that the CD95L concentration at the NK cell surface could be also reduced by metalloproteinases. Nevertheless, our data showed that CD95L is extremely stable on the NK cells surface (66 %), after 16 h of co-cultivation with HeLa target cells (ref to **Fig. 24**). The small reduction could be mediated by metalloproteinases or internalization. Nevertheless, there was still CD95L left on the surface of the NK cells but rarely any second kill induced by Casp8 was observable.

However, also the shed death receptor ligands could take part in insufficient second Casp8-mediated kill. The soluble monomer CD95L (sCD95L) cannot induce apoptosis, in contrast to CD95L homotrimers. As there was only a low reduction of CD95L surface expression measurable, the concentration may be too low to form homotrimer in the supernatant. The TRAIL expression on NK cells was reduced in a time dependent manner, which may lead to soluble TRAIL in the medium. Soluble TRAIL (sTRAIL) is able

to induce apoptosis, when it binds to membrane-bound death receptor 4 (DR4) and DR5 (Bodmer et al., 2000, Kischkel et al., 2000). In contrast, soluble CD95 ligand is able to block a second Casp8-mediated kill by binding to the receptor (CD95) (Tanaka et al., 1998).Taken together, this data demonstrate that a second Casp8-mediated kill rarely occurs, therefore, serial killing via the Casp8-initiated mechanism is unlikely.

ILC3 lack cytotoxic effector molecules like GrzB or perforin, they only express the pro-apoptotic factor TRAIL on their surface. Also these cells showed no serial killing activity via death receptor mediated apoptosis. This demonstrates that it seems to be independent of the distinct cell type, that cells are not able to kill several target cells in a serial manner by death receptors.

Both CTL and NK cells can kill multiple target cells, but operate in a sequential manner. It could also be shown that both cell types can use death receptor and granule-mediated killing pathways. In this thesis, only NK cell serial killing was examined, because of same common lymphoid precursor it appears safe to assume that CTL can use a similar switch between the cytotoxicity pathways. NK cell like cell lines, like NK92 are also able to kill several target cells in a serial manner. Using different knockout cell lines like ADAP KO markedly reduced the serial killing activity of the NK92 cells (ref. to **Fig. 11**). It is tempting to speculate that the deficient ADAP NK cells reduced the killing but did not influence the detachment or attachment of the NK cell to the target cell. In addition, other *in vivo* experiments with *Lm infected* mice showed a significant lower expression of CD107a in ADAP KO NK cells (Boning et al., 2019). This could be another explanation, why ADAP KO NK cells showed a reduced serial killing activity. This leads to the assumption that the formation of an immunological synapse failed.

The most often used target cell line in all these experiments are HeLa cells expressing CD48, which is the ligand for the activating receptor 2B4. The additional expression of CD48 on these target cells is described to result in a slight increase of the NK cell cytotoxicity but it has a high impact of the conjugate formation. There are two possible explanations for this influence. Initially CD48 can also bind to NK cell adhesion receptor CD2, increasing the adhesion (Arulanandam et al., 1993). An alternative explanation is that 2B4 binds to CD48, which increases the affinity of LFA-1 to ICAM molecule by inside-out signaling (Hoffmann et al., 2011, Urlaub et al., 2017, Anft, 2017). Interestingly, LIESCHE et al. could obtain similar results with HeLa cells without CD48 and MDA-MB-468 breast carcinoma cells in comparison to HeLa CD48 cells. As all tumor cell lines express distinguished ligands to activate NK cell receptors, it seems that the mediated switch from granule to death receptor mediated pathway is not restricted to one particular cell

activation pathway. Actually, degranulation can be induced by all activating NK cell receptors.

While all tumor cells are sensitive to lytic granule-mediated killing, for death receptor mediated killing the presence of death receptor (CD95, TRAIL-R1/2) is needed, which was seen in experiment with the co-cultivation of TRAIL KO NK cells and CD95KO HeLa target cells or CD95KO target cells and WT NK cells. In contrast, the deficiency of TRAIL on the NK cells induce a higher mortality (unpublished data), which is in line with LI et al. showing fratricide of neighboring CTLs or NK cells in CD95L deficient cells (Li et al., 2002).

On the basis of the data of this thesis, a model for the cytotoxicity mechanism of NK cells is demonstrated.

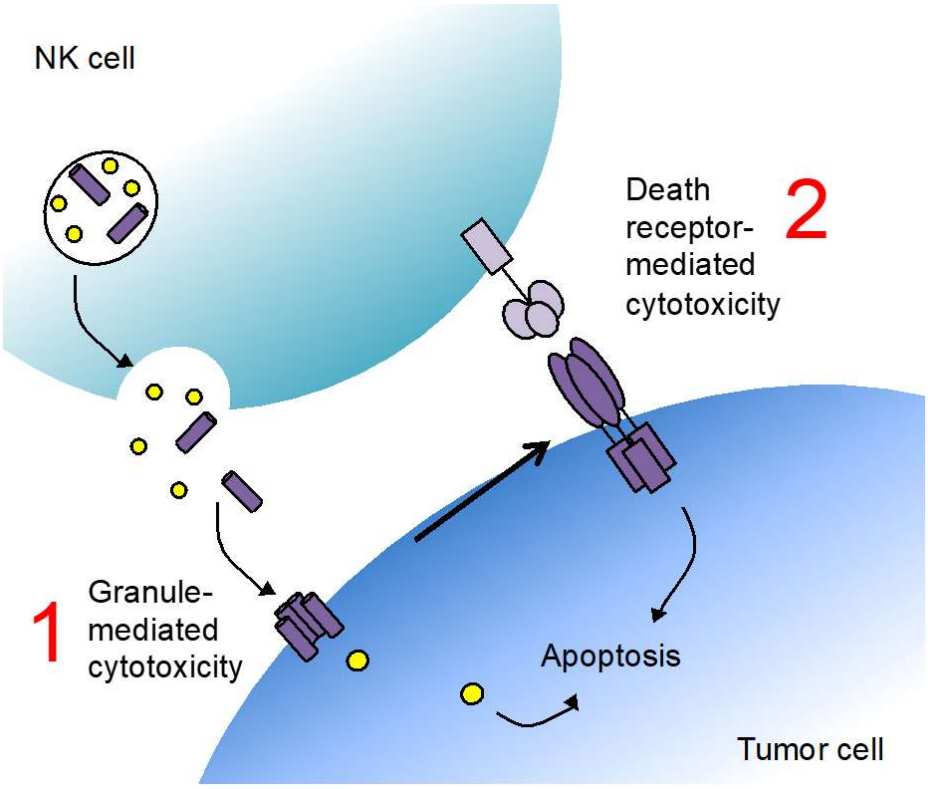

Figure 26: NK cells can induce apoptosis by two different pathways. (**1**) Initial killing mechanism is induced by GrzB. (**2**) The final killing event is mediated by death receptor pathway.

1. The initial kill is induced via the fast granule-mediated pathway. These granules contain GrzB and perforin. The lytic granules fuse with the plasma membrane and release their granule content. Perforin is able to from a pore in the target cell membrane so that GrzB can enter the target cell through this pore. GrzB initiates Casp-dependent or -independent apoptosis. After efficient killing, the cell detaches from the target cell and restores its ability to kill another target cell. Some of these NK cells are able to kill multiple targets in a strictly sequential manner. During each killing event, the NK cell releases its lytic granules, which leads to a gradual reduction of the GrzB and perforin content. This pathway can be completely inhibited by using CMA-treated NK cells or perforin KO NK cells.
2. Simultaneously to this process, CD95L is expressed on the cell surface of NK cells. After the majority of GrzB and perforin is released, the NK cell

uses the slow death receptor-mediated pathway for apoptosis induction. CD95L is accumulated within the contact area between NK and target cell. The engagement of death receptors and ligands leads to a Casp8-dependent apoptosis. After killing induced by the death receptor-mediated pathway, no further killing event can occur. Therefore, serial killing by death receptor-mediated killing is unlikely. This Casp8-mediated killing mechanism can exclusively be initiated by either CD95L or TRAIL. The knockout of CD95 results in a reduced serial killing activity, which is consistent with the fact that the final CD95-dependent kill is absent. Co-cultivation of CD95 KO target cell with TRAIL KO NK cells leads to a complete inhibition of the death receptor-mediated pathway.

6 References

ALMASAN, A. & ASHKENAZI, A. 2003. Apo2L/TRAIL: apoptosis signaling, biology, and potential for cancer therapy. *Cytokine Growth Factor Rev,* 14**,** 337-48.

ANFT, M. 2017. *THE REGULATION OF NK CELL DETACHMENT FROM TARGET CELLS AS A KEY FACTOR FOR SERIAL KILLING AND EFFECTOR FUNCTION.* PhD Dissertation, TU Dortmund.

ANFT, M., NETTER, P., URLAUB, D., PRAGER, I., SCHAFFNER, S. & WATZL, C. 2020. NK cell detachment from target cells is regulated by successful cytotoxicity and influences cytokine production. *Cell Mol Immunol,* 17**,** 347-355.

ARULANANDAM, A. R., MOINGEON, P., CONCINO, M. F., RECNY, M. A., KATO, K., YAGITA, H., KOYASU, S. & REINHERZ, E. L. 1993. A soluble multimeric recombinant CD2 protein identifies CD48 as a low affinity ligand for human CD2: divergence of CD2 ligands during the evolution of humans and mice. *J Exp Med,* 177**,** 1439-50.

ATREYA, I., KINDERMANN, M. & WIRTZ, S. 2019. Innate lymphoid cells in intestinal cancer development. *Semin Immunol,* 41**,** 101267.

BACKES, C. S., FRIEDMANN, K. S., MANG, S., KNORCK, A., HOTH, M. & KUMMEROW, C. 2018. Natural killer cells induce distinct modes of cancer cell death: Discrimination, quantification, and modulation of apoptosis, necrosis, and mixed forms. *J Biol Chem,* 293**,** 16348-16363.

BARRETT, A. J. & KIRSCHKE, H. 1981. Cathepsin B, Cathepsin H, and cathepsin L. *Methods Enzymol,* 80 Pt C**,** 535-61.

BERNINK, J. H., KRABBENDAM, L., GERMAR, K., DE JONG, E., GRONKE, K., KOFOED-NIELSEN, M., MUNNEKE, J. M., HAZENBERG, M. D., VILLAUDY, J., BUSKENS, C. J., BEMELMAN, W. A., DIEFENBACH, A., BLOM, B. & SPITS, H. 2015. Interleukin-12 and -23 Control Plasticity of CD127(+) Group 1 and Group 3 Innate Lymphoid Cells in the Intestinal Lamina Propria. *Immunity,* 43**,** 146-60.

BERTRAND, F., MULLER, S., ROH, K. H., LAURENT, C., DUPRE, L. & VALITUTTI, S. 2013. An initial and rapid step of lytic granule secretion precedes microtubule organizing center polarization at the cytotoxic T lymphocyte/target cell synapse. *Proc Natl Acad Sci U S A,* 110**,** 6073-8.

BHAT, R. & WATZL, C. 2007. Serial killing of tumor cells by human natural killer cells--enhancement by therapeutic antibodies. *PLoS One,* 2**,** e326.

BODMER, J. L., HOLLER, N., REYNARD, S., VINCIGUERRA, P., SCHNEIDER, P., JUO, P., BLENIS, J. & TSCHOPP, J. 2000. TRAIL receptor-2 signals apoptosis through FADD and caspase-8. *Nat Cell Biol,* 2**,** 241-3.

BONING, M. A. L., TRITTEL, S., RIESE, P., VAN HAM, M., HEYNER, M., VOSS, M., PARZMAIR, G. P., KLAWONN, F., JERON, A., GUZMAN, C. A., JANSCH, L., SCHRAVEN, B., REINHOLD, A. & BRUDER, D. 2019. ADAP Promotes Degranulation and Migration of NK Cells Primed During in vivo Listeria monocytogenes Infection in Mice. *Front Immunol,* 10**,** 3144.

BOSSI, G. & GRIFFITHS, G. M. 2005. CTL secretory lysosomes: biogenesis and secretion of a harmful organelle. *Semin Immunol,* 17**,** 87-94.

BRATTON, S. B., WALKER, G., SRINIVASULA, S. M., SUN, X. M., BUTTERWORTH, M., ALNEMRI, E. S. & COHEN, G. M. 2001. Recruitment, activation and retention of caspases-9 and -3 by Apaf-1 apoptosome and associated XIAP complexes. *EMBO J,* 20**,** 998-1009.

BRENNAN, A. J., CHIA, J., BROWNE, K. A., CICCONE, A., ELLIS, S., LOPEZ, J. A., SUSANTO, O., VERSCHOOR, S., YAGITA, H., WHISSTOCK, J. C., TRAPANI, J. A. & VOSKOBOINIK, I. 2011. Protection from endogenous perforin: glycans and the C terminus regulate exocytic trafficking in cytotoxic lymphocytes. *Immunity,* 34**,** 879-92.

BRENNAN, A. J., LAW, R. H. P., CONROY, P. J., NOORI, T., LUKOYANOVA, N., SAIBIL, H., YAGITA, H., CICCONE, A., VERSCHOOR, S., WHISSTOCK, J. C., TRAPANI, J. A. & VOSKOBOINIK, I. 2018. Perforin proteostasis is regulated through its C2 domain: supra-physiological cell death mediated by T431D-perforin. *Cell Death Differ,* 25**,** 1517-1529.

BRESTOFF, J. R., KIM, B. S., SAENZ, S. A., STINE, R. R., MONTICELLI, L. A., SONNENBERG, G. F., THOME, J. J., FARBER, D. L., LUTFY, K., SEALE, P. & ARTIS, D. 2015. Group 2 innate lymphoid cells promote beiging of white adipose tissue and limit obesity. *Nature,* 519**,** 242-6.

BURKHARDT, J. K., HESTER, S., LAPHAM, C. K. & ARGON, Y. 1990. The lytic granules of natural killer cells are dual-function organelles combining secretory and pre-lysosomal compartments. *J Cell Biol,* 111**,** 2327-40.

CAMPBELL, K. J. & TAIT, S. W. G. 2018. Targeting BCL-2 regulated apoptosis in cancer. *Open Biol,* 8.

CARREGA, P. & FERLAZZO, G. 2012. Natural killer cell distribution and trafficking in human tissues. *Front Immunol,* 3**,** 347.

CASCIOLA-ROSEN, L., GARCIA-CALVO, M., BULL, H. G., BECKER, J. W., HINES, T., THORNBERRY, N. A. & ROSEN, A. 2007. Mouse and human granzyme B have distinct tetrapeptide specificities and abilities to recruit the bid pathway. *J Biol Chem,* 282**,** 4545-52.

CHEN, J. J., SUN, Y. & NABEL, G. J. 1998. Regulation of the proinflammatory effects of Fas ligand (CD95L). *Science,* 282**,** 1714-7.

CHINNAIYAN, A. M., HANNA, W. L., ORTH, K., DUAN, H., POIRIER, G. G., FROELICH, C. J. & DIXIT, V. M. 1996. Cytotoxic T-cell-derived granzyme B activates the apoptotic protease ICE-LAP3. *Curr Biol,* 6**,** 897-9.

CHOI, P. J. & MITCHISON, T. J. 2013. Imaging burst kinetics and spatial coordination during serial killing by single natural killer cells. *Proc Natl Acad Sci U S A,* 110**,** 6488-93.

CHOI, Y. H., LIM, E. J., KIM, S. W., MOON, Y. W., PARK, K. S. & AN, H. J. 2019. IL-27 enhances IL-15/IL-18-mediated activation of human natural killer cells. *J Immunother Cancer,* 7**,** 168.

COHNEN, A., CHIANG, S. C., STOJANOVIC, A., SCHMIDT, H., CLAUS, M., SAFTIG, P., JANSSEN, O., CERWENKA, A., BRYCESON, Y. T. & WATZL, C. 2013. Surface CD107a/LAMP-1 protects natural killer cells from degranulation-associated damage. *Blood,* 122**,** 1411-8.

D'ANGELO, M. E., BIRD, P. I., PETERS, C., REINHECKEL, T., TRAPANI, J. A. & SUTTON, V. R. 2010. Cathepsin H is an additional convertase of pro-granzyme B. *J Biol Chem,* 285**,** 20514-9.

D'ARCY, M. S. 2019. Cell death: a review of the major forms of apoptosis, necrosis and autophagy. *Cell Biol Int,* 43**,** 582-592.

DARMON, A. J., NICHOLSON, D. W. & BLEACKLEY, R. C. 1995. Activation of the apoptotic protease CPP32 by cytotoxic T-cell-derived granzyme B. *Nature,* 377**,** 446-8.

DEVERAUX, Q. L., ROY, N., STENNICKE, H. R., VAN ARSDALE, T., ZHOU, Q., SRINIVASULA, S. M., ALNEMRI, E. S., SALVESEN, G. S. & REED, J. C. 1998. IAPs block apoptotic events induced by caspase-8 and cytochrome c by direct inhibition of distinct caspases. *EMBO J,* 17**,** 2215-23.

DICKSON, E. J., DUMAN, J. G., MOODY, M. W., CHEN, L. & HILLE, B. 2012. Orai-STIM-mediated Ca2+ release from secretory granules revealed by a targeted Ca2+ and pH probe. *Proc Natl Acad Sci U S A,* 109**,** E3539-48.

DIEFENBACH, A. & RAULET, D. H. 2001. Strategies for target cell recognition by natural killer cells. *Immunological reviews,* 181**,** 170-184.

DLUGOSZ, P. J., BILLEN, L. P., ANNIS, M. G., ZHU, W., ZHANG, Z., LIN, J., LEBER, B. & ANDREWS, D. W. 2006. Bcl-2 changes conformation to inhibit Bax oligomerization. *EMBO J,* 25**,** 2287-96.

DUAN, H., ORTH, K., CHINNAIYAN, A. M., POIRIER, G. G., FROELICH, C. J., HE, W.

W. & DIXIT, V. M. 1996. ICE-LAP6, a novel member of the ICE/Ced-3 gene family, is activated by the cytotoxic T cell protease granzyme B. *J Biol Chem,* 271**,** 16720-4.

DUNAY, I. R. & DIEFENBACH, A. 2018. Group 1 innate lymphoid cells in Toxoplasma gondii infection. *Parasite Immunol,* 40.

EBSEN, H., LETTAU, M., KABELITZ, D. & JANSSEN, O. 2015. Subcellular localization and activation of ADAM proteases in the context of FasL shedding in T lymphocytes. *Mol Immunol,* 65**,** 416-28.

ECKELMAN, B. P., SALVESEN, G. S. & SCOTT, F. L. 2006. Human inhibitor of apoptosis proteins: why XIAP is the black sheep of the family. *EMBO Rep,* 7**,** 988-94.

EINSTEIN, R. & GABEL, C. A. 1991. Cell- and ligand-specific dephosphorylation of acid hydrolases: evidence that the mannose 6-phosphatase is controlled by compartmentalization. *J Cell Biol,* 112**,** 81-94.

ELLIOTT, J. M. & YOKOYAMA, W. M. 2011. Unifying concepts of MHC-dependent natural killer cell education. *Trends Immunol,* 32**,** 364-72.

ESPOSTI, M. D. 2002. The roles of Bid. *Apoptosis,* 7**,** 433-40.

EVERAERE, L., AIT YAHIA, S., BOUTE, M., AUDOUSSET, C., CHENIVESSE, C. & TSICOPOULOS, A. 2018. Innate lymphoid cells at the interface between obesity and asthma. *Immunology,* 153**,** 21-30.

FARAG, S. S., FEHNIGER, T. A., RUGGERI, L., VELARDI, A. & CALIGIURI, M. A. 2002. Natural killer cell receptors: new biology and insights into the graft-versus-leukemia effect. *Blood,* 100**,** 1935-47.

FEHNIGER, T. A., CAI, S. F., CAO, X., BREDEMEYER, A. J., PRESTI, R. M., FRENCH, A. R. & LEY, T. J. 2007. Acquisition of murine NK cell cytotoxicity requires the translation of a pre-existing pool of granzyme B and perforin mRNAs. *Immunity,* 26**,** 798-811.

FORGAC, M. 2007. Vacuolar ATPases: rotary proton pumps in physiology and pathophysiology. *Nat Rev Mol Cell Biol,* 8**,** 917-29.

FOSTEL, L. V., DLUZNIEWSKA, J., SHIMIZU, Y., BURBACH, B. J. & PETERSON, E. J. 2006. ADAP is dispensable for NK cell development and function. *Int Immunol,* 18**,** 1305-14.

FRASER, S. A., KARIMI, R., MICHALAK, M. & HUDIG, D. 2000. Perforin lytic activity is controlled by calreticulin. *J Immunol,* 164**,** 4150-5.

FRISK, T. W., KHORSHIDI, M. A., GULDEVALL, K., VANHERBERGHEN, B. & ONFELT, B. 2011. A silicon-glass microwell platform for high-resolution imaging and high-content screening with single cell resolution. *Biomed Microdevices,* 13**,** 683-93.

FULDA, S. & DEBATIN, K. M. 2006. Extrinsic versus intrinsic apoptosis pathways in anticancer chemotherapy. *Oncogene,* 25**,** 4798-811.

GOODRIDGE, J. P., JACOBS, B., SAETERSMOEN, M. L., CLEMENT, D., HAMMER, Q., CLANCY, T., SKARPEN, E., BRECH, A., LANDSKRON, J., GRIMM, C., PFEFFERLE, A., MEZA-ZEPEDA, L., LORENZ, S., WIIGER, M. T., LOUCH, W. E., ASK, E. H., LIU, L. L., OEI, V. Y. S., KJALLQUIST, U., LINNARSSON, S., PATEL, S., TASKEN, K., STENMARK, H. & MALMBERG, K. J. 2019. Remodeling of secretory lysosomes during education tunes functional potential in NK cells. *Nat Commun,* 10**,** 514.

GRIFFITHS, G. M. & ISAAZ, S. 1993. Granzymes A and B are targeted to the lytic granules of lymphocytes by the mannose-6-phosphate receptor. *J Cell Biol,* 120**,** 885-96.

GUICCIARDI, M. E. & GORES, G. J. 2009. Life and death by death receptors. *FASEB J,* 23**,** 1625-37.

GULDEVALL, K., BRANDT, L., FORSLUND, E., OLOFSSON, K., FRISK, T. W., OLOFSSON, P. E., GUSTAFSSON, K., MANNEBERG, O., VANHERBERGHEN, B., BRISMAR, H., KARRE, K., UHLIN, M. & ONFELT, B. 2016. Microchip Screening Platform for Single Cell Assessment of NK Cell Cytotoxicity. *Front Immunol,* 7**,** 119.

GUO, X., LIANG, Y., ZHANG, Y., LASORELLA, A., KEE, B. L. & FU, Y. X. 2015. Innate Lymphoid Cells Control Early Colonization Resistance against Intestinal Pathogens through ID2-Dependent Regulation of the Microbiota. *Immunity,* 42**,** 731-43.

GWALANI, L. A. & ORANGE, J. S. 2018. Single Degranulations in NK Cells Can Mediate Target Cell Killing. *J Immunol,* 200**,** 3231-3243.

HAZENBERG, M. D. & SPITS, H. 2014. Human innate lymphoid cells. *Blood,* 124**,** 700-9.

HE, J. S. & OSTERGAARD, H. L. 2007. CTLs contain and use intracellular stores of FasL distinct from cytolytic granules. *J Immunol,* 179**,** 2339-48.

HE, Y. & TIAN, Z. 2017. NK cell education via nonclassical MHC and non-MHC ligands. *Cell Mol Immunol,* 14**,** 321-330.

HEIM, R., CUBITT, A. B. & TSIEN, R. Y. 1995. Improved green fluorescence. *Nature,* 373**,** 663-4.

HERBERT, D. R., DOUGLAS, B. & ZULLO, K. 2019. Group 2 Innate Lymphoid Cells (ILC2): Type 2 Immunity and Helminth Immunity. *Int J Mol Sci,* 20.

HOFFMANN, J. C., PAPPA, A., KRAMMER, P. H. & LAVRIK, I. N. 2009. A new C-terminal cleavage product of procaspase-8, p30, defines an alternative pathway of

procaspase-8 activation. *Mol Cell Biol,* 29**,** 4431-40.

HOFFMANN, S. C., COHNEN, A., LUDWIG, T. & WATZL, C. 2011. 2B4 engagement mediates rapid LFA-1 and actin-dependent NK cell adhesion to tumor cells as measured by single cell force spectroscopy. *J Immunol,* 186**,** 2757-64.

HOLCIK, M., GIBSON, H. & KORNELUK, R. G. 2001. XIAP: apoptotic brake and promising therapeutic target. *Apoptosis,* 6**,** 253-61.

HOLLER, N., TARDIVEL, A., KOVACSOVICS-BANKOWSKI, M., HERTIG, S., GAIDE, O., MARTINON, F., TINEL, A., DEPERTHES, D., CALDERARA, S., SCHULTHESS, T., ENGEL, J., SCHNEIDER, P. & TSCHOPP, J. 2003. Two adjacent trimeric Fas ligands are required for Fas signaling and formation of a death-inducing signaling complex. *Mol Cell Biol,* 23**,** 1428-40.

HOUSE, I. G., HOUSE, C. M., BRENNAN, A. J., GILAN, O., DAWSON, M. A., WHISSTOCK, J. C., LAW, R. H., TRAPANI, J. A. & VOSKOBOINIK, I. 2017. Regulation of perforin activation and pre-synaptic toxicity through C-terminal glycosylation. *EMBO Rep,* 18**,** 1775-1785.

HSU, H. T., MACE, E. M., CARISEY, A. F., VISWANATH, D. I., CHRISTAKOU, A. E., WIKLUND, M., ONFELT, B. & ORANGE, J. S. 2016. NK cells converge lytic granules to promote cytotoxicity and prevent bystander killing. *J Cell Biol,* 215**,** 875-889.

JANAS, M. L., GROVES, P., KIENZLE, N. & KELSO, A. 2005. IL-2 regulates perforin and granzyme gene expression in CD8+ T cells independently of its effects on survival and proliferation. *J Immunol,* 175**,** 8003-10.

JENKINS, M. R., RUDD-SCHMIDT, J. A., LOPEZ, J. A., RAMSBOTTOM, K. M., MANNERING, S. I., ANDREWS, D. M., VOSKOBOINIK, I. & TRAPANI, J. A. 2015. Failed CTL/NK cell killing and cytokine hypersecretion are directly linked through prolonged synapse time. *J Exp Med,* 212**,** 307-17.

JENNE, D. E. & TSCHOPP, J. 1988. Granzymes, a family of serine proteases released from granules of cytolytic T lymphocytes upon T cell receptor stimulation. *Immunol Rev,* 103**,** 53-71.

JEWETT, A. & BONAVIDA, B. 1996. Target-induced inactivation and cell death by apoptosis in a subset of human NK cells. *J Immunol,* 156**,** 907-15.

JOHNSEN, A. C., HAUX, J., STEINKJER, B., NONSTAD, U., EGEBERG, K., SUNDAN, A., ASHKENAZI, A. & ESPEVIK, T. 1999. Regulation of APO-2 ligand/trail expression in NK cells-involvement in NK cell-mediated cytotoxicity. *Cytokine,* 11**,** 664-72.

JOYCE, M. G. & SUN, P. D. 2011. The structural basis of ligand recognition by natural killer cell receptors. *J Biomed Biotechnol,* 2011**,** 203628.

KAJINO, K., KAJINO, Y. & GREENE, M. I. 1998. Fas- and perforin-independent mechanism of cytotoxic T lymphocyte. *Immunol Res,* 17**,** 89-93.

KANE, P. M. 2006. The where, when, and how of organelle acidification by the yeast vacuolar H+-ATPase. *Microbiol Mol Biol Rev,* 70**,** 177-91.

KANNO, A., YAMANAKA, Y., HIRANO, H., UMEZAWA, Y. & OZAWA, T. 2007. Cyclic luciferase for real-time sensing of caspase-3 activities in living mammals. *Angew Chem Int Ed Engl,* 46**,** 7595-9.

KASHII, Y., GIORDA, R., HERBERMAN, R. B., WHITESIDE, T. L. & VUJANOVIC, N. L. 1999. Constitutive expression and role of the TNF family ligands in apoptotic killing of tumor cells by human NK cells. *J Immunol,* 163**,** 5358-66.

KASSAHN, D., NACHBUR, U., CONUS, S., MICHEAU, O., SCHNEIDER, P., SIMON, H. U. & BRUNNER, T. 2009. Distinct requirements for activation-induced cell surface expression of preformed Fas/CD95 ligand and cytolytic granule markers in T cells. *Cell Death Differ,* 16**,** 115-24.

KATAOKA, T., SATO, M., KONDO, S. & NAGAI, K. 1996. Estimation of pH and the number of lytic granules in a CD8+ CTL clone treated with an inhibitor of vacuolar type H(+)-ATPase concanamycin A. *Biosci Biotechnol Biochem,* 60**,** 1729-31.

KATAOKA, T., TOGASHI, K., TAKAYAMA, H., TAKAKU, K. & NAGAI, K. 1997. Inactivation and proteolytic degradation of perforin within lytic granules upon neutralization of acidic pH. *Immunology,* 91**,** 493-500.

KAYAGAKI, N., YAMAGUCHI, N., NAKAYAMA, M., ETO, H., OKUMURA, K. & YAGITA, H. 1999a. Type I interferons (IFNs) regulate tumor necrosis factor-related apoptosis-inducing ligand (TRAIL) expression on human T cells: A novel mechanism for the antitumor effects of type I IFNs. *J Exp Med,* 189**,** 1451-60.

KAYAGAKI, N., YAMAGUCHI, N., NAKAYAMA, M., TAKEDA, K., AKIBA, H., TSUTSUI, H., OKAMURA, H., NAKANISHI, K., OKUMURA, K. & YAGITA, H. 1999b. Expression and function of TNF-related apoptosis-inducing ligand on murine activated NK cells. *J Immunol,* 163**,** 1906-13.

KEEFE, D., SHI, L., FESKE, S., MASSOL, R., NAVARRO, F., KIRCHHAUSEN, T. & LIEBERMAN, J. 2005. Perforin triggers a plasma membrane-repair response that facilitates CTL induction of apoptosis. *Immunity,* 23**,** 249-62.

KHANNA, R. 1998. Tumour surveillance: missing peptides and MHC molecules. *Immunol Cell Biol,* 76**,** 20-6.

KIESSLING, R., KLEIN, E. & WIGZELL, H. 1975. "Natural" killer cells in the mouse. I. Cytotoxic cells with specificity for mouse Moloney leukemia cells. Specificity and distribution according to genotype. *Eur J Immunol,* 5**,** 112-7.

KIRKIN, V., CAHUZAC, N., GUARDIOLA-SERRANO, F., HUAULT, S., LUCKERATH, K., FRIEDMANN, E., NOVAC, N., WELS, W. S., MARTOGLIO, B., HUEBER, A. O. & ZORNIG, M. 2007. The Fas ligand intracellular domain is released by ADAM10 and SPPL2a cleavage in T-cells. *Cell Death Differ,* 14**,** 1678-87.

KISCHKEL, F. C., HELLBARDT, S., BEHRMANN, I., GERMER, M., PAWLITA, M., KRAMMER, P. H. & PETER, M. E. 1995. Cytotoxicity-dependent APO-1 (Fas/CD95)-associated proteins form a death-inducing signaling complex (DISC) with the receptor. *EMBO J,* 14**,** 5579-88.

KISCHKEL, F. C., LAWRENCE, D. A., CHUNTHARAPAI, A., SCHOW, P., KIM, K. J. & ASHKENAZI, A. 2000. Apo2L/TRAIL-dependent recruitment of endogenous FADD and caspase-8 to death receptors 4 and 5. *Immunity,* 12**,** 611-20.

KONJAR, S., SUTTON, V. R., HOVES, S., REPNIK, U., YAGITA, H., REINHECKEL, T., PETERS, C., TURK, V., TURK, B., TRAPANI, J. A. & KOPITAR-JERALA, N. 2010. Human and mouse perforin are processed in part through cleavage by the lysosomal cysteine proteinase cathepsin L. *Immunology,* 131**,** 257-67.

KRZEWSKI, K., GIL-KRZEWSKA, A., NGUYEN, V., PERUZZI, G. & COLIGAN, J. E. 2013. LAMP1/CD107a is required for efficient perforin delivery to lytic granules and NK-cell cytotoxicity. *Blood,* 121**,** 4672-83.

KUMAR, R., HERBERT, P. E. & WARRENS, A. N. 2005. An introduction to death receptors in apoptosis. *Int J Surg,* 3**,** 268-77.

KUMAR, S. 2018. Natural killer cell cytotoxicity and its regulation by inhibitory receptors. *Immunology,* 154**,** 383-393.

KURSCHUS, F. C., FELLOWS, E., STEGMANN, E. & JENNE, D. E. 2008. Granzyme B delivery via perforin is restricted by size, but not by heparan sulfate-dependent endocytosis. *Proc Natl Acad Sci U S A,* 105**,** 13799-804.

LAW, R. H., LUKOYANOVA, N., VOSKOBOINIK, I., CARADOC-DAVIES, T. T., BARAN, K., DUNSTONE, M. A., D'ANGELO, M. E., ORLOVA, E. V., COULIBALY, F., VERSCHOOR, S., BROWNE, K. A., CICCONE, A., KUIPER, M. J., BIRD, P. I., TRAPANI, J. A., SAIBIL, H. R. & WHISSTOCK, J. C. 2010. The structural basis for membrane binding and pore formation by lymphocyte perforin. *Nature,* 468**,** 447-51.

LEE, J., DIECKMANN, N. M. G., EDGAR, J. R., GRIFFITHS, G. M. & SIEGEL, R. M. 2018. Fas Ligand localizes to intraluminal vesicles within NK cell cytolytic granules and is enriched at the immune synapse. *Immun Inflamm Dis,* 6**,** 312-321.

LETTAU, M., PAULSEN, M., KABELITZ, D. & JANSSEN, O. 2008. Storage, expression and function of Fas ligand, the key death factor of immune cells. *Curr Med Chem,* 15**,** 1684-96.

LETTAU, M., PAULSEN, M., SCHMIDT, H. & JANSSEN, O. 2011. Insights into the molecular regulation of FasL (CD178) biology. *Eur J Cell Biol,* 90**,** 456-66.

LEUNG, C., HODEL, A. W., BRENNAN, A. J., LUKOYANOVA, N., TRAN, S., HOUSE, C. M., KONDOS, S. C., WHISSTOCK, J. C., DUNSTONE, M. A., TRAPANI, J. A., VOSKOBOINIK, I., SAIBIL, H. R. & HOOGENBOOM, B. W. 2017. Real-time visualization of perforin nanopore assembly. *Nat Nanotechnol,* 12**,** 467-473.

LI, H., ZHU, H., XU, C. J. & YUAN, J. 1998. Cleavage of BID by caspase 8 mediates the mitochondrial damage in the Fas pathway of apoptosis. *Cell,* 94**,** 491-501.

LI, J., FIGUEIRA, S. K., VRAZO, A. C., BINKOWSKI, B. F., BUTLER, B. L., TABATA, Y., FILIPOVICH, A., JORDAN, M. B. & RISMA, K. A. 2014. Real-time detection of CTL function reveals distinct patterns of caspase activation mediated by Fas versus granzyme B. *J Immunol,* 193**,** 519-28.

LI, J. H., ROSEN, D., SONDEL, P. & BERKE, G. 2002. Immune privilege and FasL: two ways to inactivate effector cytotoxic T lymphocytes by FasL-expressing cells. *Immunology,* 105**,** 267-77.

LI, P., ZHENG, G., YANG, Y., ZHANG, C., XIONG, P., XU, Y., FANG, M., TAN, Z., ZHENG, F. & GONG, F. 2010. Granzyme B is recovered by natural killer cells via clathrin-dependent endocytosis. *Cell Mol Life Sci,* 67**,** 3197-208.

LIESCHE, C., SAUER, P., PRAGER, I., URLAUB, D., CLAUS, M., EILS, R., BEAUDOUIN, J. & WATZL, C. 2018. Single-Fluorescent Protein Reporters Allow Parallel Quantification of Natural Killer Cell-Mediated Granzyme and Caspase Activities in Single Target Cells. *Front Immunol,* 9**,** 1840.

LO, B. C., GOLD, M. J., HUGHES, M. R., ANTIGNANO, F., VALDEZ, Y., ZAPH, C., HARDER, K. W. & MCNAGNY, K. M. 2016. The orphan nuclear receptor RORalpha and group 3 innate lymphoid cells drive fibrosis in a mouse model of Crohn's disease. *Sci Immunol,* 1**,** eaaf8864.

LOPEZ, J. A., JENKINS, M. R., RUDD-SCHMIDT, J. A., BRENNAN, A. J., DANNE, J. C., MANNERING, S. I., TRAPANI, J. A. & VOSKOBOINIK, I. 2013a. Rapid and unidirectional perforin pore delivery at the cytotoxic immune synapse. *J Immunol,* 191**,** 2328-34.

LOPEZ, J. A., SUSANTO, O., JENKINS, M. R., LUKOYANOVA, N., SUTTON, V. R., LAW, R. H., JOHNSTON, A., BIRD, C. H., BIRD, P. I., WHISSTOCK, J. C., TRAPANI, J. A., SAIBIL, H. R. & VOSKOBOINIK, I. 2013b. Perforin forms transient pores on the target cell plasma membrane to facilitate rapid access of granzymes during killer cell attack. *Blood,* 121**,** 2659-68.

MACE, E. M., DONGRE, P., HSU, H. T., SINHA, P., JAMES, A. M., MANN, S. S.,

FORBES, L. R., WATKIN, L. B. & ORANGE, J. S. 2014. Cell biological steps and checkpoints in accessing NK cell cytotoxicity. *Immunol Cell Biol,* 92**,** 245-55.

MARIANI, S. M., MATIBA, B., BAUMLER, C. & KRAMMER, P. H. 1995. Regulation of cell surface APO-1/Fas (CD95) ligand expression by metalloproteases. *Eur J Immunol,* 25**,** 2303-7.

MASSON, D. & TSCHOPP, J. 1987. A family of serine esterases in lytic granules of cytolytic T lymphocytes. *Cell,* 49**,** 679-85.

MAY, R. M., OKUMURA, M., HSU, C. J., BASSIRI, H., YANG, E., RAK, G., MACE, E. M., PHILIP, N. H., ZHANG, W., BAUMGART, T., ORANGE, J. S., NICHOLS, K. E. & KAMBAYASHI, T. 2013. Murine natural killer immunoreceptors use distinct proximal signaling complexes to direct cell function. *Blood,* 121**,** 3135-46.

MEDEMA, J. P., TOES, R. E. M., SCAFFIDI, C., ZHENG, T. S., FLAVELL, R. A., MELIEF, C. J. M., PETER, M. E., OFFRINGA, R. & KRAMMER, P. H. 1997. Cleavage of FLICE (caspase-8) by granzyme B during cytotoxic T lymphocyte-induced apoptosis. *European Journal of Immunology,* 27**,** 3492-3498.

MONLEON, I., MARTINEZ-LORENZO, M. J., MONTEAGUDO, L., LASIERRA, P., TAULES, M., ITURRALDE, M., PINEIRO, A., LARRAD, L., ALAVA, M. A., NAVAL, J. & ANEL, A. 2001. Differential secretion of Fas ligand- or APO2 ligand/TNF-related apoptosis-inducing ligand-carrying microvesicles during activation-induced death of human T cells. *J Immunol,* 167**,** 6736-44.

MONTEL, A. H., BOCHAN, M. R., HOBBS, J. A., LYNCH, D. H. & BRAHMI, Z. 1995. Fas involvement in cytotoxicity mediated by human NK cells. *Cell Immunol,* 166**,** 236-46.

MURPHY, W. J., KOH, C. Y., RAZIUDDIN, A., BENNETT, M. & LONGO, D. L. 2001. Immunobiology of natural killer cells and bone marrow transplantation: merging of basic and preclinical studies. *Immunol Rev,* 181**,** 279-89.

NAGASAWA, M., HEESTERS, B. A., KRADOLFER, C. M. A., KRABBENDAM, L., MARTINEZ-GONZALEZ, I., DE BRUIJN, M. J. W., GOLEBSKI, K., HENDRIKS, R. W., STADHOUDERS, R., SPITS, H. & BAL, S. M. 2019. KLRG1 and NKp46 discriminate subpopulations of human CD117(+)CRTH2(-) ILCs biased toward ILC2 or ILC3. *J Exp Med,* 216**,** 1762-1776.

NAGLER, A., LANIER, L. L., CWIRLA, S. & PHILLIPS, J. H. 1989. Comparative studies of human FcRIII-positive and negative natural killer cells. *J Immunol,* 143**,** 3183-91.

NETTER, P., ANFT, M. & WATZL, C. 2017. Termination of the Activating NK Cell Immunological Synapse Is an Active and Regulated Process. *J Immunol,* 199**,** 2528-2535.

OBERST, A., POP, C., TREMBLAY, A. G., BLAIS, V., DENAULT, J. B., SALVESEN, G. S. & GREEN, D. R. 2010. Inducible dimerization and inducible cleavage reveal a requirement for both processes in caspase-8 activation. *J Biol Chem,* 285**,** 16632-42.

ORANGE, J. S. 2008. Formation and function of the lytic NK-cell immunological synapse. *Nat Rev Immunol,* 8**,** 713-25.

ORANGE, J. S., HARRIS, K. E., ANDZELM, M. M., VALTER, M. M., GEHA, R. S. & STROMINGER, J. L. 2003. The mature activating natural killer cell immunologic synapse is formed in distinct stages. *Proc Natl Acad Sci U S A,* 100**,** 14151-6.

PACKARD, B. Z., TELFORD, W. G., KOMORIYA, A. & HENKART, P. A. 2007. Granzyme B activity in target cells detects attack by cytotoxic lymphocytes. *J Immunol,* 179**,** 3812-20.

PAMARTHY, S., KULSHRESTHA, A., KATARA, G. K. & BEAMAN, K. D. 2018. The curious case of vacuolar ATPase: regulation of signaling pathways. *Mol Cancer,* 17**,** 41.

PAPAGEORGIOU, A., DINNEY, C. P. & MCCONKEY, D. J. 2007. Interferon-alpha induces TRAIL expression and cell death via an IRF-1-dependent mechanism in human bladder cancer cells. *Cancer Biol Ther,* 6**,** 872-9.

PINKOSKI, M. J., WATERHOUSE, N. J., HEIBEIN, J. A., WOLF, B. B., KUWANA, T., GOLDSTEIN, J. C., NEWMEYER, D. D., BLEACKLEY, R. C. & GREEN, D. R. 2001. Granzyme B-mediated apoptosis proceeds predominantly through a Bcl-2-inhibitable mitochondrial pathway. *J Biol Chem,* 276**,** 12060-7.

POLI, A., MICHEL, T., THERESINE, M., ANDRES, E., HENTGES, F. & ZIMMER, J. 2009. CD56bright natural killer (NK) cells: an important NK cell subset. *Immunology,* 126**,** 458-65.

PRAGER, I., LIESCHE, C., VAN OOIJEN, H., URLAUB, D., VERRON, Q., SANDSTROM, N., FASBENDER, F., CLAUS, M., EILS, R., BEAUDOUIN, J., ONFELT, B. & WATZL, C. 2019. NK cells switch from granzyme B to death receptor-mediated cytotoxicity during serial killing. *J Exp Med,* 216**,** 2113-2127.

PRAKASH, M. D., BIRD, C. H. & BIRD, P. I. 2009. Active and zymogen forms of granzyme B are constitutively released from cytotoxic lymphocytes in the absence of target cell engagement. *Immunol Cell Biol,* 87**,** 249-54.

PRAPER, T., BESENICAR, M. P., ISTINIC, H., PODLESEK, Z., METKAR, S. S., FROELICH, C. J. & ANDERLUH, G. 2010. Human perforin permeabilizing activity, but not binding to lipid membranes, is affected by pH. *Mol Immunol,* 47**,** 2492-504.

RAJASEKARAN, K., KUMAR, P., SCHULDT, K. M., PETERSON, E. J.,

VANHAESEBROECK, B., DIXIT, V., THAKAR, M. S. & MALARKANNAN, S. 2013. Signaling by Fyn-ADAP via the Carma1-Bcl-10-MAP3K7 signalosome exclusively regulates inflammatory cytokine production in NK cells. *Nat Immunol,* 14**,** 1127-36.

ROBB, R. J. & HILL, G. R. 2012. The interferon-dependent orchestration of innate and adaptive immunity after transplantation. *Blood,* 119**,** 5351-8.

ROGERS, C., ERKES, D. A., NARDONE, A., APLIN, A. E., FERNANDES-ALNEMRI, T. & ALNEMRI, E. S. 2019. Gasdermin pores permeabilize mitochondria to augment caspase-3 activation during apoptosis and inflammasome activation. *Nat Commun,* 10**,** 1689.

ROSADO, C. J., KONDOS, S., BULL, T. E., KUIPER, M. J., LAW, R. H., BUCKLE, A. M., VOSKOBOINIK, I., BIRD, P. I., TRAPANI, J. A., WHISSTOCK, J. C. & DUNSTONE, M. A. 2008. The MACPF/CDC family of pore-forming toxins. *Cell Microbiol,* 10**,** 1765-74.

SAELENS, X., FESTJENS, N., VANDE WALLE, L., VAN GURP, M., VAN LOO, G. & VANDENABEELE, P. 2004. Toxic proteins released from mitochondria in cell death. *Oncogene,* 23**,** 2861-74.

SARASTE, A. & PULKKI, K. 2000. Morphologic and biochemical hallmarks of apoptosis. *Cardiovasc Res,* 45**,** 528-37.

SCHMIDT, H., GELHAUS, C., NEBENDAHL, M., LETTAU, M., LUCIUS, R., LEIPPE, M., KABELITZ, D. & JANSSEN, O. 2011. Effector granules in human T lymphocytes: proteomic evidence for two distinct species of cytotoxic effector vesicles. *J Proteome Res,* 10**,** 1603-20.

SCHMIDT, H., GELHAUS, C., NEBENDAHL, M., LETTAU, M., WATZL, C., KABELITZ, D., LEIPPE, M. & JANSSEN, O. 2008. 2-D DIGE analyses of enriched secretory lysosomes reveal heterogeneous profiles of functionally relevant proteins in leukemic and activated human NK cells. *Proteomics,* 8**,** 2911-25.

SCHNEIDER, C. A., RASBAND, W. S. & ELICEIRI, K. W. 2012. NIH Image to ImageJ: 25 years of image analysis. *Nat Methods,* 9**,** 671-5.

SCHNEIDER, P., HOLLER, N., BODMER, J. L., HAHNE, M., FREI, K., FONTANA, A. & TSCHOPP, J. 1998. Conversion of membrane-bound Fas(CD95) ligand to its soluble form is associated with downregulation of its proapoptotic activity and loss of liver toxicity. *J Exp Med,* 187**,** 1205-13.

SECCHIERO, P., GONELLI, A., CORALLINI, F., CECONI, C., FERRARI, R. & ZAULI, G. 2010. Metalloproteinase 2 cleaves in vitro recombinant TRAIL: potential implications for the decreased serum levels of TRAIL after acute myocardial infarction. *Atherosclerosis,* 211**,** 333-6.

SHANER, N. C., CAMPBELL, R. E., STEINBACH, P. A., GIEPMANS, B. N., PALMER, A. E. & TSIEN, R. Y. 2004. Improved monomeric red, orange and yellow fluorescent proteins derived from Discosoma sp. red fluorescent protein. *Nat Biotechnol,* 22**,** 1567-72.

SHIFRIN, N., RAULET, D. H. & ARDOLINO, M. 2014. NK cell self tolerance, responsiveness and missing self recognition. *Semin Immunol,* 26**,** 138-44.

SHRESTA, S., GRAUBERT, T. A., THOMAS, D. A., RAPTIS, S. Z. & LEY, T. J. 1999. Granzyme A initiates an alternative pathway for granule-mediated apoptosis. *Immunity,* 10**,** 595-605.

SKAK, K., FREDERIKSEN, K. S. & LUNDSGAARD, D. 2008. Interleukin-21 activates human natural killer cells and modulates their surface receptor expression. *Immunology,* 123**,** 575-83.

SMYTH, M. J., MCGUIRE, M. J. & THIA, K. Y. 1995. Expression of recombinant human granzyme B. A processing and activation role for dipeptidyl peptidase I. *J Immunol,* 154**,** 6299-305.

SPITS, H., ARTIS, D., COLONNA, M., DIEFENBACH, A., DI SANTO, J. P., EBERL, G., KOYASU, S., LOCKSLEY, R. M., MCKENZIE, A. N., MEBIUS, R. E., POWRIE, F. & VIVIER, E. 2013. Innate lymphoid cells--a proposal for uniform nomenclature. *Nat Rev Immunol,* 13**,** 145-9.

SPITS, H., BERNINK, J. H. & LANIER, L. 2016. NK cells and type 1 innate lymphoid cells: partners in host defense. *Nat Immunol,* 17**,** 758-64.

SRPAN, K., AMBROSE, A., KARAMPATZAKIS, A., SAEED, M., CARTWRIGHT, A. N. R., GULDEVALL, K., DE MATOS, G., ONFELT, B. & DAVIS, D. M. 2018. Shedding of CD16 disassembles the NK cell immune synapse and boosts serial engagement of target cells. *J Cell Biol,* 217**,** 3267-3283.

SUDA, T., OKAZAKI, T., NAITO, Y., YOKOTA, T., ARAI, N., OZAKI, S., NAKAO, K. & NAGATA, S. 1995. Expression of the Fas ligand in cells of T cell lineage. *J Immunol,* 154**,** 3806-13.

SUN, J., BIRD, C. H., SUTTON, V., MCDONALD, L., COUGHLIN, P. B., DE JONG, T. A., TRAPANI, J. A. & BIRD, P. I. 1996. A cytosolic granzyme B inhibitor related to the viral apoptotic regulator cytokine response modifier A is present in cytotoxic lymphocytes. *J Biol Chem,* 271**,** 27802-9.

TALANIAN, R. V., YANG, X., TURBOV, J., SETH, P., GHAYUR, T., CASIANO, C. A., ORTH, K. & FROELICH, C. J. 1997. Granule-mediated killing: pathways for granzyme B-initiated apoptosis. *J Exp Med,* 186**,** 1323-31.

TANAKA, M., ITAI, T., ADACHI, M. & NAGATA, S. 1998. Downregulation of Fas ligand by

shedding. *Nat Med,* 4**,** 31-6.

TEUNISSEN, M. B. M., MUNNEKE, J. M., BERNINK, J. H., SPULS, P. I., RES, P. C. M., TE VELDE, A., CHEUK, S., BROUWER, M. W. D., MENTING, S. P., EIDSMO, L., SPITS, H., HAZENBERG, M. D. & MJOSBERG, J. 2014. Composition of innate lymphoid cell subsets in the human skin: enrichment of NCR(+) ILC3 in lesional skin and blood of psoriasis patients. *J Invest Dermatol,* 134**,** 2351-2360.

THIERY, J., KEEFE, D., BOULANT, S., BOUCROT, E., WALCH, M., MARTINVALET, D., GOPING, I. S., BLEACKLEY, R. C., KIRCHHAUSEN, T. & LIEBERMAN, J. 2011. Perforin pores in the endosomal membrane trigger the release of endocytosed granzyme B into the cytosol of target cells. *Nat Immunol,* 12**,** 770-7.

THORNBERRY, N. A., RANO, T. A., PETERSON, E. P., RASPER, D. M., TIMKEY, T., GARCIA-CALVO, M., HOUTZAGER, V. M., NORDSTROM, P. A., ROY, S., VAILLANCOURT, J. P., CHAPMAN, K. T. & NICHOLSON, D. W. 1997. A combinatorial approach defines specificities of members of the caspase family and granzyme B. Functional relationships established for key mediators of apoptosis. *J Biol Chem,* 272**,** 17907-11.

TOMESCU, C., CHEHIMI, J., MAINO, V. C. & MONTANER, L. J. 2009. Retention of viability, cytotoxicity, and response to IL-2, IL-15, or IFN-alpha by human NK cells after CD107a degranulation. *J Leukoc Biol,* 85**,** 871-6.

TOPHAM, N. J. & HEWITT, E. W. 2009. Natural killer cell cytotoxicity: how do they pull the trigger? *Immunology,* 128**,** 7-15.

ULLBERG, M. & JONDAL, M. 1981. Recycling and target binding capacity of human natural killer cells. *J Exp Med,* 153**,** 615-28.

URLAUB, D., HOFER, K., MULLER, M. L. & WATZL, C. 2017. LFA-1 Activation in NK Cells and Their Subsets: Influence of Receptors, Maturation, and Cytokine Stimulation. *J Immunol,* 198**,** 1944-1951.

VALIANTE, N. M., UHRBERG, M., SHILLING, H. G., LIENERT-WEIDENBACH, K., ARNETT, K. L., D'ANDREA, A., PHILLIPS, J. H., LANIER, L. L. & PARHAM, P. 1997. Functionally and Structurally Distinct NK Cell Receptor Repertoires in the Peripheral Blood of Two Human Donors. *Immunity,* 7**,** 739-751.

VANHERBERGHEN, B., OLOFSSON, P. E., FORSLUND, E., STERNBERG-SIMON, M., KHORSHIDI, M. A., PACOURET, S., GULDEVALL, K., ENQVIST, M., MALMBERG, K. J., MEHR, R. & ONFELT, B. 2013. Classification of human natural killer cells based on migration behavior and cytotoxic response. *Blood,* 121**,** 1326-34.

VON KARSTEDT, S., MONTINARO, A. & WALCZAK, H. 2017. Exploring the TRAILs less travelled: TRAIL in cancer biology and therapy. *Nat Rev Cancer,* 17**,** 352-366.

VOSKOBOINIK, I., THIA, M. C., FLETCHER, J., CICCONE, A., BROWNE, K., SMYTH, M. J. & TRAPANI, J. A. 2005. Calcium-dependent plasma membrane binding and cell lysis by perforin are mediated through its C2 domain: A critical role for aspartate residues 429, 435, 483, and 485 but not 491. *J Biol Chem,* 280**,** 8426-34.

VOSKOBOINIK, I., WHISSTOCK, J. C. & TRAPANI, J. A. 2015. Perforin and granzymes: function, dysfunction and human pathology. *Nat Rev Immunol,* 15**,** 388-400.

VOSS, M., LETTAU, M., PAULSEN, M. & JANSSEN, O. 2008. Posttranslational regulation of Fas ligand function. *Cell Commun Signal,* 6**,** 11.

VRAZO, A. C., HONTZ, A. E., FIGUEIRA, S. K., BUTLER, B. L., FERRELL, J. M., BINKOWSKI, B. F., LI, J. & RISMA, K. A. 2015. Live cell evaluation of granzyme delivery and death receptor signaling in tumor cells targeted by human natural killer cells. *Blood,* 126**,** e1-e10.

WAGNER, C. A., FINBERG, K. E., BRETON, S., MARSHANSKY, V., BROWN, D. & GEIBEL, J. P. 2004. Renal vacuolar H+-ATPase. *Physiol Rev,* 84**,** 1263-314.

WALCZAK, H., MILLER, R. E., ARIAIL, K., GLINIAK, B., GRIFFITH, T. S., KUBIN, M., CHIN, W., JONES, J., WOODWARD, A., LE, T., SMITH, C., SMOLAK, P., GOODWIN, R. G., RAUCH, C. T., SCHUH, J. C. & LYNCH, D. H. 1999. Tumoricidal activity of tumor necrosis factor-related apoptosis-inducing ligand in vivo. *Nat Med,* 5**,** 157-63.

WANG, Y., GAO, W., SHI, X., DING, J., LIU, W., HE, H., WANG, K. & SHAO, F. 2017. Chemotherapy drugs induce pyroptosis through caspase-3 cleavage of a gasdermin. *Nature,* 547**,** 99-103.

WESTPHAL, D., KLUCK, R. M. & DEWSON, G. 2014. Building blocks of the apoptotic pore: how Bax and Bak are activated and oligomerize during apoptosis. *Cell Death Differ,* 21**,** 196-205.

WILEY, S. R., SCHOOLEY, K., SMOLAK, P. J., DIN, W. S., HUANG, C. P., NICHOLL, J. K., SUTHERLAND, G. R., SMITH, T. D., RAUCH, C., SMITH, C. A. & ET AL. 1995. Identification and characterization of a new member of the TNF family that induces apoptosis. *Immunity,* 3**,** 673-82.

YANG, X., STENNICKE, H. R., WANG, B., GREEN, D. R., JANICKE, R. U., SRINIVASAN, A., SETH, P., SALVESEN, G. S. & FROELICH, C. J. 1998. Granzyme B mimics apical caspases. Description of a unified pathway for trans-activation of executioner caspase-3 and -7. *J Biol Chem,* 273**,** 34278-83.

YOUNG, J. D., DAMIANO, A., DINOME, M. A., LEONG, L. G. & COHN, Z. A. 1987. Dissociation of membrane binding and lytic activities of the lymphocyte pore-

forming protein (perforin). *J Exp Med,* 165**,** 1371-82.

ZAGURY, D., BERNARD, J., DUFER, J. & JEANNESSON, P. 1975. The biology of isolated immunocytes. I. Isolation into a closed liquid microchamber: application to PFC. *Ann Immunol (Paris),* 126**,** 23-30.

ZHANG, C., ZHANG, J., NIU, J., ZHANG, J. & TIAN, Z. 2008. Interleukin-15 improves cytotoxicity of natural killer cells via up-regulating NKG2D and cytotoxic effector molecule expression as well as STAT1 and ERK1/2 phosphorylation. *Cytokine,* 42**,** 128-36.

ZHANG, M., WEN, B., ANTON, O. M., YAO, Z., DUBOIS, S., JU, W., SATO, N., DILILLO, D. J., BAMFORD, R. N., RAVETCH, J. V. & WALDMANN, T. A. 2018. IL-15 enhanced antibody-dependent cellular cytotoxicity mediated by NK cells and macrophages. *Proc Natl Acad Sci U S A,* 115**,** E10915-E10924.

ZHANG, Z., ZHANG, Y., XIA, S., KONG, Q., LI, S., LIU, X., JUNQUEIRA, C., MEZA-SOSA, K. F., MOK, T. M. Y., ANSARA, J., SENGUPTA, S., YAO, Y., WU, H. & LIEBERMAN, J. 2020. Gasdermin E suppresses tumour growth by activating anti-tumour immunity. *Nature,* 579**,** 415-420.

ZUCCATO, E., BLOTT, E. J., HOLT, O., SIGISMUND, S., SHAW, M., BOSSI, G. & GRIFFITHS, G. M. 2007. Sorting of Fas ligand to secretory lysosomes is regulated by mono-ubiquitylation and phosphorylation. *J Cell Sci,* 120**,** 191-9.

7 Abbreviations

AA	amino acid
ADAM	A disintegrin and metalloproteinase
ADAP	adhesion and degranulating promoting adapter protein
AHR	aryl hydrocarbon receptor
Apaf-1	apoptotic protease activating factor-1
B2M	β_2-microglobulin
Bak	Bcl-2 homologous antagonist killer
Bax	Bcl-2 associated X protein
Bid	BH3-only proapoptotic Bcl-2 family member
BSA	bovine serum albumin
BV	brilliant violet
Casp	caspase
CD	cluster of differentiation
CD95L	Fas Ligand, CD178, APO-1L, FasL
CLP	common lymphoid progenitor
CTL	cytotoxic T lymphocyte
CTX	Cycloheximide
DAP10	DNAX-activating protein of 10 kDa
DD	death domain
DED	death effector domain
DISC	death inducing signaling complex
DMSO	dimethyl sulfoxide
DNAM-1	DNAX accessory molecule
EGF	epidermal growth factor
ER	endoplasmic reticulum
FA	formaldehyde
FACS	fluorescence activated cell sorter
FADD	Fas associated death domain
FCS	fetal calf serum
FRET	Fluorescence Resonance Electron Transfer
FSC	forward side scatter
GAPDH	glyerinaldehyd-3-phosphat-dehydrogenase
GFP	green fluorescent protein
GM-CSF	granulocyte macrophage-colony stimulating factor
GrzB	granzyme B

h	hour(s)
IFN-γ	Interferon-γ
Ig	immunoglobulin
IL	interleukin
ILC	Innate lymphoid cells
IO	Ionomycin
IPO8	Importin 8
IS	immunological synapse
kDa	kilo dalton
KIR	Killer-cell immunoglobulin-like receptor
LAMP-1	lysosomal-associated membrane protein 1, CD107a
LFA-1	lymphocyte Function-associated Antigen 1
LSM	lymphocyte separation medium
LTi	lymphoid tissue inducer
M6P	mannose-6-Phosphat
MACPF	membrane attack complex/perforin
MAPK	mitogen-Activated Protein Kinase
MHC	major histocompatibility complex
MMP	matrix metallopeptidase
MTOC	microtubule-organizing center
NCR	natural cytotoxicity receptor
NES	nuclear export signal
NFκB	nuclear factor 'kappa-light-chain-enhancer' of activated B-cells
NK	natural killer cells
P/S	penicillin/streptomycin
PBMC	peripheral blood mononuclear
PBS	phosphate-buffered saline
PE	phycoerythrin
PRD	proline-rich domain
PS	phosphatidylserine
RFI	relative fluorescence intensity
RT	room temperature
sCD95L	Soluble CD95L
SMAC	Second mitochondria-derived activator of caspases
sTRAIL	soluble TRAIL
tBid	truncated BH3 interacting domain death agonist

TNF	Tumor necrosis factor
TRAIL	Tumor Necrosis Factor Related Apoptosis Inducing Ligand, TL2, APO2L,CD253, TRAIL, Apo-2L, TNLG6A
TRAILR	TRAIL receptor
TSLP	Thymic stromal lymphopoietin
XIAP	X-chromosome linked inhibitor apoptosis protein

Eidesstattliche Versicherung (Affidavit)

_____ _____

Name, Vorname
(Surname, first name)

Matrikel-Nr.
(Enrolment number)

Belehrung:

Wer vorsätzlich gegen eine die Täuschung über Prüfungsleistungen betreffende Regelung einer Hochschulprüfungsordnung verstößt, handelt ordnungswidrig. Die Ordnungswidrigkeit kann mit einer Geldbuße von bis zu 50.000,00 € geahndet werden. Zuständige Verwaltungsbehörde für die Verfolgung und Ahndung von Ordnungswidrigkeiten ist der Kanzler/die Kanzlerin der Technischen Universität Dortmund. Im Falle eines mehrfachen oder sonstigen schwerwiegenden Täuschungsversuches kann der Prüfling zudem exmatrikuliert werden, § 63 Abs. 5 Hochschulgesetz NRW.

Die Abgabe einer falschen Versicherung an Eides statt ist strafbar.

Wer vorsätzlich eine falsche Versicherung an Eides statt abgibt, kann mit einer Freiheitsstrafe bis zu drei Jahren oder mit Geldstrafe bestraft werden, § 156 StGB. Die fahrlässige Abgabe einer falschen Versicherung an Eides statt kann mit einer Freiheitsstrafe bis zu einem Jahr oder Geldstrafe bestraft werden, § 161 StGB.

Die oben stehende Belehrung habe ich zur Kenntnis genommen:

Official notification:

Any person who intentionally breaches any regulation of university examination regulations relating to deception in examination performance is acting improperly. This offence can be punished with a fine of up to EUR 50,000.00. The competent administrative authority for the pursuit and prosecution of offences of this type is the chancellor of the TU Dortmund University. In the case of multiple or other serious attempts at deception, the candidate can also be unenrolled, Section 63, paragraph 5 of the Universities Act of North Rhine-Westphalia.

The submission of a false affidavit is punishable.

Any person who intentionally submits a false affidavit can be punished with a prison sentence of up to three years or a fine, Section 156 of the Criminal Code. The negligent submission of a false affidavit can be punished with a prison sentence of up to one year or a fine, Section 161 of the Criminal Code.

I have taken note of the above official notification.

_____ _____

Ort, Datum
(Place, date)

Unterschrift
(Signature)

Titel der Dissertation:
(Title of the thesis):

_____

_____

_____

Ich versichere hiermit an Eides statt, dass ich die vorliegende Dissertation mit dem Titel selbstständig und ohne unzulässige fremde Hilfe angefertigt habe. Ich habe keine anderen als die angegebenen Quellen und Hilfsmittel benutzt sowie wörtliche und sinngemäße Zitate kenntlich gemacht.
Die Arbeit hat in gegenwärtiger oder in einer anderen Fassung weder der TU Dortmund noch einer anderen Hochschule im Zusammenhang mit einer staatlichen oder akademischen Prüfung vorgelegen.

I hereby swear that I have completed the present dissertation independently and without inadmissible external support. I have not used any sources or tools other than those indicated and have identified literal and analogous quotations.

The thesis in its current version or another version has not been presented to the TU Dortmund University or another university in connection with a state or academic examination.*

*Please be aware that solely the German version of the affidavit ("Eidesstattliche Versicherung") for the PhD thesis is the official and legally binding version.

_____ _____

Ort, Datum
(Place, date)

Unterschrift
(Signature)